2017

Rheology of Thermo-Reversible Colloidal Gels

Divya Bahadur

FLORIDA STATE UNIVERSITY

FAMU-FSU COLLEGE OF ENGINEERING

RHEOLOGY OF THERMO-REVERSIBLE COLLOIDAL GELS

By

DIVYA BAHADUR

A Thesis submitted to the
Department of Chemical and Biomedical Engineering
in partial fulfillment of the
requirements for the degree of
Master of Science

2017

Divya Bahadur defended this thesis on April 06, 2017.
The members of the supervisory committee were:

Subramanian Ramakrishnan
Professor Directing Thesis

John C. Telotte
Committee Member

Sachin Shanbagh
Committee Member

The Graduate School has verified and approved the above-named committee members, and certifies that the thesis has been approved in accordance with university requirements.

ACKNOWLEDGMENTS

I cannot express enough thanks to my committee for their continued support and encouragement: Dr. Subramanian Ramakrishnan, my committee chair; Dr. John C. Telotte and Dr. Sachin Shanbhag. I offer my sincere appreciation for the learning opportunities provided by my committee.

TABLE OF CONTENTS

LIST OF FIGURES

ABSTRACT

Colloidal suspensions transform between fluid and disordered solid states when parameters such as the colloid volume fraction and the strength and nature of the colloidal interactions are varied. Seemingly subtle changes in the characteristics of the colloids can markedly alter the mechanical rigidity and flow behavior of these soft composite materials. This sensitivity creates both a scientific challenge and an opportunity for designing suspensions for specific applications. In this work, we investigate how the mechanical properties of thermo-reversible gels composed of octadecyl silica particles in decalin (sizes varying between 18 nm and 185 nm), at moderate particle concentrations change as a function of strength of attraction and particle loading. We further test the limits of applicability of scaling criteria developed within the framework of percolation theories and the more recently developed mode coupling theories. By using the experimentally measured gel boundaries and elastic moduli, the strength and range of attraction between the particles were obtained by comparison with the naïve mode coupling theory (NMCT) assuming a Yukawa interaction potential. We find reasonable agreement between theory and experiment when the data are scaled according to the relations proposed by percolation models for individual particle sizes, however these models fail to collapse the elastic moduli and yield stress data onto universal scaling curves for the entire range of particle sizes studied. The naïve mode coupling theory framework however does a remarkable job at predicting the gel boundaries, elastic moduli and the yield stresses. Finally, scaling relations are developed that collapse the elastic moduli and yield stress data onto master curves for all particle sizes and particle concentrations examined in this study.

CHAPTER 1

INTRODUCTION AND BACKGROUND

1.1 Introduction

Colloids are ubiquitous in many realms of science and technology. They are often classified as 'soft materials' since the interaction energies are of the order of thermal energy (kT) due to which small thermal and mechanical perturbations can lead to dramatic changes in properties. It is due to this sensitivity that they exhibit rich phase behavior. Colloidal suspensions can transform between fluid and disordered states by controlling the strength and nature of interaction between the colloidal particles. Understanding the mechanisms that underlie bulk property changes in colloidal systems provides fundamental insight that can be exploited to design advanced materials. Tuning inter-particle interactions electrostatically and sterically gives rise to interesting phase behavior and has been an active area of research for decades. Some examples include changing surface chemistry of the colloidal particles by grafting polymeric chains, [1-3] addition of surfactants, [4,5] [6] addition of other colloidal particles such as non – adsorbing polymer [7,8] [9], colloidal particles of different surface potentials [10], sizes (binary mixtures) [11], aspect ratios [12-14], etc. to create mixtures. Engineering stable colloidal suspensions lies at the heart of several consumer product based industries including pharmaceuticals, paints, food, personal care products and ceramics and composites processing. Even the emerging field 3D printing relies heavily on the stability and printability of dispersions which is a classical problem in colloidal science.

In addition to their use in industry, colloidal systems are also used as model systems to understand the phase behavior of pure materials at the atomic or molecular scale. The characteristic

length and time scales of colloidal dynamics are much larger than their atomic counterparts [15] [16] and can be experimentally measured using scattering and microscopy techniques down to single particle resolution. These analogues have been successful in explaining several phenomena such as crystallization [17,18], glass transition, gelation, etc.

Apart from synthetic inorganic and polymeric particles, dynamics, self – assemblies and functionalities of several biologically active systems such as complex proteins [19], viruses [20], bacteria [21], etc. have been described using experimental tools similar to those used to study colloidal dynamics as mentioned above. In addition, theories and simulations for understanding colloidal behavior have been used to model these systems since the relevant length scales are of the same order of magnitude as colloidal systems.

Colloidal dispersions, although complex in nature, can be theoretically modeled using effective interaction potentials such as the hard sphere [22], square well [23] [24], Asakura Oosawa [25,26] and Yukawa [27] potentials. Extensive work has been carried out in relating experimental results with theory and simulation. In particular, considerable efforts have gone into understanding phase behavior such as gelation and glass formation. Suspensions can transform from a liquid to a gel state at different concentrations upon introduction of short range attractions. At low concentrations, high strengths of attraction are required to induce this transition and at such concentrations, the structure is more fractal in nature. There have been efforts in literature to scale the mechanical properties of gelled suspensions based on percolation theories that are developed assuming fractal – like microstructures (which will be discussed in later sections). As concentration is increased ($\phi > 0.2$), the combined effect of crowding and attractions between

particles result in suspensions gelling at a lower strengths of attraction. At very high concentrations ($\phi > 0.5$), a transition to an amorphous glassy state is observed. When attractions are introduced at very high particle loadings, re-entrant glassy behavior is observed [28] [29] [30]. This is shown schematically in Figure 1.1 [31]. At moderate to high concentrations, the structure is no longer fractal in nature and thus an assumption of such a microstructure is no longer able to scale the mechanical properties of the system. An interplay of strength of attraction and particle concentration, thus, describes the microstructure in particle suspensions.

Gelation can occur through different routes – (1) homogenous gelation, where the gel line lies outside the traditional phase boundaries and is purely a result of dynamic arrest caused by the slowing down of particles due to particle attractions, and, (2) as a result of spinodal decomposition, where the system phase separates at the microscale. In this case, the particles form a percolated jammed network which we call a gel.

The disordered glassy and gelled states are characterized by the length and time-scales they exhibit as they dynamically arrest and how their mechanical properties evolve as they approach the ergodic to non – ergodic transition. A central question in the field of colloidal science has been whether a single framework can be developed which has the ability to capture the microstructural differences that occur at different concentrations and predict the bulk mechanical properties of the system given the nature of interactions exhibited by the particles. Theoretical models, generally classified as percolation models, were initially developed to explain the trends observed in the elastic moduli and yielding behavior relative to the gel point assuming that the system under consideration is fractal in nature [32] [33] [34] [35]. These theories have been successful in scaling the

experimental data for elastic moduli and yield strains for several systems at low to moderate particle concentrations. However, the suggested scaling relations (described in later sections) often fail at moderate to high concentrations where the contributions of particle crowding become significant. In addition, given an effective interaction potential, they cannot predict absolute elastic moduli and yield stresses/ strains.

Recent advances in this field include the development of the Activated Barrier Hopping theory by Schweizer and co-workers [36] which utilizes the framework of the Naïve Mode Coupling Theory in order to explain the mechanical properties and dynamics of colloidal gels and glasses. The strength of this framework lies in the fact that it does not assume an initial microstructure and thus, may be applicable to a larger range of concentrations. Within this framework, particles in a system are assumed to be 'caged' by their nearest neighbors. When weak attractions exist between particles, the particles may diffuse out their cages and explore larger volumes (or length scales), whereas, as attractions become stronger, the particles become more and more localized, such that they now only have the ability to explore restricted volumes. When the particles interact with very strong attractions, they become arrested within their nearest neighbor cages. Gelation is described as the condition at which they particles first become localized. This framework captures contributions of both, the interaction potential and concentration in describing the resultant microstructure and particle dynamics. Initial work by Zukoski and co – workers [27 37] utilized the framework of the barrier hopping theory to predict the gel boundaries and the mechanical properties of thermo-reversible and depletion gels containing octadecyl silica particles. Their results demonstrate good agreement between theory and experiment, however, their studies were restricted to particles of a single size (D = 40 nm) only. Till date, no work has been carried out to

test the applicability of this framework for particles of different sizes. Our motivation to study how the gel boundaries and mechanical properties change at different particle sizes lies in the need for developing design rules for processing of particle mixtures. Real life systems utilize particles of different sizes and concentrations. In addition, mixing particles of different sizes gives us a new avenue to tailor the mechanical properties of the system. With a model system well characterized at a wide range of sizes, concentrations and interaction energies, and the ability to predict their rheological behavior, we aim to set the base for future work where we will focus on studying the rheology of binary mixtures of particles.

In this work, we use thermo-reversible gels containing octadecyl silica particles of sizes varying over an order of magnitude (18-185 nm) in decahydronaphthalene (decalin), at moderate volume fractions to study the applicability of the barrier hopping theory in predicting gel boundaries, elastic moduli and yield stresses. We explore how an interplay of particle concentration and strength of attraction between particles affects the gel boundary and the bulk mechanical properties of the system. This system offers a unique advantage of good control over the strength of attraction between particles which can be achieved by controlling the temperature. Further, using the experimental data, we test the scaling criteria suggested by both, percolation and barrier hopping theory in scaling the elastic moduli and yield stresses onto universal scaling curves.

This thesis has been divided in 5 chapters. In the following section we review the relevant literature pertinent to our study. Chapter 2 describes the theoretical background for the mathematical relations used in describing our results. Chapter 3 details the materials and methods used in the current work. Chapter 4 describes the results obtained in this study and a detailed

discussion of the findings. Finally, Chapter 5 gives a summary of the important findings from this work and a brief description of the future directions.

1.2 Literature Review

1.2.1 Model Systems

Model systems are experimental systems that are designed such that their interaction potentials may be well defined by using simplified effective potentials. Three classes of model systems have been used extensively in studying particle gelation - charge stabilized systems, depletion systems and thermo-reversible systems.

In charge stabilized systems, attractions are induced through London – Van der Waal dispersion forces and attractions may be strengthened by charge screening through addition of ions. Colloidal latex, polystyrene, silica and gold [38] exhibit such interactions and their phase behavior has been studied extensively. Addition of electrolyte in these systems alters the rate of aggregation and not the net surface potential. These systems offer irreversible particle aggregation and very limited control over surface potential.

Depletion systems contain mixtures of particles and polymers (and combinations thereof) in which the size ratio (of hard cores) is large. In such a scenario, the exclusion of the small particles from between the large particles creates a local disturbance in the osmotic pressure thereby introducing attractions between large particles. One well-studied depletion system is octadecyl – silica in decalin with low molecular weight polystyrene [39]. Particle interactions are modeled using the AO potential and the system has been shown to undergo gelation through

spinodal decomposition [7,8]. Quantification of the strength of attraction in these systems and accounting for the partitioning of the components on phase separation has proven to be very challenging [23]. In addition, similar to electrostatically stabilized systems, introduction of attractions in these systems is an irreversible process.

Thermo-reversible systems contain sterically stabilized colloidal particles in index matched solvents which can be made to reversibly aggregate by controlling the sample temperature. Steric stabilization by grafting short chain alkanes and suspension in an in index matched solvent neutralizes surface charges and minimizes the contribution of Van der Waals interactions in the system. At high temperatures, the attractions in the system are negligible and the particles behave as hard spheres whereas quenching the temperature induces particle attraction. Some prominent examples of such systems are octadecyl-silica in decalin [27,37,40] and tetradecane [23 41 42]. In solvents which are structurally different from the grafted chains, such as decalin, attractions are introduced as a result of poor solvency of the grafted chains at low temperatures. However, when solvents are structurally similar to the grafted chains, such as tetradecane, the solvent molecules are seen to interdigitate and freeze in the grafted chains at low temperatures [23]. Thermo - reversible systems, as the name suggests can be reversibly made to transition between fluid and arrested states. Strength of attraction in these systems can be controlled very systematically and with great precision since it only requires good temperature control. In our study, we use octadecanol grafted silica suspended in decalin as the model system and carry out rheological measurements for samples of different particle sizes at moderate volume fractions.

1.2.2 Aggregation Theories

1.2.2.1 Percolation Models

Percolation models for particle gelation utilize the theoretical framework that was developed to describe the microstructure and mechanical properties of polymeric gels. It assumes that particles cluster to form fractal flocs which grow in size and eventually overlap to form a percolated, space – filling network. A percolated network that can sustain its own weight is defined as a gel. Close to the percolation transition, the system exhibits very high viscosities and upon percolation, attains a finite shear modulus. Clustering has been observed at low concentrations as seen in Ref 37 and 44 [35,43]. Space filling networks are formed when the mass of a floc (M) increases with the characteristic size of the floc (ξ) as a power law given by: $M = \xi^{D_f}$ such that D_f, the fractal dimension of the floc, is less than 3. Diffusion limited cluster aggregation (DLCA), a mechanism proposed for physical gelation is reported to have a characteristic floc dimension of $D_f \sim 1.75$ which is characteristic of fast aggregation [32]. Reaction limited cluster aggregation (RLCA) occurs when gelation occurs as a result of formation of chemical bonds, and is reported to have $D_f \sim 2 – 2.2$ which is characteristic of slow aggregation kinetics [43]. Floc sizes are estimated by assuming that all particles in the system participate in clustering and each particle floc has grown to achieve a volume fraction of random close packing ~ 0.64 yielding $\frac{\xi}{D} = \left(\frac{\phi}{\phi_m}\right)^{\frac{1}{D_f - 3}}$. Several theories based on this fractal framework have been developed to explain the trends observed for the kinetics of gelation and the mechanical properties of the resultant gels relative to the gel point, some of which are described below.

Using the fractal gel framework, Shih and co – workers [32] developed scaling criteria for elastic moduli and yield strains for gels formed far from the gelation threshold. They suggested

that in the regime where the links between fractal flocs are stronger than links between particles within the flocs the elastic modulus scales as $G' \sim \phi^{\left[\frac{3+b}{3-D_f}\right]}$ and the limit of linearity scales as $\gamma_M \sim \phi^{\left[\frac{1+b}{3-D_f}\right]}$ where D_f is the characteristic fractal dimension described earlier and b is the fractal dimension of the backbone of the percolated network. For alumina particles, they observed $G' \sim \phi^{4.1}$ and $\gamma_M \sim \phi^{-2.1}$. Using a similar framework of percolation, several models were developed that demonstrate a power law dependence of G' on ϕ. Buscall et al. [44-46] predicted $G' \sim \phi^x$ where x = 4.5 for reaction limited cluster formation and x = 3.5 for diffusion limited cluster formation where the power exponent depends upon the fractal dimensions of the flocs and the rigid backbone.

A micro-rheological model was developed by De Rooij et al. [33,47] and Potanin et al. [48,49] to describe the aggregation kinetics and linear viscoelastic properties of aggregated suspensions with weak particle interactions. In deriving this model, the authors assume fractal clusters are formed which percolate to form space spanning networks and that these networks are transient. The aggregates (assumed to be impermeable spheres) form chains upon collisions through two types of bonds – rigid bonds which impart the structural stability as they form the elastic backbone of the percolated network and soft bonds which are elastically inactive, i.e., they don't contribute to the elasticity of the network, and form inter-aggregate connections. The strength of the elastic network is thus determined by the rate at which rigid bonds form. The rigid chains respond elastically to deformation caused either mechanically or thermally and are assumed to transmit stress as Hookean springs. The system is then viewed as an interconnected system of beads and springs. The relaxation processes in such a system are characterized by the lifetime of the rigid bonds. This model predicts a power law dependence of G', $G' \sim \phi^x$, with theoretically calculated exponent x ~ 6.15 – 7.15, normalized rate of gel growth, $\Gamma_g t_D \sim \phi^a$, with exponent a ~ 6.7 - 9.2 [40]

and $\tau_y \sim \phi^b$ where b ~ 1.13 at low volume fractions and b ~ 2.5 – 4.3 at high volume fractions for sterically stabilized polystyrene latex particles. The power law exponents in this model, as seen earlier in the results of Shih et al. [32] and Buscall et al. [44], are dependent upon fractal dimensions.

In the work carried out by Rueb and Zukoski [40] using octadecyl silica in decalin as a model system that gels thermo-reversibly, they observed the same power law dependence of G' and rate of gel growth. They found that x ~ 5.6 close to the gel point and x ~ 4.4 away from the gel point, and, a ~ 2 – 3 close to the gel point and systematically decreases away from the gel point. They also observed that the dependencies of elastic modulus or yield stress on strength of attraction and particle concentration are very different. They observed that the power law exponents diverge at conditions close to the gelation transition when approached either by systematically changing particle concentration or system temperature. They concluded that the power law exponents, themselves, must have a temperature and/ or volume fraction dependence. Further, they noticed that at high particle concentrations, fractal arguments suggest that the effective number of particles in a 'cluster' is reduced to just two or three particles. In dense colloidal gels, thus, crowding would become significant and the concept of open fractal networks may have to be modified further.

Alternate percolation models exist which, unlike the models shown earlier, do not assume that the system percolates at all particle concentrations. In such systems, a threshold volume fraction, ϕ_G, is defined as the minimum particle concentration at which the system can percolate. Universal scaling behavior has been observed when the bulk modulus is scaled as a function of the distance from the percolation threshold at a given strength of attraction. Percolation model by Stauffer (1985) [34] suggests that G' should scale as $G' \sim \left(\phi - \phi_G\right)^s$ or $G' \sim \left(\frac{\phi}{\phi_G} - 1\right)^p$ where the

quantities $(\phi - \phi_G)$ and $\left(\frac{\phi}{\phi_G} - 1\right)$ represent the distance from the percolation threshold. The advantage of such scaling arguments lies in the fact that the scaling exponents p and s at these normalized 'distances' from the gel point don't change significantly with the aggregation mechanism. These models, however, are expected to hold true strictly at conditions close to the percolation threshold and seem to fail at high particle loadings. Experimental studies carried out by Grant and Russel (1993) [35] using octadecyl silica in hexadecane show excellent collapse of data when the bulk modulus is scaled as $G' \sim (\phi - \phi_G)^s$ with s ~ 3 for a large range of volume fractions up to $(\phi - \phi_G)$ = 0.3. They claim that $(\phi - \phi_G)$ represents the variable that describes the probability of bond formation as particle fraction is increased above the gelation threshold. Experiments carried out by Rueb and Zukoski [40] on octadecyl silica in decalin, however, suggest that both the elastic moduli and limit of linearity scale significantly better with $\left(\frac{\phi}{\phi_G} - 1\right)$ with p ~ 2. The authors suggest that at the same $\frac{\phi}{\phi_G}$, the density of the cluster may be assumed to be constant at all strengths of attraction. Thus, this variable is able to account for the effect of both strength of attraction and particle concentration in determining the final microstructure and aggregation rates and thus results in a better collapse of data than $(\phi - \phi_G)$, which only takes volume exclusion effects into account.

1.2.2.2 Activated Barrier Hopping Theory Framework

The activated barrier hopping model developed by Schweizer and co-workers [50] [36] within the framework of the Naïve Mode Coupling Theories (NMCT) has gained a lot of recognition in predicting both the location of the dynamic arrest transition well as the mechanical properties of the resultant gel. This theory describes how particle dynamics can be related to density fluctuations

arising in a system in which the particles are close enough for their collective motions to be sufficiently correlated. In this framework, the suspension is treated as an Einstein solid, i.e.: each particle is modeled as a harmonic oscillator, with the particles having a Gaussian positional dependence. A concept of caged particle motion is proposed such that a particle can diffuse freely within a "cage" of its nearest neighbors. The concept of a characteristic localization length is established which describes the length over which the particles can freely move around. In this regime, single particle transport requires thermally activated hopping over the entropic free energy barrier that is established as a result of interactions of the said particle with its nearest neighbors. At low strengths of attraction or particle loadings, thermal motion may be sufficient to allow particles to hop over the energy barriers and diffuse over large distances compared to the particle diameter. The system in this case behaves like a fluid containing freely diffusing particles and the localization length is effectively infinity since the particle motion is not restricted by its nearest neighbors. Conversely, as interaction strength or particle concentration is increased, the particle motion starts to become more confined and caging starts to become more prominent. In this regime, localization length decreases to attain a finite value – a fraction of the particle size. Gelation in such a system, is said to occur when the localization length first takes up a finite value [27]. Consequently, as the localization length decreases, it indicates that the particles are packed more tightly. The following sections will demonstrate the calculations required to predict the gel boundaries, elastic moduli and yield stresses for the octadecyl – silica – decalin system using the barrier hopping framework.

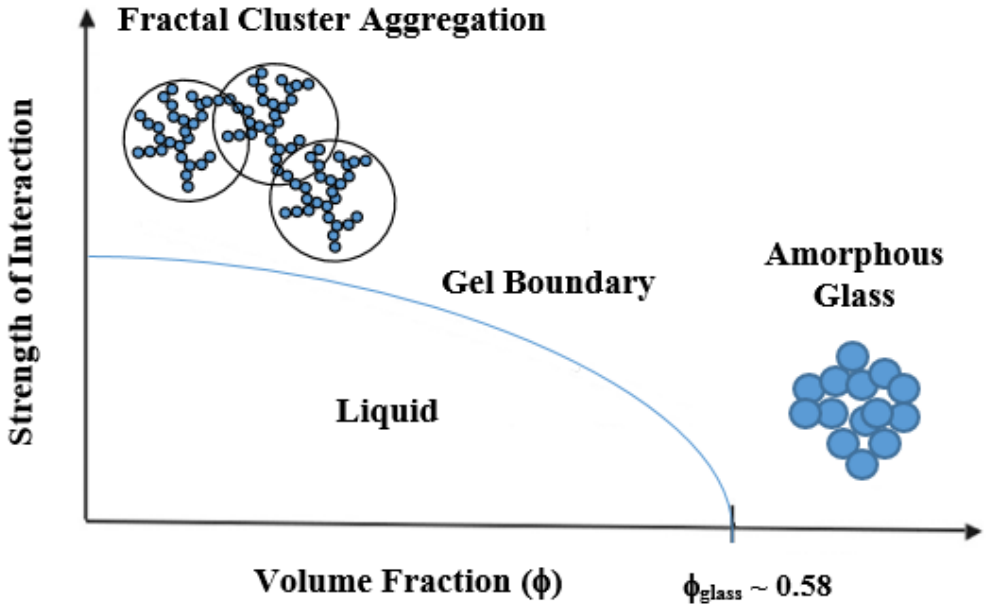

Figure 1.1 (Color Online) - Schematic phase diagram of colloidal suspensions depicting the transition between the fluid and disordered states with volume fraction ϕ and strength of interaction.

CHAPTER 2

THEORETICAL BACKGROUND

In this chapter we will detail the theoretical principles and assumptions underlying the models used to scale and predict the kinetics of gel growth, elastic moduli and yield stresses based on the framework of the percolation theories and the activated barrier hopping theory respectively. Our discussion for the percolation models describes the work carried out by Derooij and Potanin [48], Shih et al. [32] and Rueb and Zukoski [40]. For the discussion of the activated barrier hopping theory, we discuss the work carried out by Schweizer and co – workers [51 36 52], Ramakrishnan and Zukoski [27]and Gopalakrishnan and Zukoski [37].

2.1 Percolation Theory

2.1.1 Determination of Elastic Moduli

An appropriate interaction potential U (r) is assumed to model inter – particle interaction where 'r' is the surface to surface distance between the particles. The particle separation at which the potential energy is minimum corresponds to the condition at which particles form strong, rigid connections. The location of the energy minimum is denoted as r_c and the energy minima is denoted as U_{min}. The end to end chain length that forms the rigid backbone of the cluster is denoted by 'q'. Assuming all the particles in the system participate in cluster formation, the volume fraction is given by $\phi \sim \left(\frac{q}{a}\right)^{D_f-3}$ where 'a' is the particle radius. It is assumed that the rigid particle network is elastic and the particles behave as Hookean springs, thus, the force, 'f' that would be exerted on a particle as it is driven away from the energy minima, $r > r_c$ can be written as:

$$f = k_e \Delta q$$

Here k_e is the elastic constant given as $k_e = k_{el}\left(\frac{q}{a}\right)^{-(2+b)} = k_0 \frac{U_{min}}{r_c^2}\left(\frac{q}{a}\right)^{-(2+b)}$, k_{el} is the bond bending elastic constant, k_0 is the elastic constant when the potential is the steepest, b is a fractal parameter corresponding to the rigid backbone of the aggregate and Δq is the displacement of the particle from r_c [49]. The stress on a microscopic volume, may be given as:

$$\tau \sim nqf \sim N_r\, q^{-2} k_e \Delta q \qquad 2.1$$

Here, n is the number density of elastically active chains, n1 is the number of elastically active chains in a correlation volume of q^3 given by $n_1 \equiv nq^3$. When the stresses are small such that the system can respond elastically, the bonds break due to thermal and mechanical fluctuations of the system. A characteristic time – scale designated for this process is called the bond lifetime and is denoted by t_L. No bond/chain can exist longer than this characteristic timescale regardless of whether it is subjected to any external stresses [49]. The chain responds viscoelastically when subjected to small stresses. The elastic modulus, G' may be written as:

$$G' = \frac{\tau}{\gamma_0} \sim n_1 \xi^3 \frac{k_{el}}{2a}\left(\frac{\xi}{2a}\right)^{-(3+b)} \sim \phi^y \qquad 2.2$$

Here $y \sim \frac{6-b+D_f}{3-D_f}$, γ_0 is the strain given by $\Delta q/q$ and $q \sim q_{corr} \sim \xi$ is the correlation length scale of the fractal aggregate. We can assume here that $\phi \sim n_1 \xi^3$ and $\phi \sim \left(\frac{\xi}{2a}\right)^{(D_f-3)}$. Thus, we expect the elastic modulus to scale as a power law function of volume fraction.

2.1.2 Determination of Initial Growth Rate of the Elastic Modulus

Using the framework developed by Derooij and Potanin [48], Rueb and Zukoski [40] derived a simplified expression to study the initial growth rate of the elastic modulus, Γ_g, for weakly aggregating systems. Under conditions of shear flow, the aggregates forming the rigid backbone of the percolated network shrink such as:

$$N_r(t) \sim -1/\dot{\gamma}$$

Here, N_r represents the number of rigid bonds in the system and $\dot{\gamma}$ represents the shear rate the system is exposed to. Soon after the cessation of shear, it may be assumed that all inter-floc bonds are soft and these soft bonds transform to rigid bonds as the structure develops. The number of rigid bonds at short times (after cessation of shear) may be written as:

$$N_r(t) \sim \frac{N_{so} t}{t_D}$$

Here, N_{so} is the number of soft bonds that exist in the structure at time t = 0 and t_D is the time scale corresponding to diffusion of the particles, given by $t_D = kT/6\pi\eta_c a^3$. The elastic modulus is given as in equation 2.2:

$$G'(t) \sim N_r(t)\xi^3 \frac{k_{el}}{2a}\left(\frac{\xi}{a}\right)^{-(3+b)}$$

Here, ξ is the cluster size at time t, k_{el} is the pair elasticity constant given by $k_{el} \sim \left[\frac{dU}{dr}\right]_{max} \frac{U_{min}}{r_c^2}$ where the first term represents maximum force required by the particle to diffuse out of its potential energy well, U_{min} represents the energy of the particle in the potential energy well and r_c represents the position of the well in terms of distance from the particle surface.

Experimentally, the growth of G' in time is modeled using the following expression [40 53]:

$$G'(t) = G'(\infty)\left[1 - \exp\left(-\Gamma_g\left(t - t_g\right)\right)\right] \qquad 2.3$$

Here G' (∞) is the modulus at long times, once it reaches a plateau value, Γ_g is the initial rate of gel growth and t_g is the lag time. At short times, when $(t - t_g) \rightarrow 0$, equation 2.3 may be approximated using $\exp(x \rightarrow 0) \sim 1 + x$ as:

$$G'(t \longrightarrow 0) \sim G'(\infty)\left[\Gamma_g\left(t - t_g\right)\right] \qquad 2.4$$

The initial rate of growth of G', Γ_g, may thus be defined as:

$$\Gamma_g \sim \lim_{t \to 0} \frac{G'(t \longrightarrow 0)}{G'(\infty)\,(t - tg)}$$

Using the model developed by Potanin et al., thus, the initial growth rate may be given as:

$$\lim_{t \to 0} \frac{G'(t \longrightarrow 0)}{G'(\infty)} \; \frac{t_D}{t - t_g} \sim \Gamma_g t_D \sim \frac{N_{so}}{N_r(\infty)} \left(\frac{\xi_0}{\xi_\infty}\right)^{-b} \qquad 2.5$$

Here, ξ_0 and ξ_∞ represent the cluster size at time t = 0 and at long times when the network is percolated. In terms of volume fraction, rigid floc volume fraction, $\phi_r \sim N_r(\infty)\,\xi_\infty^3 \sim 1$ and total particle fraction at time t = 0, $\phi \sim N_{so}\,\xi_0^3$ and the cluster size may be approximated as 2a = D if we assume that the shear broke up all space spanning clusters [40]. Then, on expressing volume fraction as a function of cluster size, using $\phi \sim \left(\frac{\xi_\infty}{\xi_0}\right)^{(D_f - 3)}$ [47], the initial growth rate from equation 2.5 may then be expressed as a power law function of volume fraction given as:

$$\Gamma_g t_D \sim \phi^{\frac{D_f + b}{D_f - 3}} \sim \phi^s \qquad 2.6$$

Thus, a power law dependence of Γ_g may be expected as a function of particle concentration.

2.1.3 Determination of Yield Stress

The yield stress is defined as the maximum stress that a structure can sustain before it ruptures. As a first estimate, if we neglect the internal aggregate structure and assume that only one bond per cluster is required to break up the aggregate, then the yield stress may be approximated as:

$$\tau_y \sim \frac{F_{max}}{\Delta A} \sim \frac{1}{q^2}\left[\frac{dU}{dr}\right]_{max,\ r_c} \sim \frac{\phi^2}{a^3}\left[\frac{dU}{dr}\right]_{max,\ r_c} \qquad 2.7$$

Here, F_{max} is the maximum inter - particle force which is defined as the first derivative of the total interaction potential which would be required to separate particles when their separation is ~ r_c. Assuming that the internal aggregate structure is composed of a rigid backbone, equation 2.1 describes the relation between stress and strain in a viscoelastic system with a fractal microstructure. The system would yield when the stress is high enough to break the rigid inter – aggregate bonds. In order to break the bond, the applied mechanical energy must be greater than the energy stored in an elastic bond, $U_{bond} \sim k_{el}(\Delta q)^2$. Thus the strain at bond rupture and the corresponding yield stress may be written as:

$$\frac{\Delta q_{rup}}{q} \sim k_0^{-\frac{1}{2}} \left(\frac{r_c}{a}\right)\left(\frac{q}{a}\right)^{-b} \qquad 2.8$$

$$\tau_y \sim \left[k_0^{\frac{1}{2}} n_1 \left(\frac{U_c}{a^2 r_c}\right)\right] \phi^{\left(\frac{3}{3-D_f}\right)} \sim \phi^d \qquad 2.9$$

Thus, a power law dependence of yield stress may be expected on particle concentration.

2.1.4 Prediction of the Gel Boundary

Rueb and Zukoski [40] verified the power law dependence of elastic modulus at long times, G'_∞, on volume fraction and also found that for thermo - reversible systems, G'_∞ varies as an

exponential function of temperature. G'_{∞} was found to scale on a universal scaling curve as a function of non – dimensionalized volume fraction, $\frac{\phi}{\phi_G}$ such that,

$$G'_{\infty}(\phi, T) \sim \left(\frac{\phi}{\phi_G}\right)^{y} \qquad 2.10$$

Where ϕ_G is the volume fraction at the gel boundary at temperature T. The following expression was developed to determine the strength of attraction for octadecyl silica particles by Jansen et al. [24]:

$$\frac{\epsilon}{kT} = -A'\left(1 - \frac{T}{T_\theta}\right) \qquad 2.11$$

The exponential dependence of the elastic modulus on temperature was assumed to be related to the strength of attraction such that $G'_{\infty} \sim \exp\left(-\frac{\epsilon}{kT}\right)$ and thus,

$$G'_{\infty}(\phi, T) = G'_{\infty}(\phi, T_R) \exp\left\{\frac{A'T_R}{T_\theta}\left(1 - \frac{T}{T_R}\right)\right\} \qquad 2.12$$

Here T_R is a reference temperature at which the volume fraction at the gel boundary is known for the system. Using equations 2.10 and 2.12, thus, we can determine the gel boundary using the following simplification:

$$\phi_G = \phi_G(T_R) \exp\left(\frac{[T - T_R]}{y}\right) \qquad 2.13$$

It must be noted that this method of determining ϕ_G is only approximate and depends upon the accuracy of the experimental data. In general, no consensus has been reached in predicting ϕ_G theoretically [27].

2.2 Activated Barrier Hopping Theory

2.2.1 Prediction of the Gel Boundary

A simplified form of the activated barrier hopping theory focusses on the short ranged aspect of the dynamics such as hard core collisions. This simplification is referred to as the "Ultra - local Limit" of the activated barrier hopping theory and is expected to be applicable to any system that interacts through a near hard core repulsion or short ranged attraction [36]. Within this framework, the model describes the localization length as:

$$\frac{1}{r_{loc}^2} = \frac{1}{9}\int_0^\infty \frac{4\pi q^2 dq}{2\pi^3}\, q^2 \rho\, C^2(q)\; S(q) \exp\left(-\frac{q^2 r_{loc}^2}{6\left(1+\frac{1}{S(q)}\right)}\right) \qquad 2.14$$

Here, q is the wave-vector (m^{-1}), a Fourier transformed length scale, S (q) is the structure factor that represents density fluctuations at length scales of the order of 1/q, C (q) is the direct correlation function which can be determined from S (q) such that $S(q) = \left(\frac{1}{1-\rho C(q)}\right)$ [36] and $\rho = \left(\frac{\phi}{\frac{1}{6}\pi D^3}\right)$ is the number density. With an appropriate choice of interaction potential and closure relation, S (q) and consequently the localization length can be calculated using equation 2.14. As described in Section 1.2, the transition to dynamic arrest is indicated when the localization length attains its first finite value. Ramakrishnan and Zukoski [27] have used this method to theoretically predict the gel boundaries assuming a Yukawa interaction potential (described in Section 2.2.2) to model the particle interactions is shown in Figure 2.1. As can be seen, the barrier hopping theory predicts a power law dependence of strength of attraction at the gel boundary on volume fraction.

2.2.2 Determination of Elastic Moduli

The glassy (or zero frequency) modulus may be determined using the Green – Kubo relation and MCT factorization approximation [36 27 37] and is given as:

$$G'(\omega = 0) = \frac{kT}{60\pi^2}\int_0^\infty dq\, q^4 \left(\frac{d\ln S(q)}{dq}\right)^2 \exp\left(-\frac{q^2 r_{loc}^2}{\left(\frac{3}{S(q)}\right)}\right) \qquad 2.15$$

Non - dimensionalizing this equation using q' = qD and r_{loc}' = r_{loc}/D gives:

$$G'(0) = \frac{kT}{60\pi^2 D^3}\int_0^\infty d(q')\,(q')^4 \left(\frac{d\ln S(q')}{d(q')}\right)^2 \exp\left(-\frac{(q' r_{loc}')^2}{\left(\frac{3}{S(q')}\right)}\right)$$

$$\frac{G'D^3}{kT} = \frac{1}{60\pi^2}\int_0^\infty d(q')\,(q')^4 \left(\frac{d\ln S(q')}{d(q')}\right)^2 \exp\left(-\frac{(q' r_{loc}')^2}{\left(\frac{3}{S(q')}\right)}\right) \qquad 2.16$$

The term on the left hand side of equation 2.16 is non – dimensionalized elastic modulus. We know that the function on the RHS of equation 2.16 can be written as a function of ϕ and a non - dimensionalized temperature, f (ϕ, T), since the RHS is essentially a complex function expressed in terms variables that determine S (q) such as q, T and ϕ. Taking a first order approximation of this function in ϕ for cases when concentrations are low, we get:

$$\frac{G'D^3}{kT} = f(\phi, T) = \phi * g(\phi, T) \qquad 2.17$$

Simplifications made to the Green Kubo expression for G' (0) in the ultra - local limit yields an expression that relates the localization length to G' (0) given as[36]:

$$G'(0) = \frac{9}{5\pi}\frac{\phi kT}{D\, r_{loc}^2} \qquad 2.18$$

Since rloc itself is dependent on volume fraction, equation 2.18 may be used to demonstrate the power law dependence of G' on volume fraction. In an article by Ramakrishnan and Zukoski [27],

similar calculations have been carried out to predict the elastic modulus using the Yukawa interaction potential along with a modified Mean Spherical Approximation closure for the same octadeyl – silica – deaclin system. The Yukawa potential is a three parameter interaction potential that has been used extensively to model strong short range attractions in colloidal systems. It is characterized by three potential parameters – particle diameter, D (m), strength of interaction at contact given as $\frac{\epsilon}{kT}$ and range of attraction given as κ^{-1} (m) and is given as:

$$\frac{u_{yukawa}(r)}{kT} = \begin{bmatrix} \infty & \text{for } r < D \\ -\frac{\frac{\epsilon}{kT}\exp\left(-\kappa D\left(\frac{r}{D}-1\right)\right)}{\frac{r}{D}} & \text{for } r > D \end{bmatrix}$$

The octadecyl – silica – decalin system has been extensively studied and its strength of attraction is well described using the Flory – Higgins theory for polymers [54,55] as:

$$\frac{\epsilon}{kT} = A\left(\frac{T}{T_\theta} - 1\right) \qquad 2.19$$

Here, A is defined as the overlap volume fraction of the octadecyl chains upon aggregation and T_θ is the theta temperature of the octadecane – decalin system. These variables are dependent on particle size and solvent properties. Given the particle diameter and the range and strength on interaction, thus, the elastic modulus can be predicted upon numerically integrating equation 2.15.

2.2.3 Prediction of the Interaction Potential Parameters

It must be stated here that determining absolute values for the range and strength of attraction for a system under a certain set of conditions is a non – trivial exercise. An empirical relation was developed by Ramakrishnan and Zukoski [27] using the barrier hopping framework for particles modeled using short range Yukawa interactions that allows one to back-calculate the

interaction potential parameters using experimentally measurable properties such as particle diameter, volume fraction, absolute temperature and equilibrium elastic modulus given as:

$$\frac{G'D^3}{kT} = \frac{0.58\,\phi\,[\kappa D]^2}{M^2(\phi,\kappa D)} \exp\left[1.6\,\chi(\phi,\kappa D) A\,T_\theta \left(\frac{1}{T} - \frac{1}{T_{gel}}\right)\right] \qquad 2.20$$

Here, $M(\phi,\kappa D)$ and $\chi(\phi,\kappa D)$ are constants that depend on volume fraction and the range of interaction. This empirical scaling relation is found to hold in the limit $0.15 \leq \phi \leq 0.38$ and $11 \leq \kappa D \leq 100$. This framework showed excellent collapse of experimental data for the octadecyl – silica – decalin system for a single particle size and varying volume fractions as seen in the two studies carried out for 90 nm particles and volume fractions varying between 0.253 and 0.446 by Ramakrishnan and Zukoski [27] and for 48 nm particles and volume fractions between 0.25 and 0.38 for the studies carried out by Gopalakrishnan and Zukoski [37] when $\frac{G'D^3}{kT}$ is plotted as a function of $\left[\frac{1}{T} - \frac{1}{T_{gel}}\right]$. The range and strength of interaction is then determined using the slope and intercept of the exponential fit. If the volume fraction is known, the range of interaction, κD may be determined from the intercept using the following empirical relation developed by Ramakrishnan and Zukoski:

$$\left(\frac{\kappa D}{M(\phi,\kappa D)}\right)^2 = (3.11 - 27.31\phi + 106.37\phi^2 - 137.45\phi^3)(\kappa D)^{2.2} \qquad 2.21$$

From the knowledge of κD, the χ parameter may be obtained from Table 1 in Ramakrishnan and Zukoski [27]. An average value of χ over the range of volume fractions studied is used to determine the product AT_θ. Next, individual values of A and T_θ may be determined by solving equation 2.19 with one known experimental point on the gel boundary.

2.2.4 Determination of Yield Stress

In the activated barrier hopping framework, particle localization is expressed in terms of an effective non-equilibrium free energy function, F (in units of kT) which is dependent on separation distance, r. This free energy function describes the effective interaction energy imposed on a primary particle from surrounding particles in the limit of zero stress and is given as:

$$F(\alpha) = \frac{3}{2}\ln(\alpha) - \int \frac{dq}{2\pi^3}\rho C^2(q)S(q)[\{1 + S^{-1}(q)\}^{-1}] * \exp\left(-\frac{q^2}{4\alpha}[1 + S^{-1}(q)]\right)$$

Here, $\alpha = \frac{3}{2r^2}$, ρ is the particle number density, S(q) is the structure factor dependent on wave – vector q (m^{-1}) and C (q) is the direct correlation function which can be determined from the structure factor. Kobelev and Schweizer [51] derived an expression for the free energy function by incorporating effects of external stress, τ, in units of kT/D^3, given as:

$$F(\alpha) = \frac{3}{2}\ln(\alpha) - \int \frac{dq}{2\pi^3}\rho C^2(q)S(q)\left[\left\{\frac{1}{1 + S^{-1}(q)}\right\}\right] * \exp\left(-\frac{q^2}{4\alpha}\left[1 + \frac{1}{S(q)}\right]\right) - \frac{\tau}{\phi^{\frac{2}{3}}}\sqrt{\frac{3}{2\alpha D^2}} \quad \cdots 2.22$$

Gopalakrishnan and Zukoski [37] calculate F (α) using the experimentally backed out values of range and strength of attraction as described in Section 2.2.3 based on the work carried out by Ramakrishnan and Zukoski [27] and experimental values of shear stress as shown in Figure 2.2. The minimum if F (α) is the localization length of the particles. This localization length may then be used to calculate the elastic modulus at a given shear stress using equation 2.18. Gopalakrishnan and Zukoski define the yield stress as the shear stress corresponding to the point where the G' drops to 90% of its linear viscoelastic value.

At low stresses, it can be assumed that the imposed external stress is constant throughout the material, thus, the macroscopic and microscopic stresses are equal. The microscopic force acting on a unit cross section area of the particle area may be given by assuming an averaged length scale of the system given by $\langle L \rangle \sim \left(\frac{\phi}{n}\right)^{\frac{1}{3}}$ where ϕ is the volume fraction of particles and n is the number density of particles in the system. The averaged characteristic area may thus be given by $\langle A \rangle \sim \left(\frac{\phi}{n}\right)^{\frac{2}{3}}$ and the corresponding force may be written as:

$$f = \tau\left(\frac{\phi}{n}\right)^{-\frac{2}{3}} = \left(\frac{\pi D^3}{6}\right)^{\frac{2}{3}} \frac{\tau}{\phi^{\frac{2}{3}}}$$

The system is thought to yield when the external stress can impose an external force greater than the maximum cage restoring force, f_{max} given as $f_{max} \sim \left[\frac{dF}{dr}\right]_{R^*}$ where R* is the displacement at which the slope of the free energy function is maximum. The yield stress may thus be approximated as:

$$\tau_y \sim \frac{\phi^{\frac{2}{3}}}{D^2} f_{max} \qquad 2.23$$

Here, the yield stress is non – dimensionalized using characteristic stress kT/D^3.

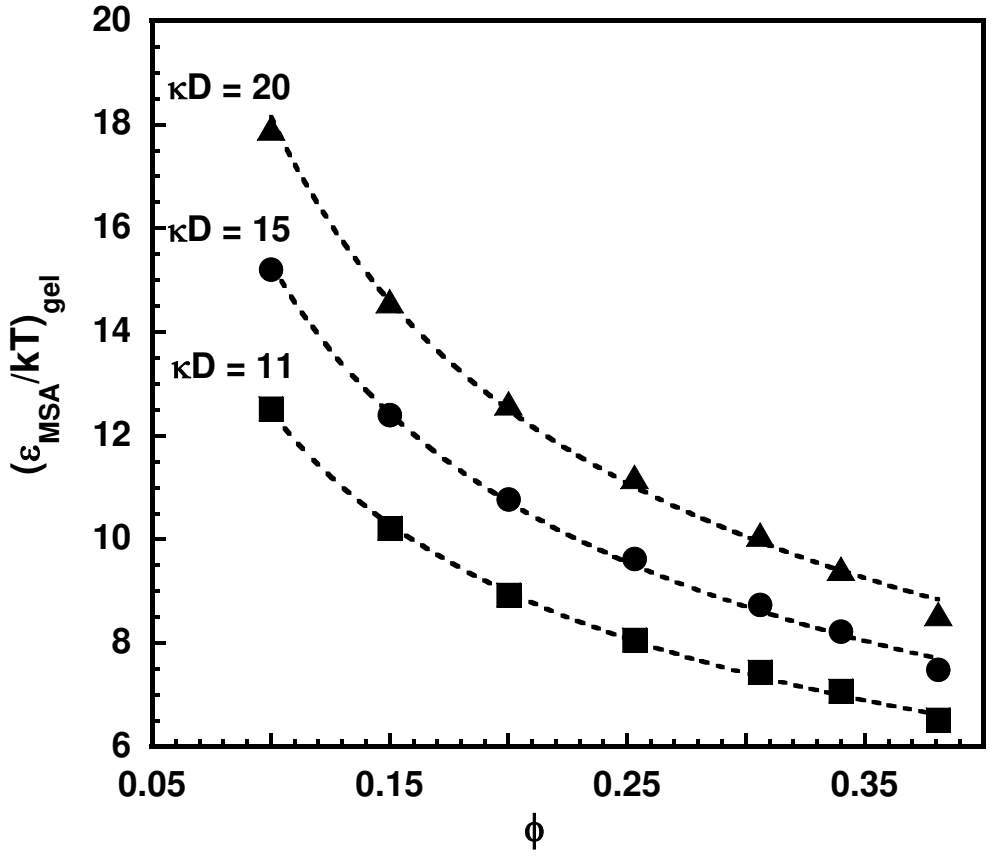

Figure 2.1 - ϵ_{MSA}/kT at the calculated gel boundary vs ϕ for particles interacting with short-range Yukawa potential at different κD values using the NMCT framework. Solid symbols are theoretically calculated points on the gel boundary while the lines are power law fits to data

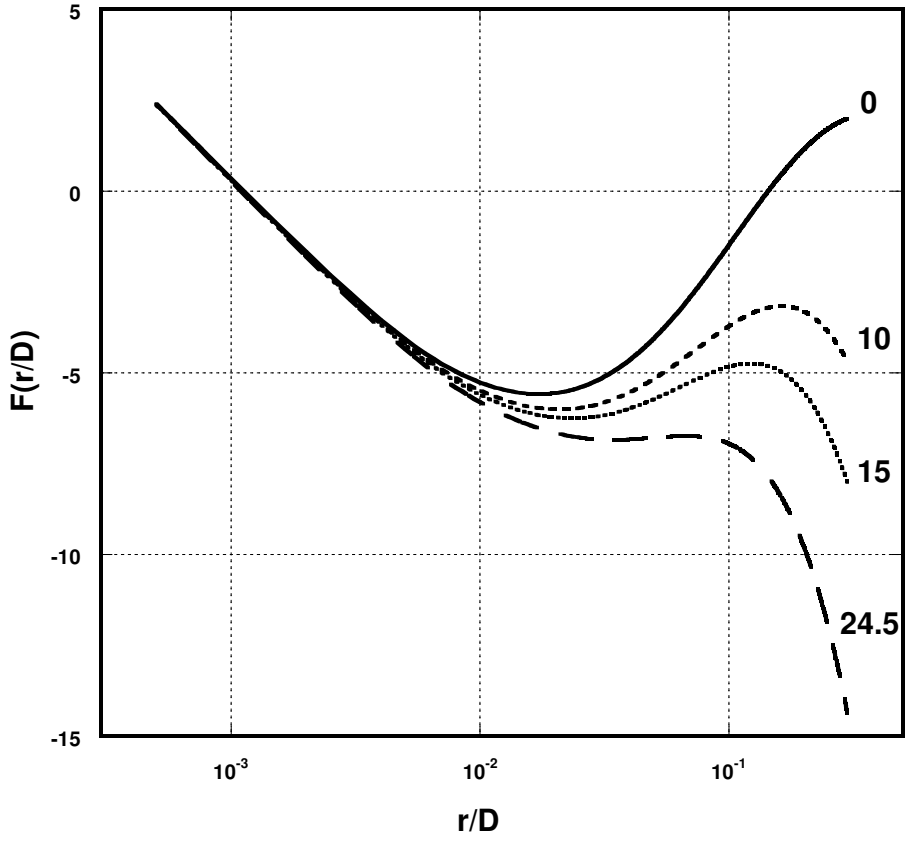

Figure 2.2 – Non-equilibrium free energy F, in units of kT, as a function of the normalized particle displacement (r/D). With increasing stress (values next to the curves, in units of kT/D^3), the non-equilibrium free energy barrier height decreases while the position of the minima, or the localization length shifts to higher values.

CHAPTER 3

MATERIALS AND METHODS

This chapter describes the synthesis of silica particles, coating of the particles with octadecanol, suspension preparation, protocols for particle characterization, and protocols for rheological measurements.

3.1 Synthesis of Octadecyl Silica Dispersions

The system under investigation is composed of monodisperse octadecyl silica spheres suspended in decahydronaphthalene (Decalin). Monodisperse silica cores were synthesized using the Stöber synthesis technique detailed in Section 3.1.1. To prepare larger particle sizes, these core particles were grown via double additions using a Seeded Growth Technique proposed by Bogush et al. [56] mentioned in Section 3.1.2 and finally surface functionalized with n-octadecanol using the method developed by Van Helden et al. [57] to neutralize the surface charges as described in Section 3.1.3. Stock solutions of ~45% volume fraction of octadecyl silica in decalin are prepared initially and then diluted to 40%, 35%, 30%, 25% and 20% by diluting with Decalin.

3.1.1 Stöber Synthesis

An elegant method for controlled synthesis monodisperse silica particles through the hydrolysis of silicon alkoxides and subsequent condensation of SiO_2 into uniform spheres was proposed by Stöber et al. [58]. Silica particles of a particular size were synthesized from the hydrolysis of tetra-ethyl orthosilicate (TEOS) in an ethanol medium with ammonia as a catalyst (added as ammonium hydroxide). Good control of the particle size was achieved by tuning the

concentrations of TEOS, ammonia, water and the solution temperature. The hydrolysis reactions governing the process are described as follows:

$$Si(OC_2CH_5)_4 + 4H_2O \xrightarrow{NH_3,\ Alcohol} Si(OH)_4 + 4C_2H_5OH \qquad \text{(Hydrolysis)}$$

$$Si(OH)_4 \xrightarrow{NH_3,\ Alcohol} SiO_2 \downarrow + 2H_2O \qquad \text{(Condensation)}$$

3.1.1.1 Synthesis of 30 nm Particles

Initial reactions were carried out in a 5 L round flask inserted with a stir rod and placed in a hot water bath set to 49 ^{o}C. 3620 mL 200-Proof Ethanol and 89.2 mL de-ionized water were added to the reaction vessel and allowed to thermally equilibrate for 1 hour before simultaneously adding 152 mL of tetra ethyl orthosilicate (TEOS) and 139 mL of ammonia hydroxide (13% by weight), initializing the reaction. The system was covered with aluminum foil to reduce the rate of evaporation from the water bath and glass stoppers on the flask were secured with parafilm to avoid leakage of the vapors and to avoid the stoppers from getting pushed out due to pressure in the vessel. This batch reaction was allowed to go to completion overnight before the water bath was switched off to stop the reaction. Six batches were synthesized using this technique and combined before coating with octadecanol.

3.1.1.2 Synthesis of 82 nm Particles

The first step in synthesizing 82 nm particles is the 30 nm seed particles as detailed above. 30 nm seed particles were synthesized in a 5 L round bottom flask with a stir rod, placed in a hot water bath at 49 C. 1818 mL of 200-Proof Ethanol and 46.8 mL of deionized water were equilibrated at 49 C for 1 hour after which 77 mL TEOS and 77ml ammonium hydroxide were

simultaneously added to initiate the reaction. The water bath was covered with aluminum foil to avoid evaporation and the stoppers on the flask were sealed using parafilm. The batch reaction was allowed to go to completion overnight. In order to attain the desired particle sizes, the seed particles were grown to the desired size by the Seeded Growth technique proposed by Bogush et al. [58]. A double addition reaction is carried out by adding 154 mL TEOS and 25 mL of deionized water to the seed particles in the ethanolic medium at 25 C. This reaction is carried out for at least 7 hours. Eight double addition reactions were carried out to synthesize particles of size for 82 nm particles respectively.

3.1.1.3 Synthesis of 185 nm Particles

72 nm seed particles of were synthesized in a 5 L round bottom flask containing 1818 mL of 200-Proof Ethanol and 46.8 mL of deionized water thermally equilibrated at 25 C by placing the apparatus in a water bath maintained at 25 C and stirring constantly using a stir rod. 77 mL TEOS and 77 mL ammonium hydroxyl are added to the ethanolic medium to initiate the reaction at 25C. The reaction was allowed to undergo completion overnight. Double Additions were carried out at 25 C by adding 154 mL TEOS and 25 mL deionized water each time. Nine double additions were used to grow the particles to a size of 185 nm particles.

3.1.2 Surface Functionalization

After synthesis of the silica particles, the particles were coated with 1-octadecanol using an esterification reaction according to the protocol followed in Van Helden et al [57]. Volume reduction was carried out prior to transferring the sol into a 1000 mL beaker in order to reduce the amount of water and ethanol in the mixture. Care was taken to avoid excess ethanol and water

from evaporating which can cause the system to crash out. Addition of pure ethanol in this step enhances the removal of water. Once the volume is significantly reduced, 1000 g of anhydrous octadecanol is added in excess (3-5 times the amount of silica present by weight) to the sol. The esterification reaction takes place at 215 °C for 5 hours under constant stirring using a magnetic stirrer on a hot plate. The temperature is carefully monitored and recorded every 15-20 minutes. Once the reaction is completed, the temperature is slowly lowered down to room temperature and the remaining ethanol and water is allowed to evaporate overnight. The surface functionalized silica particles and unreacted octadecanol forms a cake at the bottom of the beaker.

3.1.3 Purification

The purification of the coated particles from excess octadecanol takes place through a series of centrifugation and vacuum drying steps. The cake obtained from the previous step is dispersed in excess chloroform, a good solvent for octadecanol, by heating it up to a temperature of 35-45 °C and stirring it simultaneously. Once the particles are well dispersed in chloroform, the solution is poured in 500ml polypropylene centrifuge bottles and centrifuged at 18000 rpm for 3 – 4 hours at a temperature of 25-30 °C. The supernatant is poured off and the suspended silica particles are dried under vacuum alone until dry powder is obtained without applying any heat. The dry powder is weighed and then re-dispersed in chloroform and the centrifugation and vacuum drying steps are repeated. For all particle sizes 4 cycles of centrifugation and vacuum drying were carried out, first two using chloroform as solvent and last two using cyclohexane. Cyclohexane offers a larger density difference between the particles and the media thus enabling better separation.

3.1.4 Sample Preparation

After the final vacuum drying step, the dried powder is weighed and dispersed in calculated amounts of decalin to make a stock solution of ~45% by volume silica. To prepare samples of different volume fractions for the rheology experiments, the stock solution was diluted by adding requisite amounts of decalin to the stock. To verify the volume fractions, the samples were dried at 100°C in an oven overnight, the dry weight was recorded and the volume fractions were back-calculated both before and after the rheological measurements.

3.2 Particle Sizing and Characterization using SAXS

Particle sizing during synthesis was carried out using a Dynamic Light Scattering (DLS) Apparatus. DLS gave initial estimates of the hydrodynamic radius of the particles and their polydispersity. Small Angle X-Ray Scattering (SAXS) was employed in order to get an accurate estimate of the particle size, polydispersity and nature of particle interactions.

X-ray scattering experiments were carried out at Sector 12-ID of the Advanced Photon Source at Argonne National Laboratory. Dilute samples (volume fractions ~ 0.02) were loaded into a glass capillary of 1 mm thickness and mounted on the beamline. The energy of the incident X-ray beam was ~ 10 keV and the sample to detector distance was ~ 4 m. The wave vector (q) range accessed in this experiment was between 0.002 to 0.5 $Å^{-1}$. The experimental data measured scatter intensity as a function of q. These data were fit to a model (form factor for a sphere with a size distribution) to back out the size and polydispersity of the particle using the Irena SAS Modeling Macro on Igor Pro.

3.3 Rheological Characterization

Rheological experiments were carried out using the Bohlin Gemini Rotonetic Z, stress controlled rheometer in a C-14 couette geometry (Outer cup diameter = 14 mm; Gap = 0.7 mm) and the temperature was controlled using a Peltier drive setup with an accuracy of ± 0.2C. A 3ml sample volume was loaded each time and evaporation of the sample was prevented by using a solvent trap to cover the geometry. Samples remained unchanged in the rheometer for at least a 20 hour period. Experiments were carried out up to 3 times to ensure repeatability.

3.3.1 Determining the Gel Temperature

The test sample was loaded into the cup at room temperature and then quenched quickly at a rate of 4 K/min to the desired temperature. It was then pre-sheared at 300 s^{-1} for 180 s in order to remove any thermal history that may have built up in the gel structure during the rapid quench so as to ensure reproducibility. The sample is then oscillated at a constant frequency of 1 Hz and a low stress between 0.1 – 0.5 Pa for 3600 s during which the modulus of the gel grows to a time independent equilibrium value G' (∞).The sample is then subject to a temperature ramp of 0.1 K/min and oscillated at 1 Hz and a very low stress of 0.05 Pa. As the sample is heated, both the storage and loss moduli undergo a rapid decrease in a small temperature window. The gel point is defined as the temperature at which the storage and the loss moduli first cross over. Summary of steps involved in determining the gel temperature –

1. Load sample at 25C
2. Rapid quench at 4 K/min to T_low
3. Pre-shear at 300 s^{-1} at T for 180 s

4. Gel growth – 1 Hz, low stress (0.1-0.5 Pa), 1 hour
5. Temperature ramp up at 0.1K/min at 0.05 Pa from T_low

3.3.2 Rheological Characterization at Steady Temperatures

The sample is rapidly quenched from room temperature at which the particles behave like hard spheres to a temperature below the gel point. Once the desired temperature is attained, the sample is pre-sheared at a shear rate of 300 s^{-1} for 180 s, and is then subject to - (1) a stress controlled oscillation at 1 Hz at a low stress between 0.1 and 0.5 Pa - low enough so that the growth of the gel structure is not disrupted, however, high enough so that the strain doesn't approach instrument limits and result in noise in the measurement. Depending on how far the temperature is from the gel temperature, it takes from 2 – 3.75 hours for the modulus to reach a time invariant value. Once the modulus plateaus, (2) a frequency sweep is carried out where the sample is subject to stress controlled oscillation and a frequency ramp between 0.1Hz – 50Hz to probe the dependence of the moduli on frequency. The frequency sweep is followed by (3) a stress sweep where the magnitude of the shear stress is increased logarithmically from a low value of 0.1 Pa to ~ 100 Pa to determine the yield stress. Summary of steps involved in rheological characterization of a sample at a given temperature and concentration –

1. Load sample at 25°C
2. Rapid quench at 4 K/min to T
3. Pre-shear at 300 s^{-1} at T for 180 s
4. Gel growth – 1 Hz, low stress (0.1 - 0.5 Pa), > 3 hours
5. Frequency Sweep – constant stress, 0.1 - 50Hz
6. Stress Sweep – 1 Hz, 0.1 - 100 Pa

CHAPTER 4

RESULTS AND DISCUSSION

This chapter discusses the experimental results obtained from the SAXS and rheological measurements. Further, the experimentally obtained data are compared with the predictions of the barrier hopping theories for elastic moduli and yield stresses. In addition, scaling criteria proposed by percolation theories and mode coupling theories to collapse the experimental data for elastic moduli and yield stresses are tested.

4.1 Particle Characterization using Small Angle X-Ray Scattering (SAXS)

Octadecyl silica particles of sizes 30 nm, 82 nm, and 185 nm were successfully synthesized using the protocol described in Section 3.1. The particles were sized using SAXS which measures scattered intensity (I) as a function of wave vector (q) for a dilute sample. Figure 4.1 shows a sample static X-ray scattering plot for a dilute sample (ϕ ~ 0.02) of 82 nm particles at 25 °C - symbols represent experimental data and the solid lines are curve fits to the experimental data based on Equation 4.1 which represents the form factor for a sphere with a Gaussian (or log normal) distribution.

$$f(q) = \int_0^\infty f_s(q)\ R^6 \frac{1}{\delta\sqrt{2\pi}} \exp\left(-\frac{1}{2}\left(\frac{R - \langle R\rangle}{\delta}\right)^2\right) dR \quad \cdots 4.1$$

Where $f_s(q)$ is the form factor of a perfect sphere given as:

$$f_s(q) - \left[\frac{3(\sin(qR) - qR\cos(qR))}{(qR)^3}\right]^2$$

Here q is the wave-vector, R is the radial distance, δ is the Gauss width and ⟨R⟩ is the Gauss mean particle radius. The mean value and the standard deviation of the particle sizes as determined from the curve fit for all particle sizes are given in the Figure 4.1 for 82 nm particles and in Appendix A for 18, 30 and 185 nm particles.

Figure 4.2 is a plot of I vs q for a concentrated sample of 82 nm particles ($\phi = 0.3$) in decalin at 25°C. The experimental points are open symbols while the solid lines are a curve fit to the experimental data using the Hard Sphere equation of state with the Percus - Yevick (PY) closure. The good agreement of experiments with theory suggests the particles indeed behave as hard spheres at room temperature even at high concentrations. In this work, attractions are introduced between the particles by reducing the system temperature. Below a critical threshold temperature, the particles form a gel. Good control over the strength of interaction is obtained by controlling temperature.

4.2 Analysis of Rheology Data

4.2.1 Gel Boundaries and Extraction of Interaction Potential Parameters

A sample plot showing the temperature ramp carried out to determine the gel temperature (T_{gel}) for 30 nm octadecyl silica particles in decalin ($\phi = 0.4$) using the protocol described in section 3.3.1 is shown in Figure 4.3. A well - formed gel at $T_{low} = 13$°C is slowly melted at a heating rate of 0.1 K/min. Initially, at T_{low}, the sample is a strong gel as indicated by well separated G' and G'' and a high G' (~ 15 kPa). As the temperature is increased, the strength of attraction between particles $\left(\frac{\epsilon}{kT}\right)$ decreases and the structure is expected to loosen which can be seen as a sharp decline in G' and G'' in Figure 4.3. At a certain temperature through the ramp, here, 15.9 C, the structure

loosens to the extent that it can't sustain its own weight and collapses. This transition to a predominantly liquid-like regime is indicated by the intersection of G' and G'' and is defined as the gel point. Experimentally, if G'' is greater than or equal to G' and the oscillatory strains are high, it is indication of a fluidized regime as opposed to a solid-like structure. The sharp decline of G' and G'' within ~1°C from the gel point is noteworthy and is observed for every sample. It indicates the fragility of the gel at temperatures very close to the gel point. This method of determining the gel point is found to be reproducible to within 0.5°C. Gel point determination plots for all particle sizes and volume fractions studied are given in Appendix B.

The effect of conducting a heating ramp versus a cooling ramp to determine the gel point was examined in the study as shown in Figure 4.4 for 82 nm octadecyl silica particles in decalin (ϕ = 0.2). The experimental protocol followed to carry out a cooling ramp is similar to that described in section 3.3.1. The sample is first quenched from 25°C to 5°C and thermally equilibrated. The cooling ramp is then carried out from 5°C to 1°C at a cooling rate of 0.1 K/min, 1% strain and a frequency of 1 Hz. Once T_{low} is attained, the heating ramp is carried out immediately after, at the same ramp rate, strain and frequency conditions from 1°C to 5°C. Figure 4.4a shows that the heating ramp doesn't re-trace the cooling ramp. This hysteresis between the two temperature ramps indicates that the gel is evolving differently in time during the cooling and heating ramp when the ramping rates are the same in the two cycles. The effect of the heating and cooling rate on the determination of the gel point was examined by Guo et al. (2011) [59] for the same octadecyl silica - decalin system. They claimed that heating rates between 0.05 – 1 K/min don't show a significant difference in the determination of the gel point, whereas changing cooling rates within the same range yield very different gel points. This indicates that the loosening/melting

of the gel structure upon heating from an initially arrested state is fast and, thus, not sensitive to the rate at which the temperature, or inter-particle strength of attraction is changed. Formation of a gelled network by increasing the strength of attraction (cooling) however, is a slower process and thus the evolution of the moduli is different with different cooling rates.

Another approach used to determine the gel point, utilizes the idea that the gelation transition should occur at the same temperature over a range of probing frequencies [60]. Thus, the frequency of oscillation during the heating ramp conducted in our experiments may affect the gel point slightly. However, Guo et al. [53] found that gel temperature measurements carried out for the same octadecyl silica - decalin system yield similar values of gel temperatures which show similar trends with increasing particle concentration using both the approaches of determining the gel point.

Figure 4.5 shows how the gel temperature varies with particle size and volume fraction. We see that for a given particle size T_{gel} increases as a weak power law function of volume fraction, ϕ_G for the range of volume fractions between 0.2 and 0.4. As can be seen from Figure 4.5, as the volume fraction decreases, a lower temperature or higher strength of attraction is needed for gelation to occur. This is because particle crowding contributes significantly to hindered particle motion and dynamic arrest and since the particles are closer together at higher volume fractions, a lower strength of attraction is sufficient to form a space spanning network thereby inducing gelation. However, we also see that the gel temperatures don't change systematically with particle size for a given volume fraction. The 30 nm particles have the highest T_{gel} followed by the 185 nm particles and finally the 82 nm particles. It is not clear what gives rise to this non-monotonic trend

in T_{gel}. We hypothesize that this may be due to a difference in surface density of octadecanol between different particle sizes. Although we added octadecanol in excess during synthesis and care was taken while handling the particles during the purification process, there is a chance that octadecyl chains may have cleaved from the surface of the silica particles resulting in a difference in the surface coating between different particle size dispersions.

The dashed lines in Figure 4.5a are curve fits of the experimental data using equation 2.13 developed by Rueb and Zukoski [40] as discussed in Section 2.1.4 while the solid symbols are the experimentally determined gel temperatures at different volume fractions. These equations are used to fit T vs ϕ at the gel point so that ϕ_G can be determined at a given temperature. These will be used to test the scaling functions $(\phi - \phi_G)$ and $(\phi/\phi_G - 1)$ suggested by the percolation theories. As can be seen, equation 2.13 shows reasonable agreement in determining the gel boundary for the different particle sizes. The predicted values of the gel points lie well within the experimental error limits (± 0.3°C). Similar results were observed by Rueb and Zukoski [40] in determining the gel boundary for the same experimental system.

Using the experimental data in Figure 4.5, we can back out the parameters determining the strength of attraction, A and T_θ as outlined by Ramakrishnan and Zukoski [27]. For the same system of octadecyl particles in silica, the work carried out by Ramakrishnan and Zukoski, Gopalakrishnan and Zukoski [37] and Breuer and Ramakrishnan [61] showed that particles interacting with a range parameter, $\kappa D = 11$ was able to predict the gel boundary, elastic moduli and yield stresses for different sized particles. Using the exponential fit suggested in equation 2.20, we can obtain the product of AT_θ from the slope of the exponential fit obtained by plotting $\frac{G'D^3}{kT}$ as a

function of $\left(\frac{1}{T} - \frac{1}{T_{gel}}\right)$ (Figure 4.21, details given in a later section). By assuming κD = 11 we obtain the χ parameter by averaging the data obtained by Ramakrishnan and Zukoski (Table 1) [27] over all volume fractions under consideration. Upon the knowledge of AT_θ, individual values of A and T_θ were determined by matching the experimentally determined gel point (Figure 4.5b) to the theoretically predicted gel point (Figure 2.1) at one volume fraction (here, at $\phi = 0.3$) using equation 2.19. The values of A and T_θ for the different particle sizes extracted from $AT_\theta = 9147.72$ are listed in Table 4.1. Once the interaction potential parameters A and T_θ are determined, we can predict the gel boundary at other volume fractions using the data for κD = 11 given in Figure 2.1 using equation 2.19. The predicted gel boundaries are depicted as solid lines in Figure 4.5b. As can be seen from the plot there is excellent agreement between theory and experiment at other volume fractions as well.

Table 4.1: Interaction potential parameters for different particle sizes at κD = 11

Parameter	**30 nm**	**82 nm**	**185 nm**
A	28.85	29.93	29.39
T_θ	317.02	305.64	311.22

4.2.2 Growth of Elastic Modulus with Time

Once the sample is quenched to the desired temperature below the gel point, it is first pre-sheared at very high strains in order to ensure consistency between the thermal and shear history of different samples [40]. One may expect that pre-shearing would break up any clusters that may have formed during the sharp temperature quench from room temperature to T_{low} as a result due to

shear thinning. On the contrary, Brownian simulations of sheared aggregating suspensions by Melrose and Heyes [62] suggest the formation of dense regions, many particle diameters in size during shear thinning; simulations by Chen and Doi [63] suggest that the structure doesn't change during shear thinning and Lin et al. [64] and Muzny et al. [65] report shear densification in fractal gold sols and dilute silica gels respectively. However, Ramakrishnan and co – workers [7] demonstrated that for octadecyl silica in decalin, at low temperatures, shear produces clusters, however they break up once the shear is stopped. Immediately after the temperature quench, the sample is probed through oscillatory measurements carried out at a frequency of 1 Hz and very low stresses. Figure 4.6 shows a sample plot of how the structure evolves in time after pre-shear. Three distinct phases of structure evolution are observed – the lag phase, indicated by a very low/unmeasurable G' and G'', often with G' ≤ G'' indicating liquid-like behavior; the exponential growth phase where both G' and G'' show a steep exponential increase and intersect such that G' becomes greater than G''. This phase is characterized by cluster-formation and growth to form a percolated structure that can support its own weight. This is indication of a cross-over to a solid-like regime. Clustering may occur through the lag phase as well, however since we don't see a measurable elasticity, we can assume that the clusters may not have percolated through the sample volume. Finally, the structure evolves to a point where the modulus changes either very slowly or just fluctuates about a constant mean value indicated by G' (∞). The slow increase of modulus is called ageing of the gel. Appendix C contains plots for G' as a function of time for all particle sizes, volume fractions and temperatures. Equation 4.1 has been used in literature [59] [40] to describe the evolution of the gel in time.

$$G'(t) = G'(\infty)\left[1 - \exp\left(-\Gamma_g\left(t - t_g\right)\right)\right] \qquad 4.1$$

Here G' (∞) is the plateau elastic modulus at long times, Γ_g is the exponential growth rate of the elastic modulus, t is the waiting time after pre-shear and t_g is the lag time through which the modulus is unmeasurable. Figure 4.6 is a sample plot of the growth of the elastic modulus with time for a sample containing 40 % by volume 82 nm silica particles in decalin at different temperatures. The dashed lines represent curve fits of the experimental data using Equation 4.1. As can be seen, equation 4.1 doesn't fit the experimental data at early times for our system, however does a very good job fitting the data at long times. Hence, in this work, in order to back out initial rates of growth of the elastic modulus, data at short times was taken where the modulus grows linearly with time and a linear curve fit was used to back out the initial growth rate according to the following simplification:

$$\lim_{t\to 0} \exp\left(-\Gamma_g\left(t_w - t_g\right)\right) \sim 1 - \Gamma_g(t - t_g)$$

$$G'(t) = G'(\infty)\left[1 - \Gamma_g(t - t_g)\right] \qquad 4.2$$

In Figure 4.7, we plot ($\Gamma_g t_D$) vs volume fraction and temperature for 185 nm octadecyl silica particles in decalin. Here t_D is the single particle diffusive time scale given as $t_D = (6\pi\eta_c a^3)/kT$ as described in Section 2.1.2. As can be seen, the absolute values of $\Gamma_g t_D$ decreases as temperature is increased from 4°C to 9°C. A similar trend can be seen in the results obtained by Rueb and Zukoski [40]. As can be seen, at the same temperature, as the volume fraction increases, the normalized rate of growth of G' increases. We also find that at high temperatures, the growth rate increases more rapidly with increasing ϕ. These results are in line with those obtained by Potanin et al. [49] who obtain power law exponents ranging between 6.7 and 9.2 as a function of ϕ for a system of sterically stabilized polystyrene latex particles, decreasing as one moves away from the gel point. Rueb and Zukoski [40] obtain power law exponents between 2 and 3 on plotting normalized growth rate as a function of ϕ for octadecyl silica in decalin such that the exponent decreases as

one moves deeper into the gel. Although we see the same qualitative trends, qualitatively, we don't have enough data points to fit the experimental data to obtain good power law fits.

Figure 4.8 shows how $\Gamma_g t_D$ changes as a function of quench temperature for different volume fractions for 185 nm particles. As can be seen, the growth rate of G' decreases as temperature is increased. At weaker strengths of attraction, thus, it takes longer to form a gel. This is seen for all particle sizes and the relevant plots are given in Appendix F. When the strength of attraction is low, we can anticipate the potential energy well to be shallow. Thus, a larger fraction of particles could acquire energy from local temperature and mechanical fluctuations and diffuse out of their nearest neighbor cages. It would take much longer for the system to become dynamically arrested in this case as opposed to the case where the temperature is low and particles become localized in steep energy minima such that diffusion out of nearest neighbor cages is considerably restricted.

4.2.3 Elastic Modulus as a Function of Temperature

Figure 4.9 is a plot of G' (∞), the plateau elastic modulus as a function of temperature for 82 nm particles at different volume fractions. The solid symbols are experimental data points while the dashed lines are curve fits to the data. As can be seen from the figure, the plateau elastic modulus scales exponentially with time $G'(\infty) \approx \exp(-zT)$ with an exponent z ~ 1 ± 0.05. This is in agreement with previous experiments on a similar particle system as studied by Ramakrishnan and Zukoski [27] and Rueb and Zukoski [40]. At high temperatures, strength of attraction between the particles is low and thus, the resultant gel network is weak, as indicated by a lower elastic modulus. At a fixed particle concentration, this exponential dependence on strength of attraction is predicted

by the activated barrier hopping theory as seen from equation 2.18. We see a significant, yet non - systematic spread in the exponent for different particle sizes - 0.65 – 1.3 for 30 nm particles and z ~ 0.8 – 1.21 for 185 nm particles. Plots for the different particle sizes are given in Appendix F.

4.2.4 Elastic Modulus as a Function of Volume Fraction

G' (∞) is plotted against volume fraction ϕ at different temperatures in Figure 4.10a for samples containing 82 nm particles. Solid symbols indicate experimental data points and the dashed lines represent power law fits $G'(\infty) \approx \phi^{y}$ to data. The modulus has a power law dependence on volume fraction with exponents y ~ 6.6 close to the gel temperature and y ~ 3.8 deeper into the gel. For 30 nm particles, y ~ 4.6 and 5.7 between 11°C and 13°C and for 185 nm particles, y ~ 5.2 at 5°C and y ~ 7 at 9°C. This result is in agreement with literature where higher exponents are observed close to the gel boundary while as one gets deeper in the gel phase, the exponents become lower (Potanin et al. (1995) [48], Rueb and Zukoski (1996) [40] , Ramakrishnan and Zukoski (2005) [27], Shih et al. (1990) [32]; Chen and Russel (1993) [66]; Derooij et al. (1994) [47]). In the case of gels formed by addition of a non-adsorbing polymer to a hard sphere system, Ramakrishnan and co-workers [7] [39] measured exponents of 9 closer to the gel boundary and the exponents decreased to 5 deeper inside the gel phase while for thermo - reversible gels at deep quenches, T_{gel}–T ~ 1–8K, y ~ 5 at all temperatures. In Figure 4.10b, we see that exponent y systematically increases as a weak exponential function of temperature for each particle size with exponents varying between 0.08 – 0.1 for the three particle sizes. The final elasticity of the network depends upon its microstructure which in turn is a result of an interplay between the strength of attraction and the crowding of the nanoparticles in the system. At a given strength of interaction, both activated barrier hopping and percolation theories predict a power law dependence of elastic

moduli on volume fraction. Our results suggest that at weaker strengths of attraction, rapid increase of moduli is seen as one increases the volume fraction of particles as opposed to conditions in which attractions are strong. This complex interplay of strength of attraction and crowding determines how the modulus changes with volume fraction. From a NMCT point of view both of these factors influence the localization length and how this localization length changes with both ϕ and T determines how the modulus changes. Plots for other particle sizes are given in Appendix F.

4.2.5 Prediction of Elastic Moduli

Using the interaction potential parameters given in Table 4.1, one can predict the plateau elastic modulus of the gel at different temperatures, concentrations and for different particle sizes using equation 2.20 based on the framework developed by Ramakrishnan and Zukoski [27]. In our analysis, we use $\kappa D = 11$ and the parameter $\chi(\kappa D, \phi) = 3.77$ (averaged for $\kappa D = 11$ for all volume fractions under consideration using Table 1 given in Ref 2 [27]) to theoretically predict G' and compare it to the experimentally obtained G'. Figure 4.11 (in color) is a plot of normalized elastic modulus, $\frac{G'D^3}{kT}$ as a function of temperature showing experimental data (solid symbols) and theoretical predictions (solid lines). We find excellent agreement between the results predicted by the barrier hopping theory and the experimental data at deep quenches below the gel point. We observe however, that the agreement becomes poor as we approach the gel boundary (at high temperatures, close to the gel boundary). This may be due to the fact that even after waiting for nearly 4 hours for the modulus to develop and show a plateau, the gels may age to achieve higher moduli. Aging is seen for the same experimental system in the work carried out by Guo et al. [53].

Such agreement between theory and experiment is also observed by Ramakrishnan and Zukoski [27] for the same experimental system. Plots for other particle sizes are given in Appendix F.

4.2.6 Elastic Modulus as a Function of Frequency

Once a gel is formed at a certain temperature, indicated by a plateau in G' in time, a frequency sweep is performed to study the dependence of G' and G'' on oscillation frequency. Figure 4.12 shows how G' and G'' vary with oscillation frequency for a sample containing 20% by volume 82 nm octadecyl silica particles in decalin at different temperatures. As expected for a gelled system, there is a weak dependence of G' and G'' on frequency. The symbols denote experimental data points and the dashed lines represent power law fits to the data. Power law exponents close to 0.15 are observed at temperatures close to the gel boundary and 0.09 deeper inside the gel phase. We do not observe a minima in G' or G'', nor a crossover between the two in the experimentally measured frequency window suggesting the existence of a solid like network. These trends are observed for all particle sizes. Plots for the data obtained for different volume fractions and particle size particles are given in Appendix D.

4.2.7 Yield Stress as a Function of Temperature and Volume Fraction

After the frequency sweeps, amplitude sweeps were carried out in order to study the yielding behavior of the gels. Stress amplitude, τ, was increased logarithmically and elastic and loss moduli were measured as a function of τ. Figure 4.13 shows a sample plot of an amplitude sweep for 82 nm particles in decalin loaded at a 20% volume fraction. As can be seen, G' and G'' are characterized by a plateau in moduli at low stresses. This plateau region is called the Linear Viscoelastic (LVE) regime. The LVE regime gives us information about the maximum stress/strain

a structure can endure before it yields. At a certain critical stress, the structure loses its elasticity, in that, the structure prior to the oscillatory perturbation and after are drastically different. Since the structure can no longer recover to its original modulus, it suggests that some permanent deformation has taken place. On applying more stress, the structure further loosens and eventually fluidizes. This is characterized by high strains, a sharp drop in both G' and G'' until they cross over, after which G'' becomes equal to or greater than G' indicating liquid like behavior. It must be noted that determining the yield stress experimentally can be tricky as it may be influenced by the rate of the stress ramp. Although, care was taken in carrying out amplitude sweeps in a logarithmic fashion, such that the majority of data points are taken at low stresses, the errors in determining absolute yield stresses that match the theoretical framework may be significant. Plots for different particle sizes are given in Appendix E.

Three different definitions of the yield point from literature are examined in this work. These include – (i) When G' reaches 90% of its LVE limit [37], (ii) when G' reached 95% of its LVE limit [40] and (iii) when G' and G'' intersect [67]. The extracted yield stresses from the three different approaches though different in magnitude show very similar qualitative dependence on temperature and volume fraction. For the sake of discussion in this chapter, we restrict ourselves to definition number (i).

Figure 4.14 shows how yield stress varies with temperature at different volume fractions for the system containing 82 nm particles. We see a systematic increase in yield stress as temperature is decreased at a fixed volume fraction. In this plot, the symbols represent the experimental data points and the dashed lines represent exponential fits to $\tau_y \sim \exp(-cT)$. Here,

the exponent c changes non-systematically between 0.50 and 0.83 for all three particle sizes. Figure 4.15a is a plot of yield stress vs volume fraction for a system of 82 nm particles plotted at different temperatures. The lines represent power law fits of experimental data to $\tau_y \sim \phi^d$. The power law exponent varies between 4.5 at 2°C and 8.8 at 5°C. For 30 nm particles, d varies between 3.7 at 11°C and 6.4 at 13°C, and between 5.8 at 5°C and 8.0 at 9°C for 185 nm particles. Plots for different particle sizes are given in Appendix F. The trends observed for yield stress as a function of volume fraction and temperature track those observed for elastic moduli for these samples. A stronger microstructure, indicated by a higher G' (∞), also has a higher yield stress. At a constant volume fraction, as the strength of attraction is increased, the potential energy minima becomes more negative and the slope of the free energy function becomes steeper. Thus, higher stresses would be required to separate particles/aggregates. At a constant strength of attraction, as the particle loading is increased, we see an increase in G' due to an increased contribution of crowding in the system. As with G', we see a systematic power law increase in yield stress as a function of volume fraction. Figure 4.15b shows how the exponent d changes as a function of temperature for the three particle sizes. We see a power law dependence of d on temperature with the exponent varying non-systematically between 0.08 and 0.28 for the different particle sizes.

4.2.8 Predicting Yield Stresses

Following the protocol developed by Gopalakrishnan and Zukoski [37], we attempt to theoretically determine yield stress using the framework of the activated barrier hopping theory as discussed in Section 2.2.4. The interaction potential parameters A and T_θ listed in Table 4.1 and $\kappa D = 11$ are used to numerically calculate the free energy function (in units of kT) at different input stresses (in units of kT/D^3) described using Equation 2.22 for the three particle sizes at a

given particle concentration and temperature. Next, the derivative of the free energy function in 'r' is numerically calculated to determine the localization length as the point where $\frac{dF}{dr}$ first attains a value of 0 (at the energy minima). The elastic modulus can be calculated using the localization length using the relation given in equation 2.18. According to definition (i) of yield stress, we calculate the stress at which G' ~ 0.9 G' (∞). Figure 4.16 (in – color) is a plot of experimentally determined and theoretically calculated yield stress, τ_y (in units of kT/D^3) as a function of temperature for the three particle sizes at volume fractions 0.2 and 0.35. Solid symbols denote experimental data points and solid lines are theoretical predictions of the yield stress. We see reasonable agreement between theory and experiment for the data corresponding to the all particle sizes. We find that for the majority of the data, the theory underestimates the yield stresses. This may be due to the fact that while carrying out the amplitude sweep, we are increasing the stress in steps which logarithmically increase in step size. The stress predicted by the barrier hopping theory may lie between two data points and may not be captured well experimentally. Additionally, the barrier hopping theory assumes that prior to the reduction of the bulk modulus to 90% of its original value, the system is in the linear viscoelastic regime – i.e.: no deformation has taken place. In reality, however, the system has deformed appreciably well before the modulus is reduced to 0.9G'∞. Through the sweep, thus, we are applying a high stress on an already deformed system. This may also lead to discrepancies between theoretical predictions and experimental observations which we observe in our results.

4.3 Scaling Relationships

Figure 4.17 is a plot of G' (∞) as a function of temperature for different particle sizes and volume fractions. As can be seen from the plot, there is considerable scatter in the data with G'

ranging from 10 to 10^5 Pa. Our aim in this section is to check if scaling relationships exist that can collapse the initial growth rates, elastic moduli and yield stresses on-to master curves in order to better understand their dependencies on the strength of interaction and particle loading.

4.3.1 Scaling Initial Growth Rates

Figure 4.18a, b and c shows how $\Gamma_g t_D$ scales as a function of $(\phi - \phi_G)$, $\left(\frac{\phi}{\phi_G} - 1\right)$ and $\frac{T_{gel} - T}{T_{gel}}$. These three functions are measures of proximity of the system to the gel boundary and may be related to the probability of rigid bond formation as discussed in Section 1.2.4. These functions have been used to scale experimental data at different temperatures and volume fractions on to universal scaling curves. In all three plots, symbols represent experimental data and lines represent power law fits for the different particle sizes. As can be seen, $\Gamma_g t_D$ increases roughly by two orders of magnitude as the particle size is increased from 30 nm to 185 nm. This is due to the strong dependence of t_D on particle size. Although our data don't scale on a single master curve for different particle sizes, we attempt to scale data for a single particle size at different volume fractions and temperatures onto master curves. We see substantial scatter in the data in all three plots for all particle sizes. We note that as temperatures and concentrations close to the gel boundary, the power law fits similar to those carried out by Rueb and Zukoski [40] don't scale the data well. Finally, we observe marginally better power law fits in Figure 4.18c as a function of reduced temperature. We conclude that normalization of the rate with diffusion time greatly enhances the size dependence of the normalized function $\Gamma_g t_D$ and may not be an appropriate choice of scaling variable.

In an attempt to scale the initial growth rate data for all particle sizes onto a single master plot, we determine α, the initial rate at which non-dimensionalized elastic modulus, $G'D^3/kT$ grows in time using a similar linear fit as used to determine Γ_g. As can be seen in Figure 4.18d, we find that α for all particle sizes, concentrations and temperatures collapses onto a universal exponential scaling curve. Equation 2.18 shows that $G'D^3/kT$ is essentially a measure of the normalized localization length $\frac{\phi D^2}{r_{loc}^2}$ and thus the rate, α (1/s) represents the rate at which the normalized localization length changes for a system at early times. The universal scaling as a function of $\frac{T_{gel}-T}{T_{gel}}$ then tells us that the rate of change of localization length for a system only depends upon the proximity to the gel boundary. It must be noted that scaling these data as a function of $(\phi - \phi_G)$ and $\left(\frac{\phi}{\phi_G} - 1\right)$ as suggested by percolation models resulted in a lot of scatter. The significant improvement in scaling as a function of $\frac{T_{gel}-T}{T_{gel}}$ suggests that it is better able to capture the interplay of concentration and strength of attraction as compared to $(\phi - \phi_G)$ and $\left(\frac{\phi}{\phi_G} - 1\right)$ [68].

4.3.2 Scaling Elastic Moduli

We first examine how G' scales as a function of $(\phi - \phi_G)$ and $\left(\frac{\phi}{\phi_G} - 1\right)$ as suggested by percolation models in Figure 4.19a and b for 82 nm particles. As can be seen from the figure, $(\phi - \phi_G)$ does a much better job at scaling the data for all different temperatures onto a single master curve with power law exponents varying systematically between 1.80 and 1.92, increasing as particle size decreases. In comparison, the fits in Figure 4.19b as a function of $\left(\frac{\phi}{\phi_G} - 1\right)$ are much poorer and the power law exponents vary non – systematically between 1.23 and 1.88. For

a similar system, octadecyl silica in hexadecane, Grant and Russel [35] found G' to scale as a power law function of $(\phi - \phi_G)$ at a range of volume fractions, up to 0.3 and obtained a power law exponent of ~ 3. For the same system as ours, Rueb and Zukoski [40] found the data to scale better as a function of $\left(\frac{\phi}{\phi_G} - 1\right)$with a power law exponent of ~ 2.

In order to scale the data onto a universal scaling curve, we must account for the particle size dependence on G' since we use a very large range of particle sizes, from 18 nm to 185 nm. We utilize $G'D^3/kT$ (also predicted by the barrier hopping theory, equation 2.17) to scale the data. Figures 4.18a and b show how $G'D^3/kT$ scales as a function of non – dimensionalized volume fraction, $(\phi - \phi_G)$ and $\left(\frac{\phi}{\phi_G} - 1\right)$. We find that data collected at different temperatures collapses well for each individual particle size, however, while the data for the 30 nm and 82 nm particles lies in the same vicinity, data for 185 nm particles has much higher overall values of $G'D^3/kT$. Power law fits to data yield exponents between 1.84 – 1.93 when plotted as a function of $(\phi - \phi_G)$ and exponents between 1.37 and 1.79 when plotted as a function of $\left(\frac{\phi}{\phi_G} - 1\right)$.

Next, we examine the scaling relations suggested by equation 2.20 derived from the activated barrier hopping theory approach [27] as explained in Section 2.2. In Figure 4.21 we plot $\frac{G'D^3}{kT}$ as a function of $\left(\frac{1}{T} - \frac{1}{T_{gel}}\right)$. We find that the data collapses reasonably when fit using an exponential function as suggested by equation 2.20. In Figure 4.22 we have plotted the experimental data obtained by Ramakrishnan and Zukoski [27] as well as Breuer and Ramakrishnan[61] for the same system, within the same range of volume fractions however, using particles of

different sizes along with the data we obtained. We have also plotted equation 2.20 which predicts how the modulus should scale with re-scaled temperature at $\kappa D = 11$ (lower limit for the validity of empirical fitting relation given in equation 2.4), $\chi = 3.77$ and $AT_\theta = 9147.72$. Symbols represent experimental data points and lines indicate exponential fits to the data. We find that our data points correlate very well with the experimental data found for other independent studies carried out for the same particle system as well as the with the barrier hopping model.

An exponential fit to our experimental data shown in Figure 4.20 however yield a lower intercept of 8.55, nearly 2 - 3 times less than that predicted by the barrier hopping model and a slope of 83650, roughly 2 - 3 times higher than that predicted by the model as shown in Figure 4.22. This discrepancy may be attributed to the range of temperatures studied in this work. In our study, we have carried out measurements of the elastic moduli at fairly shallow temperature quenches, $T_{gel} - T \sim 3 - 4°C$ in comparison with the studies carried out by Ramakrishnan and Zukoski Breuer and Ramakrishnan in which $T_{gel} - T \sim 6 - 7°C$. We expect the data to scale along the activated barrier hopping model curve at deeper quenches.

The change in scaling at lower quenches, however, is interesting to note. A reduction in elastic modulus from that predicted by the activated barrier hopping theory may be indicative of a change in the mechanism of aggregation. For depletion gels, Ramakrishnan and Zukoski [7] observed that the experimentally measured elastic modulus is significantly lower than that predicted for depletion systems by the barrier hopping theory. Using ultra - small angle x – ray scattering techniques, they found evidence of cluster formation in the system and re-scaled the modulus with the number of particles, N_c, in a cluster such that $G' = G'_{MCT}/N_c$

where $N_c \sim 8\phi_c \left(\frac{\xi}{D}\right)^3$. Here, ϕ_c is the particle volume fraction in a single cluster (ϕ_c = 0.5 for dense clusters) and ξ is the characteristic size of the cluster. We used SAXS measurements to measure the structure factor for the 82 nm particles at a volume fraction of 0.2 at a range of temperatures both above and below the gel transition temperature as shown in Figure 4.23. At low temperatures (T_{gel} – T ~ 2°C), we see up-turns in the structure factor at low qD values which are indicative of cluster formation and a shift of the structure factor peak to very high qD values ~ 7 which indicates that the particles are extremely closely packed in the gelled system. Although these observations are indicative of the existence of densely packed clusters in the system, we don't have any quantitative proof to suggest that particles are clustering at shallow quenches.

4.3.3 Scaling Yield Stresses

In Section 2.2.4, we established that yield stress normalized with characteristic stress, (kT/D^3), should theoretically scale as a power law function of volume fraction, $\phi^{\frac{2}{3}}$. We thus scale $\frac{\tau_y D^3}{\phi^{\frac{2}{3}} kT}$ as a function of rescaled temperature, $\left(\frac{1}{T} - \frac{1}{T_{gel}}\right)$ in Figure 4.24a. We find that although the data collapses onto a single exponential – like curve, there is significant scatter that corresponds to the 82 nm and 185 nm data. Plotting as a function of $\left(\phi - \phi_g\right)$ and $\left(\frac{\phi}{\phi_g} - 1\right)$ resulted in very poor power law fits and thus have not been shown. Figure 4.24b shows that normalizing the data with a volume fraction contribution of ϕ^2 suggested by equation 2.7 does a significantly better job at collapsing the data for the different particle sizes onto an exponential master curve. When the volume fraction dependence of the interaction potential is ignored, the function $\frac{\tau_y D^3}{\phi^2 kT}$ represents the slope of the free energy function as shown in equation 2.7. When scaled as a function of

rescaled temperature (or reduced temperature), the excellent collapse of data indicates the similarity of the potential energy surface for all particle sizes (varying by a factor of 10) and volume fractions at the same distance away from the gel point. Evidently, as one moves deeper into the gel, the slope of the potential energy function would become steeper and thus more force would be required for the system to yield. This function, thus, does an excellent job at capturing the particle size and concentration dependence of yield stress.

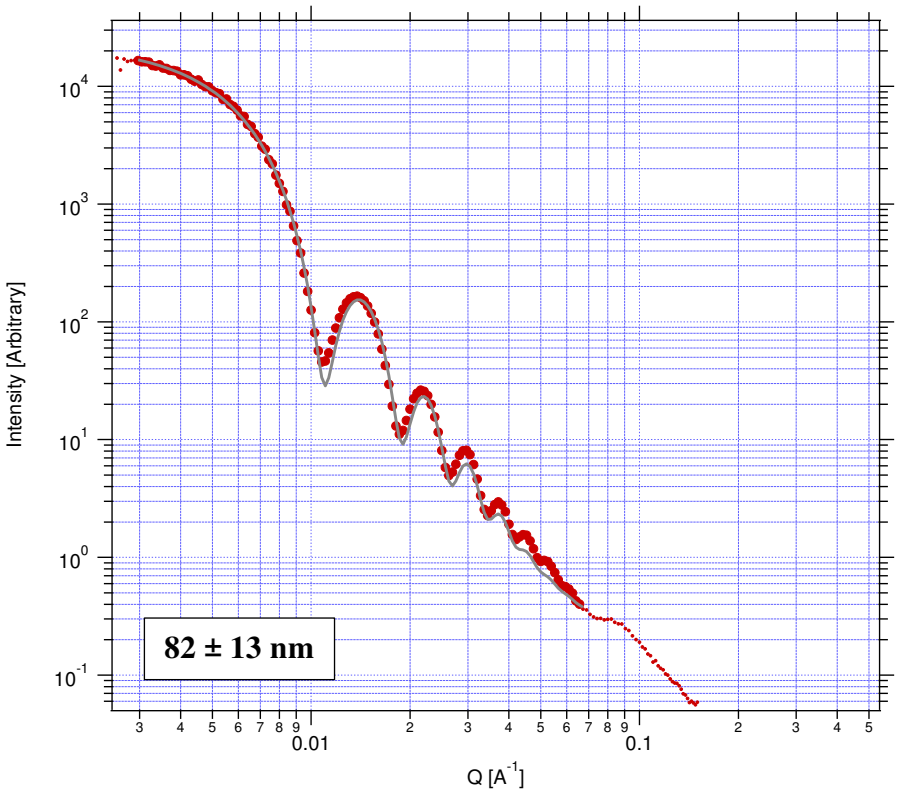

Figure 4.1 – Intensity (A.U.) vs. Wave Vector (Q) (Å^{-1}) form factor fit for 82nm octadecyl silica particle sample in Decalin (dilute - ϕ ~ 2%). Large red solid-filled circles represent the data points fitted to the Hard Sphere model, small red solid filled dots represent data points that were excluded from the fitting and the solid grey line represents the model fit.

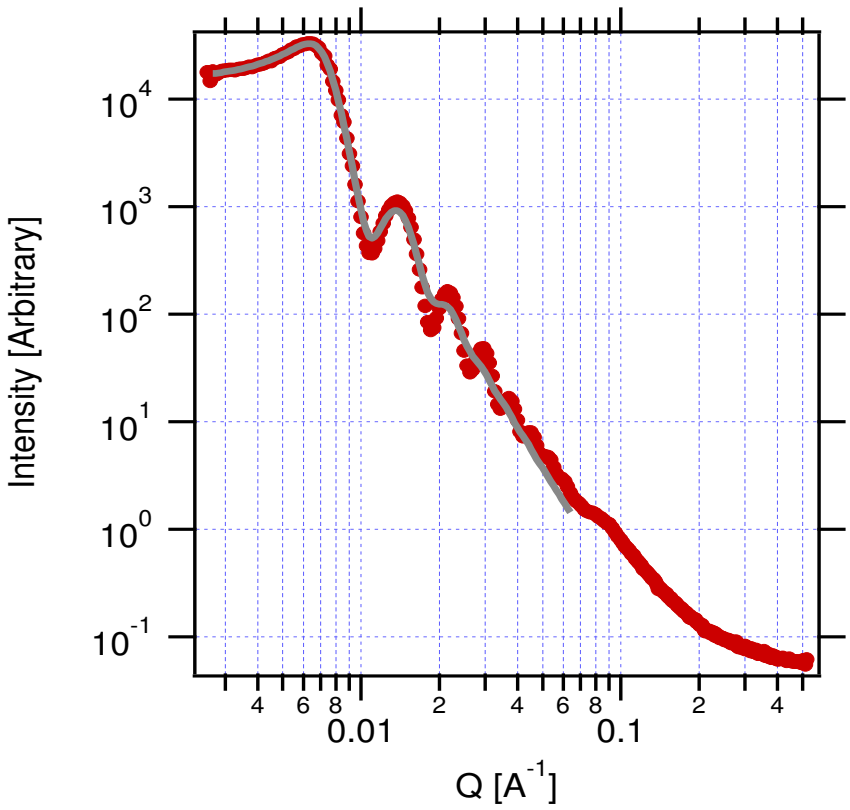

Figure 4.2 – Intensity (A.U.) vs. Wave Vector (Q) ($Å^{-1}$) form factor fit for 82 nm octadecyl silica particle sample in Decalin ($\phi = 0.3$). Red solid-filled circles represent the data points fitted to the Hard Sphere equation of state with a Percus – Yevick (PY) closure and the solid grey line represents the model fit.

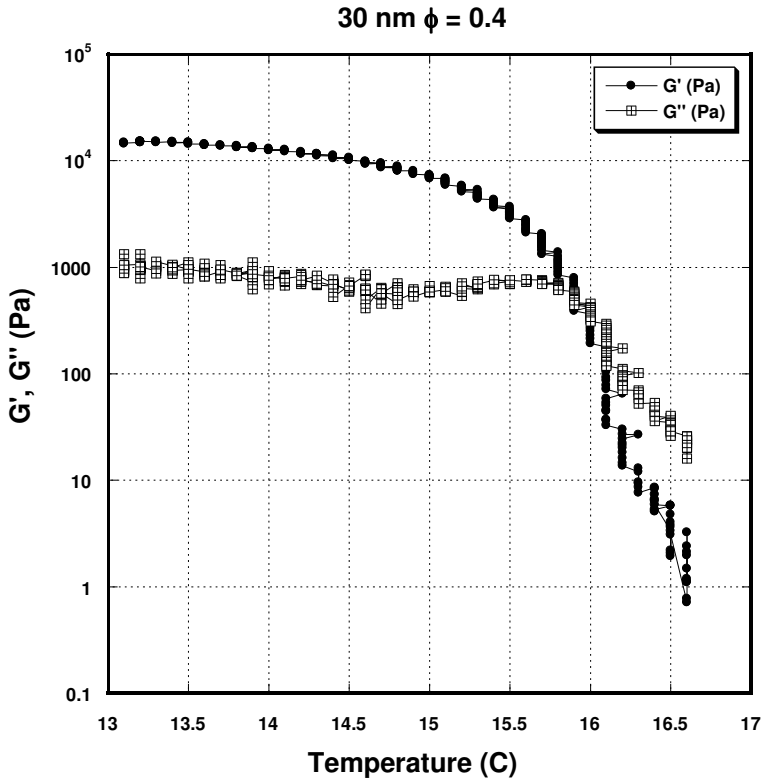

Figure 4.3 – Determination of the Gel Temperature for 30 nm octadecyl silica particles in decalin ($\phi = 0.4$). Symbols represent experimental data points and solid lines are drawn to guide the eye. On heating the sample from 13 C to 16.6 C, the temperature at which G' and G'' first intersect is regarded as the Gel Point.

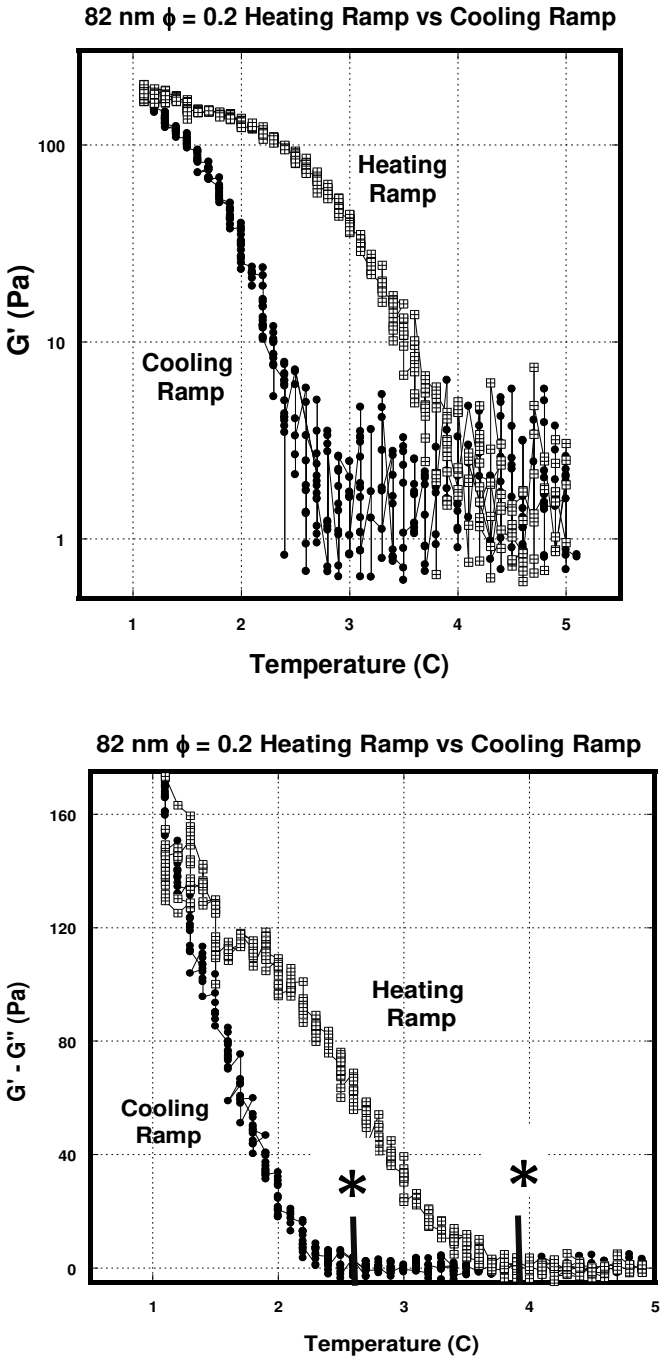

Figure 4.4 – Plot showing hysteresis between heating ramp and cooling ramp for 82 nm octadecyl silica particles in decalin. (a) Evolution of G' (Pa) during heating and cooling at 0.1 K/min (b) Difference between the G' and the G'' during heating and cooling. The gel point (T_{gel}) is defined as the point where G' – G'' first becomes zero (indicated by *). For the heating ramp, T_{gel} = 3.7°C and for the cooling ramp, T_{gel} = 2.4°C.

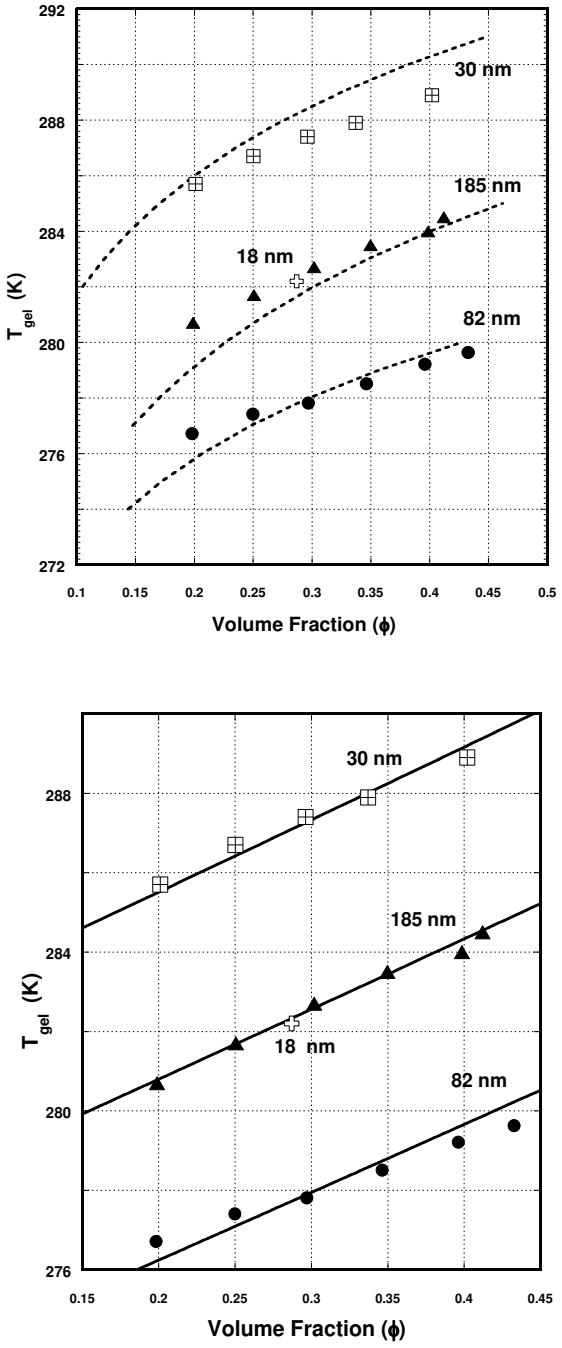

Figure 4.5 – Experimentally determined Gel Temperatures T_{gel} (K) as a function of Volume Fraction (ϕ) for different particle size. Solid filled points represent experimental data points, lines represent (a) fits to equation 2.13, (b) fits to equation 2.19 using interaction potential parameters listed in Table 4.1.

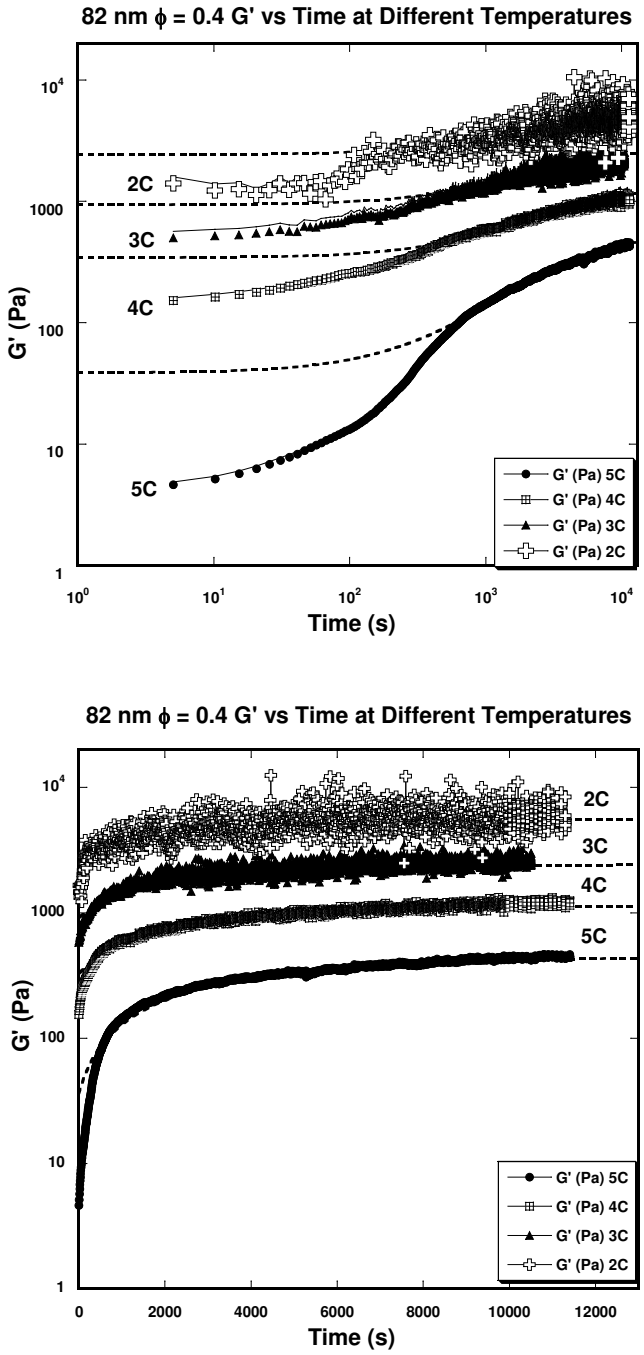

Figure 4.6 – Growth of G' and G'' with time for 82 nm particles ($\phi = 0.4$) symbols with solid line represents experimental data points, dashed line represents fits of experimental data to equation 1 (a) log-log plot showing poor curve fits at short times. (b) Log – linear plot shows curve fits of equation 1 are good at long times.

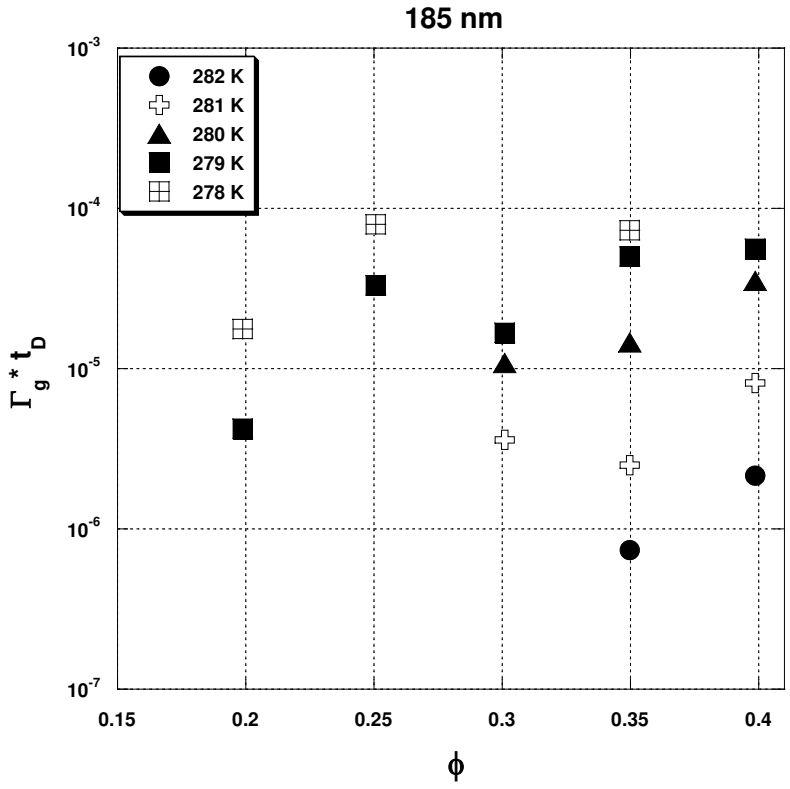

Figure 4.7 – $\Gamma_g\, t_D$ vs Volume Fraction at different temperature for 185 nm particles. Symbols indicate experimental data points.

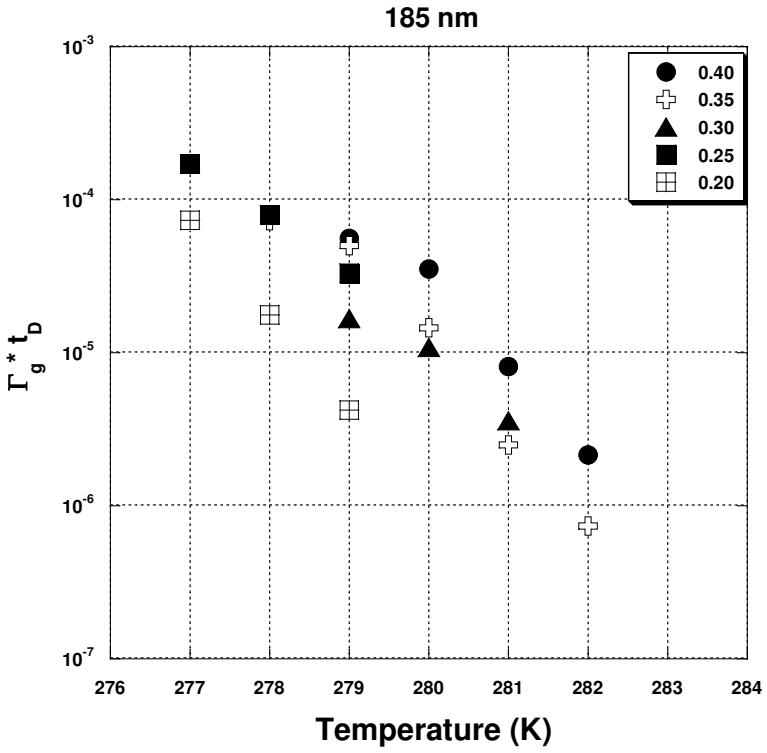

Figure 4.8 – $\Gamma_g t_D$ vs Temperature at different volume fractions for 185 nm particles. Symbols indicate experimental data points.

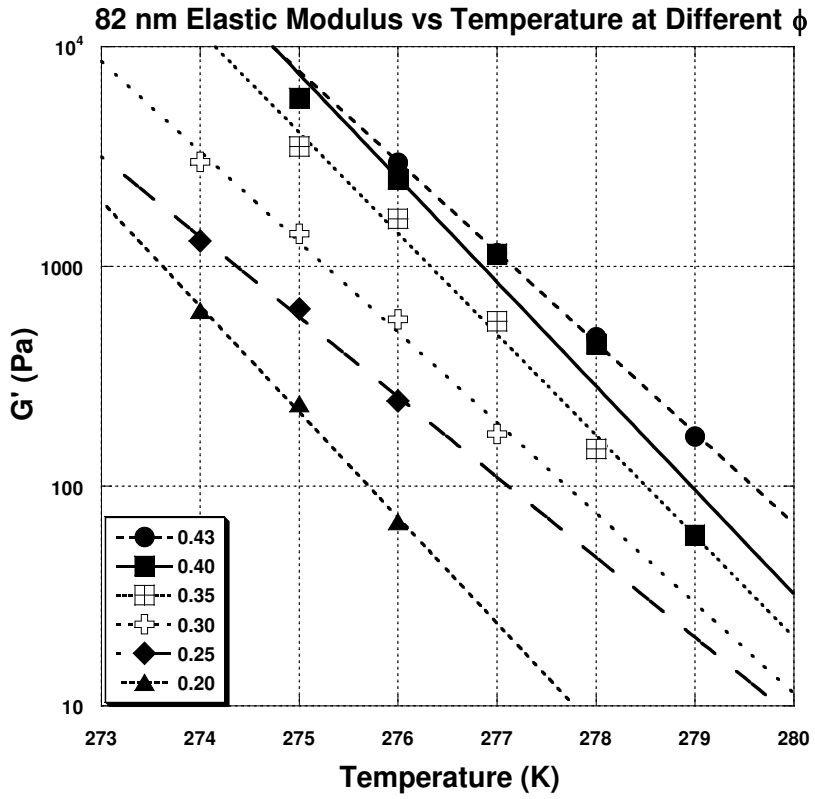

Figure 4.9 – Sample plot showing the regularity of G' (∞) with Temperature for 82 nm particles. Solid circular markers indicate experimental data and dashed lines represent exponential fits $G'(\infty) \approx \exp(-zT)$ such that z ~ 1 ± 0.05.

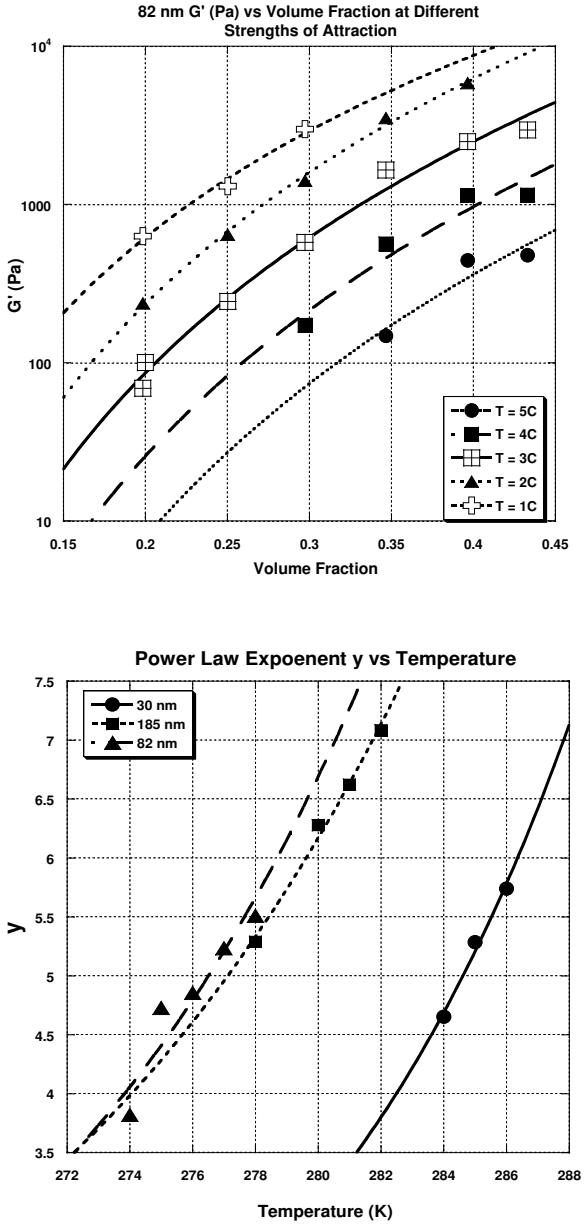

Figure 4.10 – (a) Sample plot showing the regularity of G' (∞) with Volume Fraction for 82 nm particles. Solid circular markers indicate experimental data and dashed lines represent power law fits to $G'(\infty) \approx \Phi^{-y}$ such that y ~ 3.8 at T = 274 K and y ~ 6.6 at T = 277 K. (b) Plot showing the exponential scaling of the power law exponents for all particle sizes - $y \sim \exp(mT)$. m = 0.1 for 30 nm particles, 0.08 for 82 nm particles and 0.07 for 185 nm particles.

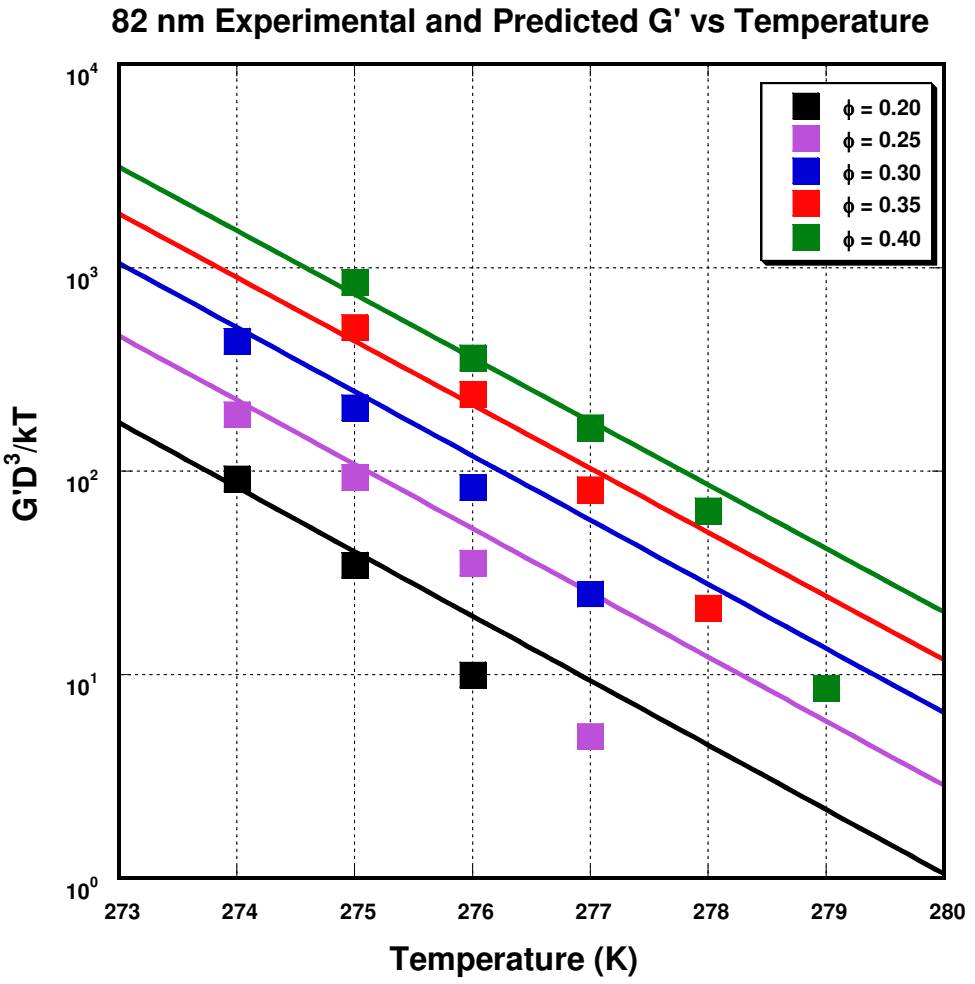

Figure 4.11 (color online) – Theoretically predicted and experimental $\frac{G'D^3}{kT}$ as a function of temperature for 82 nm particles for volume fractions between 0.2 and 0.4. Symbols represent experimental data points and lines represent theoretical predictions using equation 2.20.

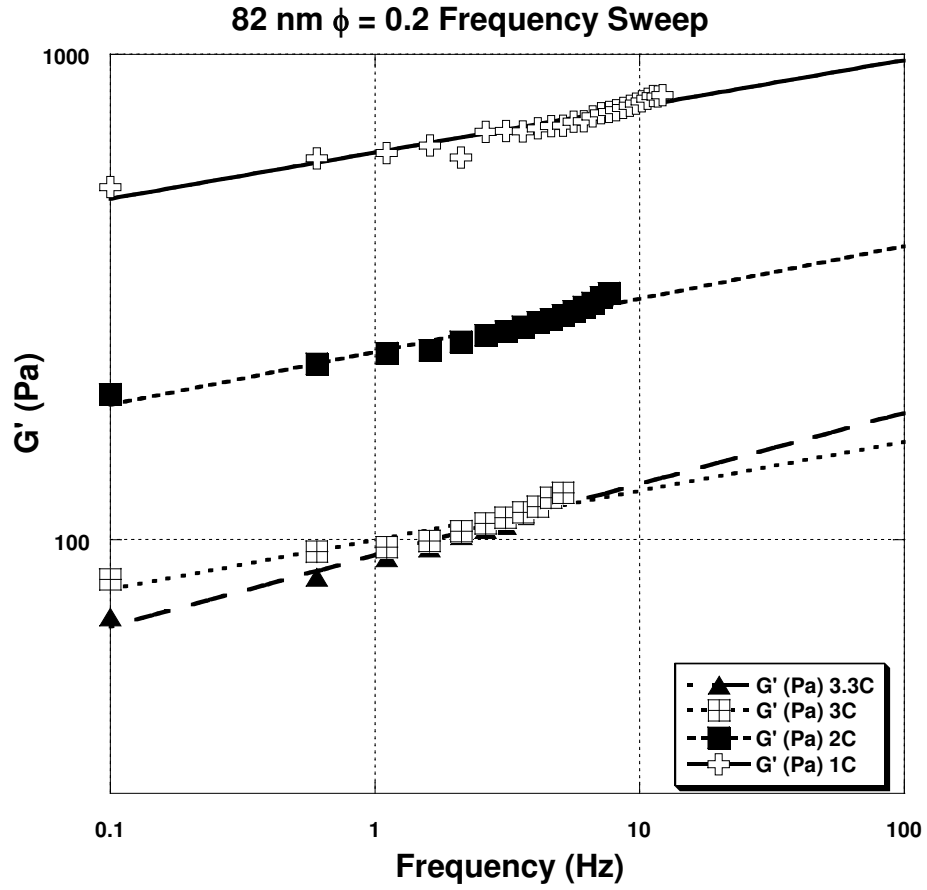

Figure 4.12 – Frequency Sweep Plots for 82 nm particles, $\phi = 0.2$ at different temperatures. Symbols represent experimentally determined data points and the solid, dashed and dotted lines represent power law fits to experimental data. Power law exponent systematically increases from 0.9 to 1.5 as temperature is decreased.

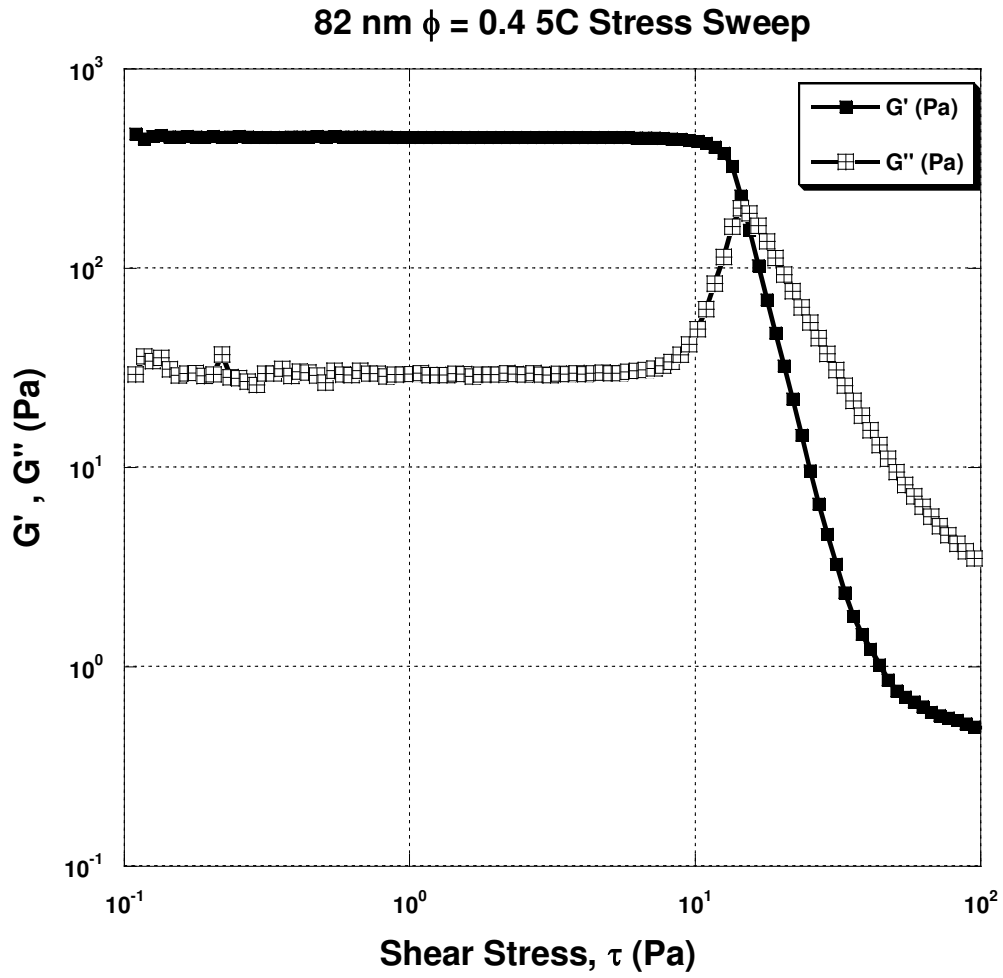

Figure 4.13 – Representative plot for an amplitude sweep for 82 nm particles, $\phi = 0.4$ at 5°C. Symbols represent experimental data points while the lines are drawn to guide the eye.

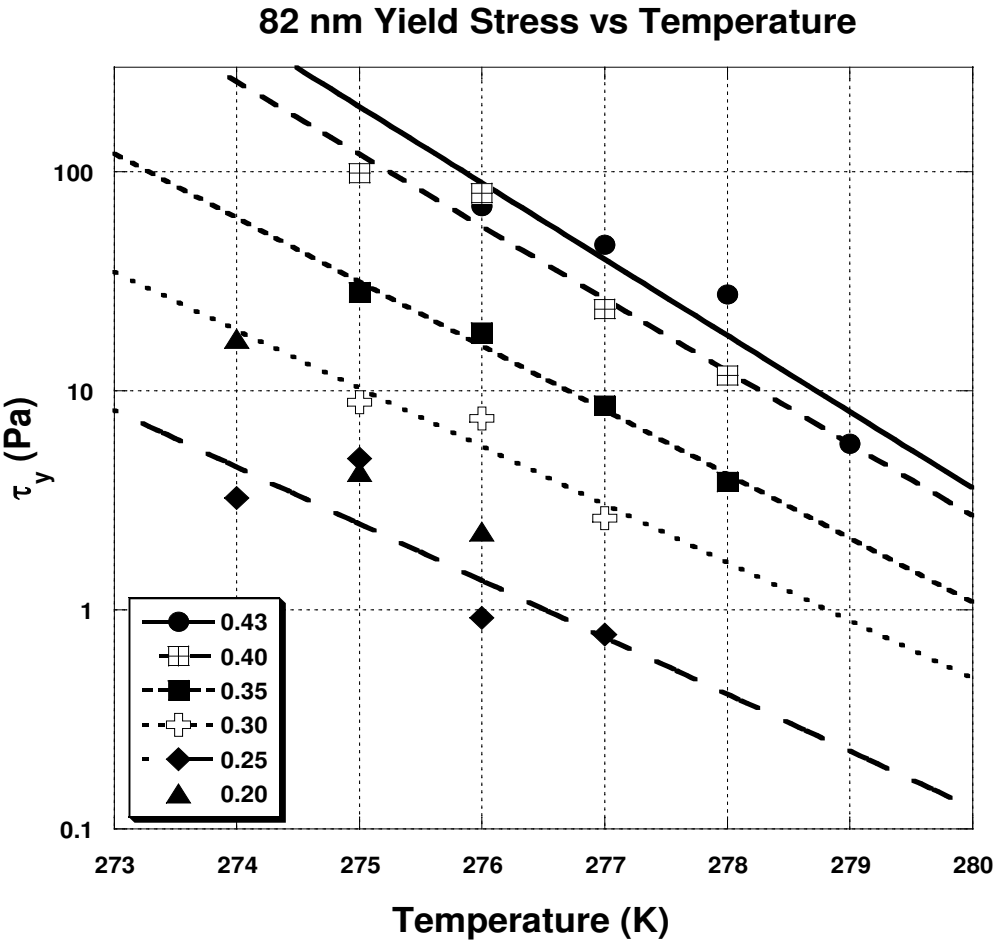

Figure 4.14 – Sample plot showing Yield Stress (Pa) vs Temperature (K) for 82 nm octadecyl silica in decalin. Symbols represent experimental data and dashed lines represent exponential fits to $\tau_y \sim \exp(-cT)$. For this system, c ~ 0.55 – 0.8.

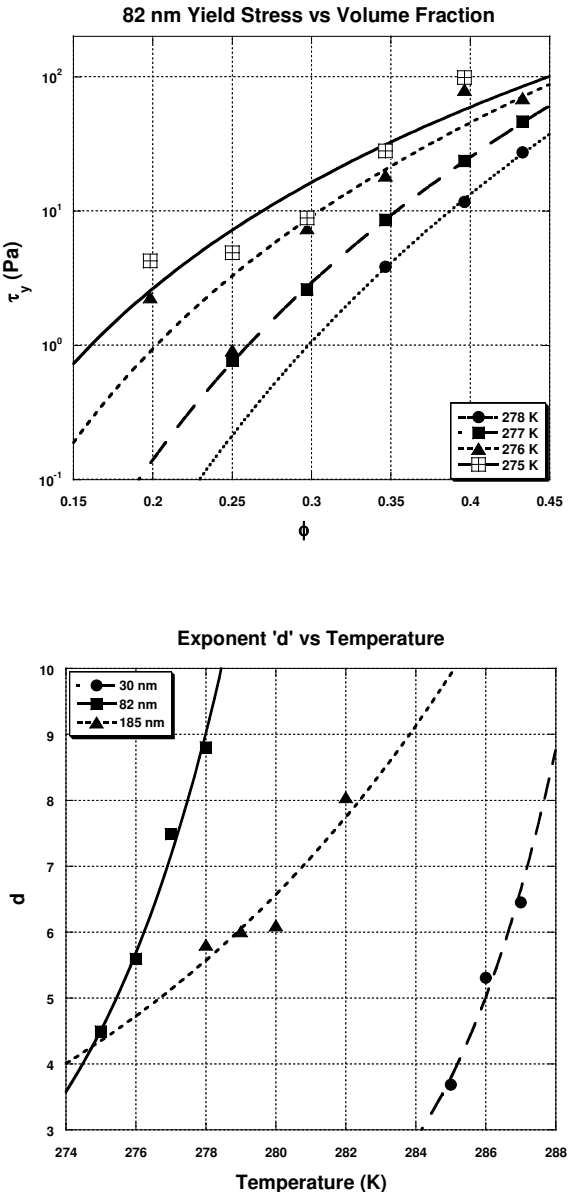

Figure 4.15 – (a) Sample plot showing Yield Stress (Pa) vs Volume Fraction (ϕ) for 82 nm octadecyl silica in decalin. Symbols represent experimental data and dashed lines represent power law fits to $\tau_y \sim \phi^d$. (b) Exponent d as a function of Temperature for different particle sizes. Symbols represent experimental values of d and dashed lines represent power law fits.

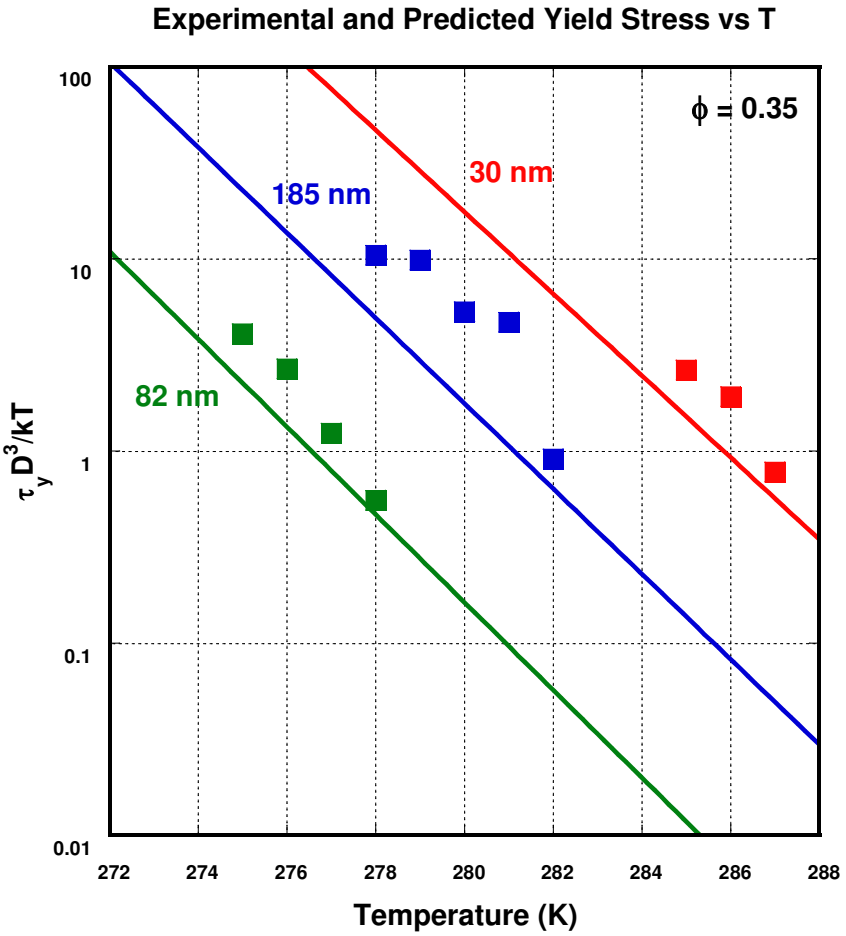

Figure 4.16 (color online) – Theoretically predicted and experimental $\frac{\tau_y D^3}{kT}$ as a function of temperature for 30 nm, 82 nm and 185 nm particles at $\phi = 0.35$. Symbols represent experimental data points and lines represent theoretical predictions determined using the protocol described in Section 4.2.8.

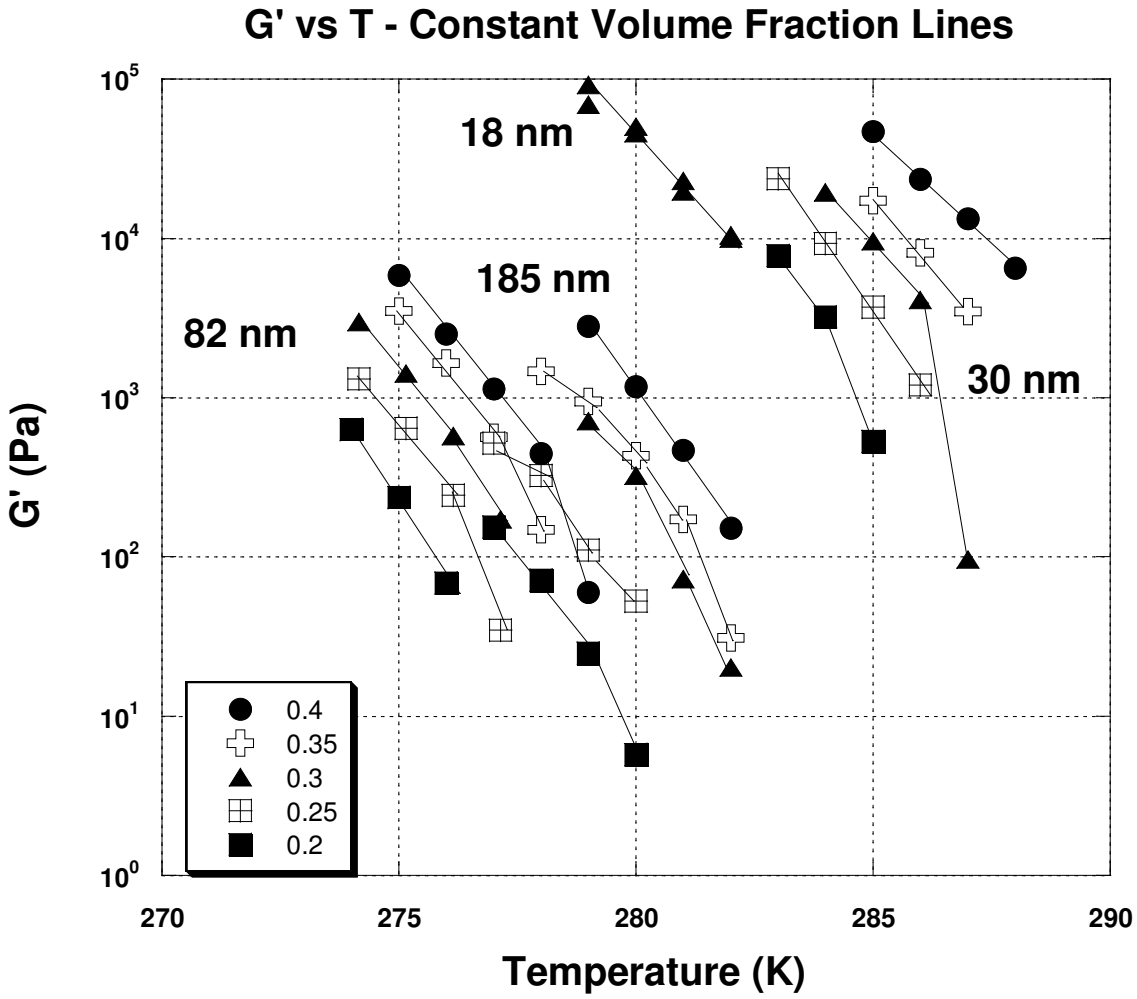

Figure 4.17 – Elastic Modulus (Pa) plotted as a function of temperature for all particle sizes and volume fractions shows a lot of scatter.

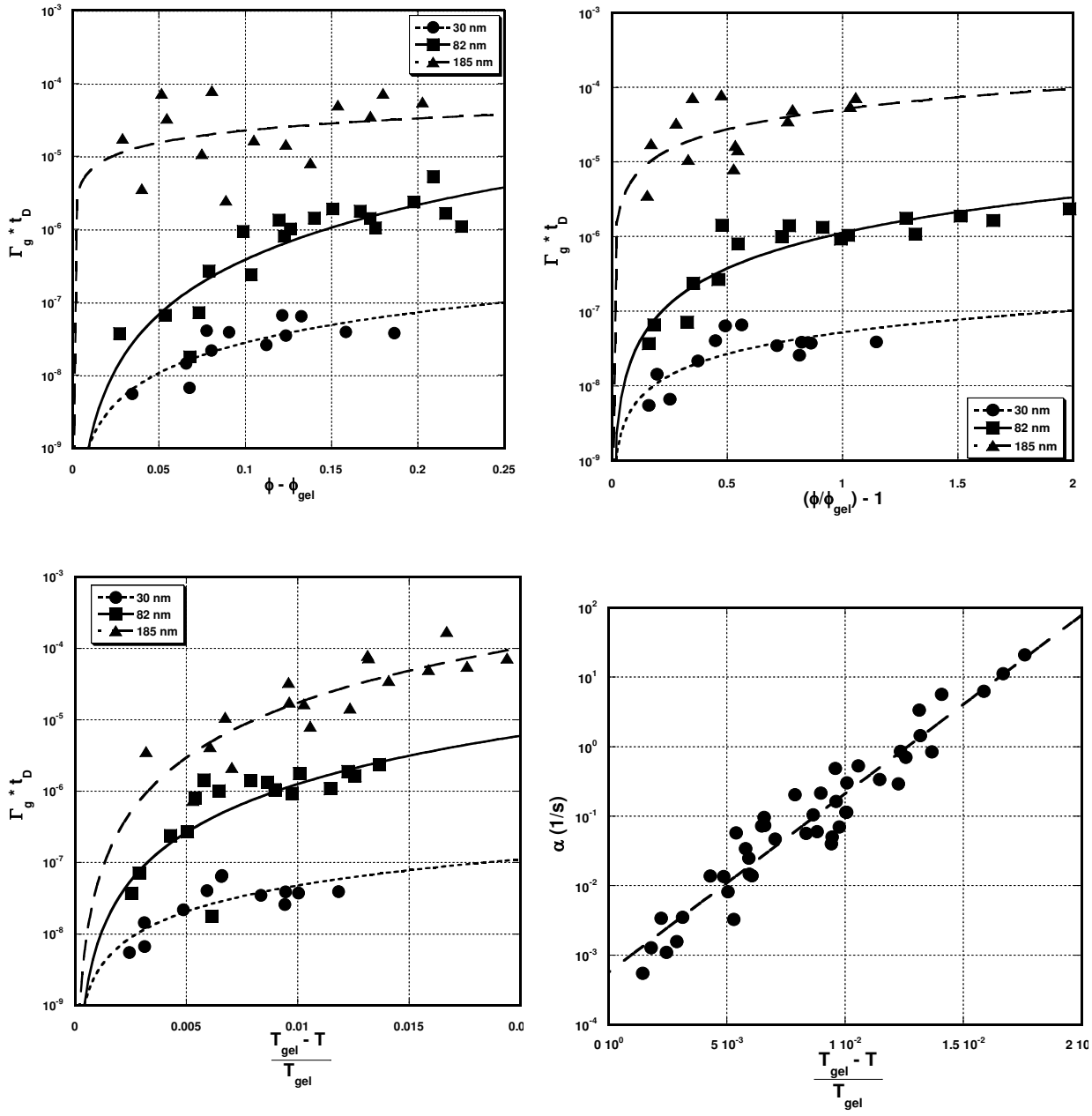

Figure 4.18 – (a) $\Gamma_g\, t_D$ vs $(\phi - \phi_G)$, (b) vs $\left(\frac{\phi}{\phi_G} - 1\right)$ and (c) vs $s = \frac{T_{gel} - T}{T_{gel}}$. Solid symbols indicate experimental data points and lines indicate power law fits to data. (d) Universal scaling curve α vs $\frac{T_{gel} - T}{T_{gel}}$. Solid symbols indicate data points and the dashed line indicates an exponential fit to data.

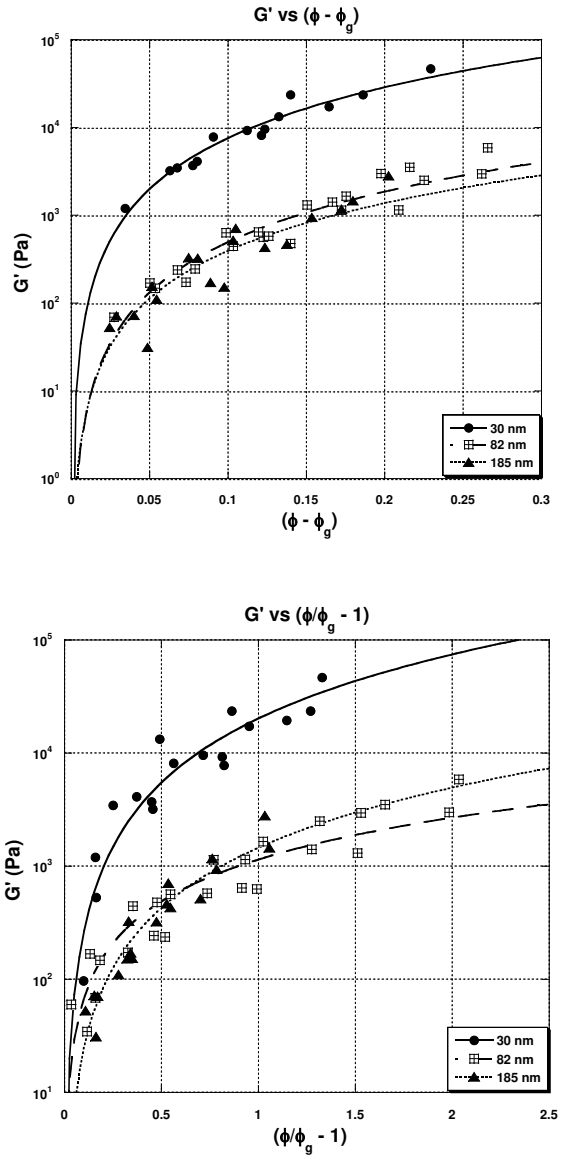

Figure 4.19 – (a) G' vs $\left(\phi - \phi_g\right)$ and (b) G' vs $\left(\frac{\phi}{\phi_g} - 1\right)$ for all particle sizes. Symbols represent experimental data points and lines represent power law fits. Power law exponent in (a) lies between 1.80 – 1.92 and systematically decreases with increasing particle size. Power law exponent in (b) varies non - systematically for the different particle sizes between 1.23 – 1.88.

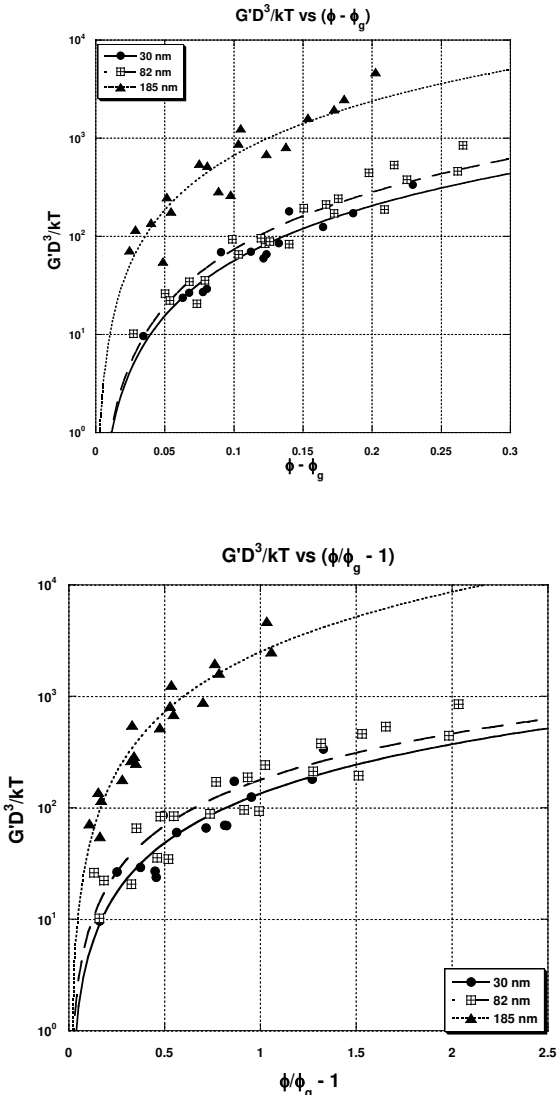

Figure 4.20 – (a) $\frac{G'D^3}{kT}$ vs $\left(\phi - \phi_g\right)$ and (b) $\frac{G'D^3}{kT}$ vs $\left(\frac{\phi}{\phi_g} - 1\right)$ for all particle sizes. Symbols represent experimental data points and lines represent power law fits. Power law exponent in (a) lies between 1.84 – 1.93 and systematically decreases with increasing particle size. Power law exponent in (b) varies non - systematically for the different particle sizes between 1.37 – 1.79.

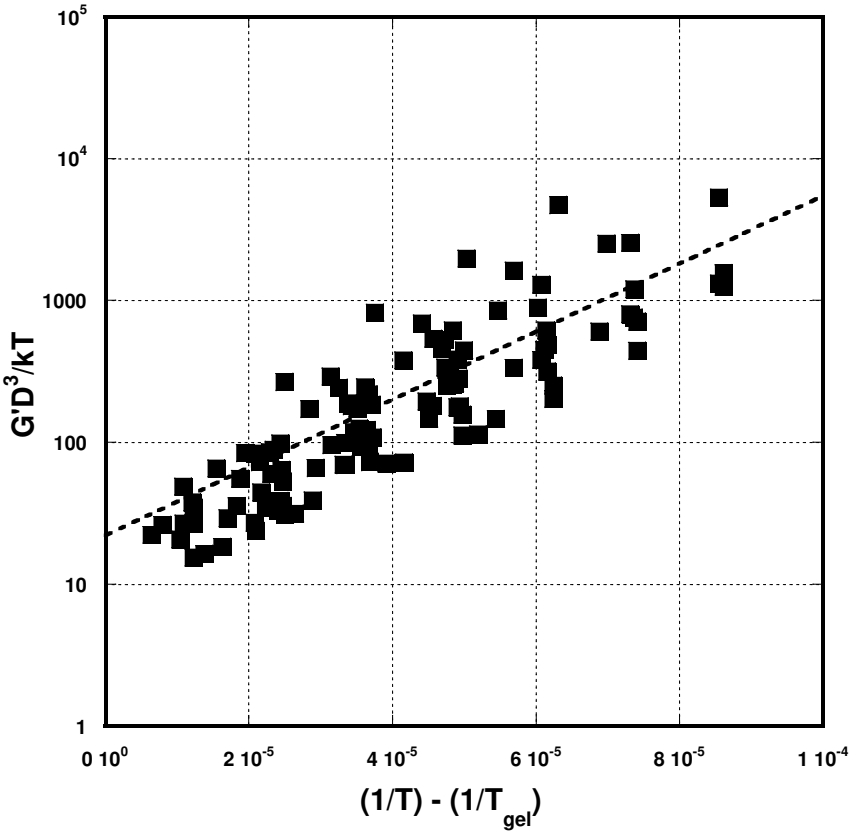

Figure 4.21 – $\frac{G'D^3}{kT}$ vs $\left(\frac{1}{T} - \frac{1}{T_{gel}}\right)$ for all particle sizes and volume fractions. Symbols indicate experimental data points and dashed line indicates the model fit obtained evaluating equation 2.19 using the parameters listed in Table 4.1.

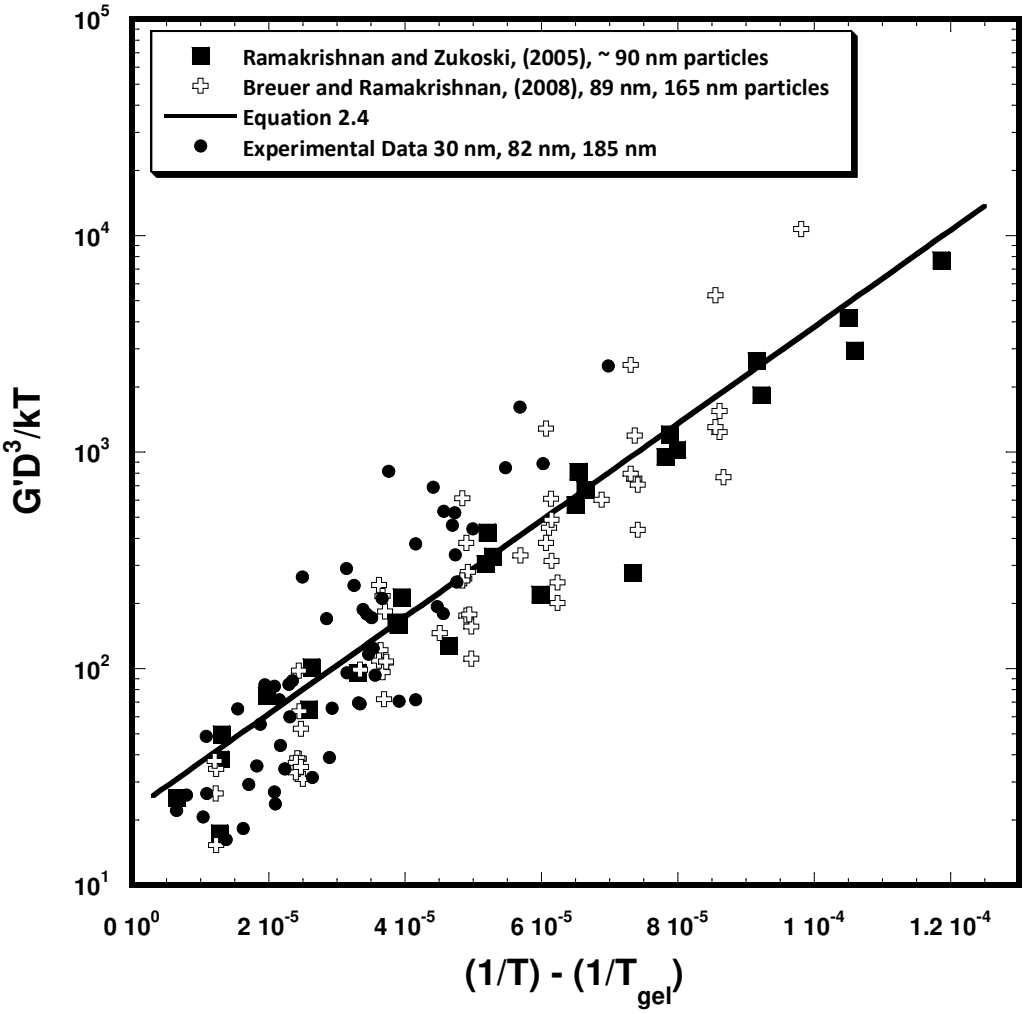

Figure 4.22 - $\frac{G'D^3}{kT}$ vs $\left(\frac{1}{T}-\frac{1}{T_{gel}}\right)$ for experimental data obtained by Ramakrisnan and Zukoski (2006), Breuer and Ramamkrishnan (2008) and the data obtained for 18, 30, 82 and 185 nm particles (same as in Figure 4.21). Solid line represents the model fit to equation 2.21 with $\kappa D = 11$, $AT\theta = 46578$ and $\chi = 3.77$. Symbols represent experimental data points. Solid and dotted lines indicate exponential fit to experimental data.

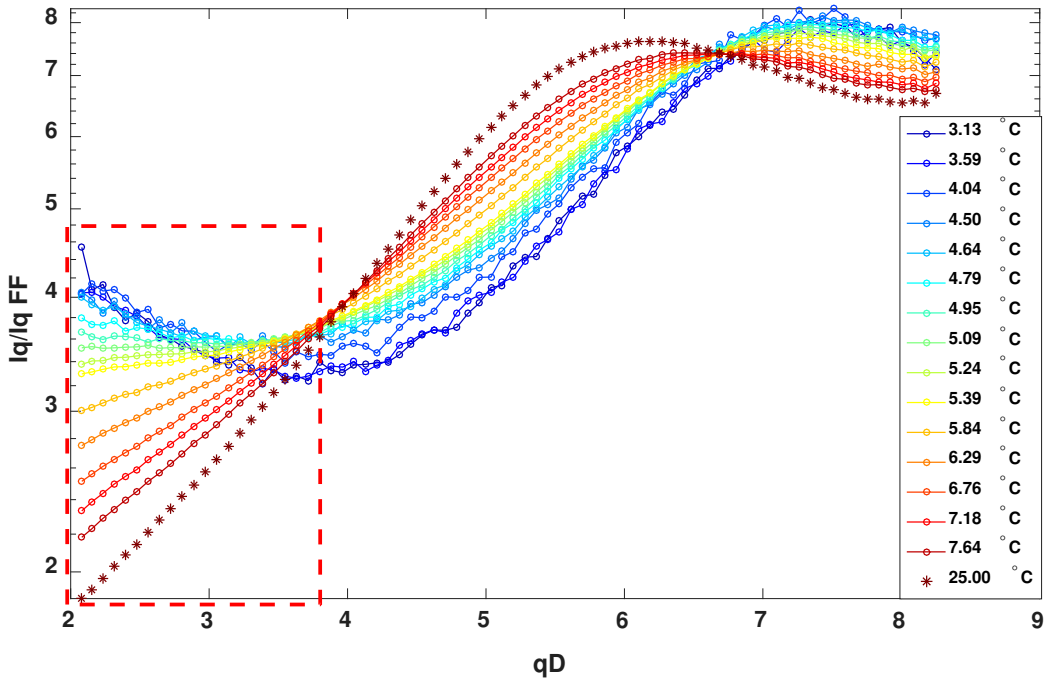

Figure 4.23 – Normalized Intensity $\left(\frac{I(q)}{I(q)_{\text{Form Factor}}}\right)$ vs normalized wave vector qD for 82 nm particles at a volume fraction of 0.2 at different temperatures. We find upturns at low qD values that indicate the possibility of clustering in the system.

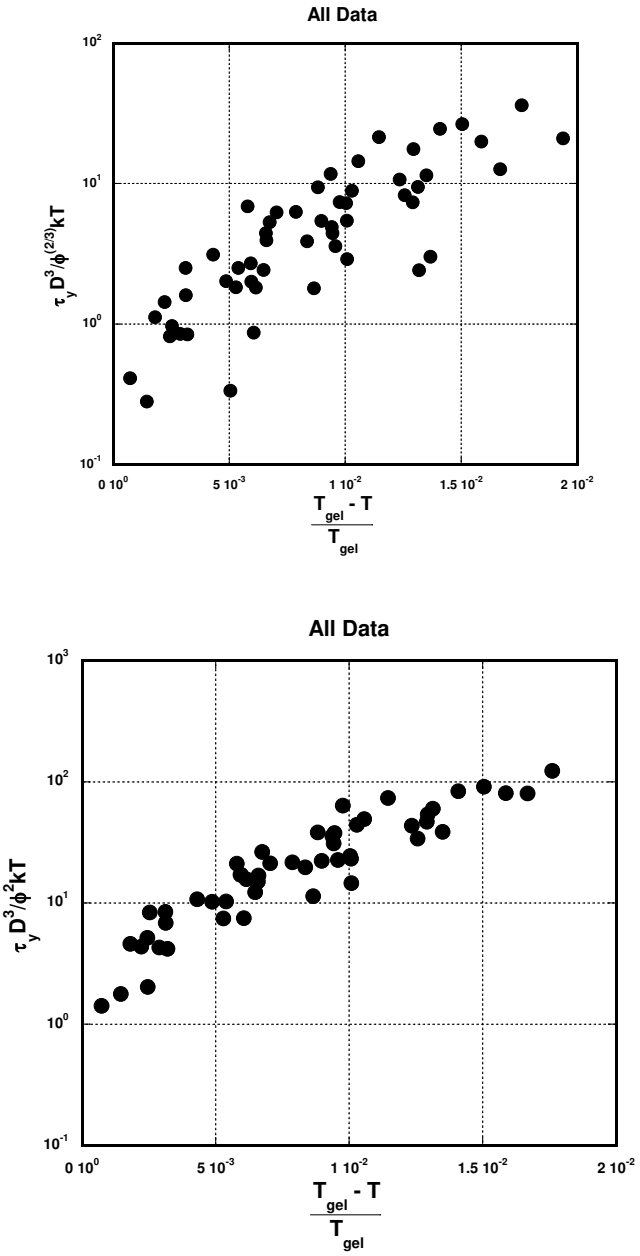

Figure 4.24 – (a) $\frac{\tau D^3}{\phi^{2/3} kT}$ and (b) $\frac{\tau D^3}{\phi^2 kT}$ vs $\left(\frac{1}{T} - \frac{1}{T_{gel}}\right)$ data for 30 nm, 82 nm and 185 nm particles.

CHAPTER 5

CONCLUSIONS AND FUTURE DIRECTION

5.1 Conclusions

We find that the gel temperatures increase as a power law function of volume fraction for a single particle size. We observe very similar slopes for the three particle sizes, however, we don't see the gel boundaries change systematically in terms of particle sizes. We hypothesize that this non – monotonicity in terms of particle size may be a result of different surface graft densities for the different particle sizes. Further, we extract the interaction potential parameters used to determine the strength of attraction at a range which was seen to be appropriate for the octadecyl silica – decalin system based on previous studies carried out by Ramakrishnan and Zukoski [2] and Breuer and Ramakrishnan [62] and our results are of the same order of magnitude as seen in literature.

Upon examining how the elastic moduli and yield stresses vary as functions of temperature and volume fraction, we find that the qualitative trends observed for the two are very similar. They vary as exponential functions of temperature with relatively similar exponents (z ~ 1) for all volume fractions and particle sizes, while they vary as power law functions of volume fraction with the power law exponent decreasing systematically on decreasing temperature. The power law exponents observed in this work match those observed by Rueb and Zukoski for the same experimental system [41].

We studied how the initial growth rates, elastic moduli and yield stresses scaled with functions denoting proximity to the gel point, $\left(\phi - \phi_G\right)$ and $\left(\frac{\phi}{\phi_G} - 1\right)$. These functions describe the

probability of bond formation as one moves deeper into the gel, away from the gel point within the framework of percolation models and have been employed in literature to universally scale data for the properties mentioned earlier on universal scaling curves. We find that $\left(\phi - \phi_G\right)$ does a much better job at scaling data for different temperatures and volume fractions onto master curves for individual particle sizes compared to $\left(\frac{\phi}{\phi_G} - 1\right)$ (the fits to both these functions are very similar for scaling initial growth rates). These results match those obtained by Russel and Grant [37] for a similar system of octadecyl silica particles in hexadecane, however don't match the results obtained by Rueb and Zukoski [41] whose data scale well with $\left(\frac{\phi}{\phi_G} - 1\right)$ for the same experimental system. A temperature analog of $\left(\frac{\phi}{\phi_G} - 1\right)$ defined as reduced temperature, $\frac{T_{gel} - T}{T_{gel}}$ gives the best fits for all three properties. Thus for a given range of interaction, a non-dimensional strength of interaction scales the viscoelastic properties well.

The interaction potential parameters extracted from the gel boundaries are used to predict the elastic moduli and yield stresses using the barrier hopping framework. We find very good agreement between the predicted and experimentally obtained yield stresses for the 30 nm and 82 nm particles, while poor agreement is seen for samples containing 185 nm particles. Excellent agreement is seen between the predicted and experimentally determined values of G' at high volume fractions for the 82 nm particles while the agreement between the two becomes poor as one moves closer to the gel boundary upon increasing temperature or decreasing volume fraction at a fixed temperature. These results are consistent with what is found in literature [2] for the same model system.

In order to collapse the data on to a universal scaling curve for all particle sizes and concentrations, elastic moduli and yield stresses were re – scaled to incorporate the contributions of particle size and volume fraction and plotted as a function of $\left(\frac{1}{T}-\frac{1}{T_{gel}}\right)$ using the framework proposed by Ramakrishnan and Zukoski [2]. We find reasonable collapse of our data on universal scaling curves plotted as $\frac{G'D^3}{kT}$ and $\frac{\tau_y D^3}{\phi^2 kT}$ vs $\left(\frac{1}{T}-\frac{1}{T_{gel}}\right)$.

This scaling of the elastic modulus confirms that it is indeed the localization length that determines the final modulus of the gel. i.e.: if two systems have the same $\phi D^2/r_{loc}^2$ then they will have the same modulus. As for the universality in scaling observed for yield stress, non dimensionalized yield stress given by $\frac{\tau_y D^3}{\phi^2 kT}$ essentially describes the slope of the potential energy surface. The scaling tells us that at the same distance from the gel boundary, rescaled as $\left(\frac{1}{T}-\frac{1}{T_{gel}}\right)$, the collapse in data is due to the fact that the slope $\frac{dF}{dr}$ is the same while this force increases as we go deeper into the gel.

5.2 Future Directions

In this work we have characterized a well-defined system of particles which gel upon reducing temperature. Good control of strength is obtained by controlling the sample temperature and the kinetics of gel growth, mechanical properties and yielding behavior are characterized for wide range of temperatures for different size particles at moderate concentrations. This sets the stage for the following work:

1) Understanding the microscopic dynamics of nanoparticles as one traverses the gel boundary and how it relates to the growth in elastic modulus. We'd like to understand what a gel point is at the microscopic level and what happens to the dynamics of the particles at the gel point.

2) Temperature Quench vs Shear Melting: One of the questions of interest to the community is how the rheological properties evolve when different routes are taken to traverse the gel boundary. From a liquid state one can form a gel by reducing temperature and the gel can be fluidized again by applying high shear then, upon the cessation of shear, at the same temperature, the system gels again. But do properties evolve in the same manner along different routes to the gel boundary? The current system is ideal for such investigations.

3) Rheology of Mixtures: Most industrial formulations utilize mixtures of particles of different sizes and nature of interactions. However, processing of mixtures of high complexity can be challenging and limited progress has been made in developing design criteria for their processing. Our well characterized system may be an ideal choice to study the mechanical and yielding properties of particle mixtures. We'd like to study if there are there any scaling relationships that can be developed for predicting the mechanical properties of particle mixtures or if we can identify design criteria that enable us to independently tune the elastic moduli and yield stresses of mixtures of particles. Initial studies carried out on bimodal mixtures of octadecyl silica particles in decalin show that using mixtures of particles (16 nm and 32 nm), we see an enhancement in gel points. A 1:1 mixture of the 16 nm and 32 nm particles gel at a higher temperature than the individual

particles at the same concentration. We hope to be able to use such results to tune the rheological properties of particle mixtures.

APPENDIX A

FORM FACTORS FOR DIFFERENT PARTICLE SIZES

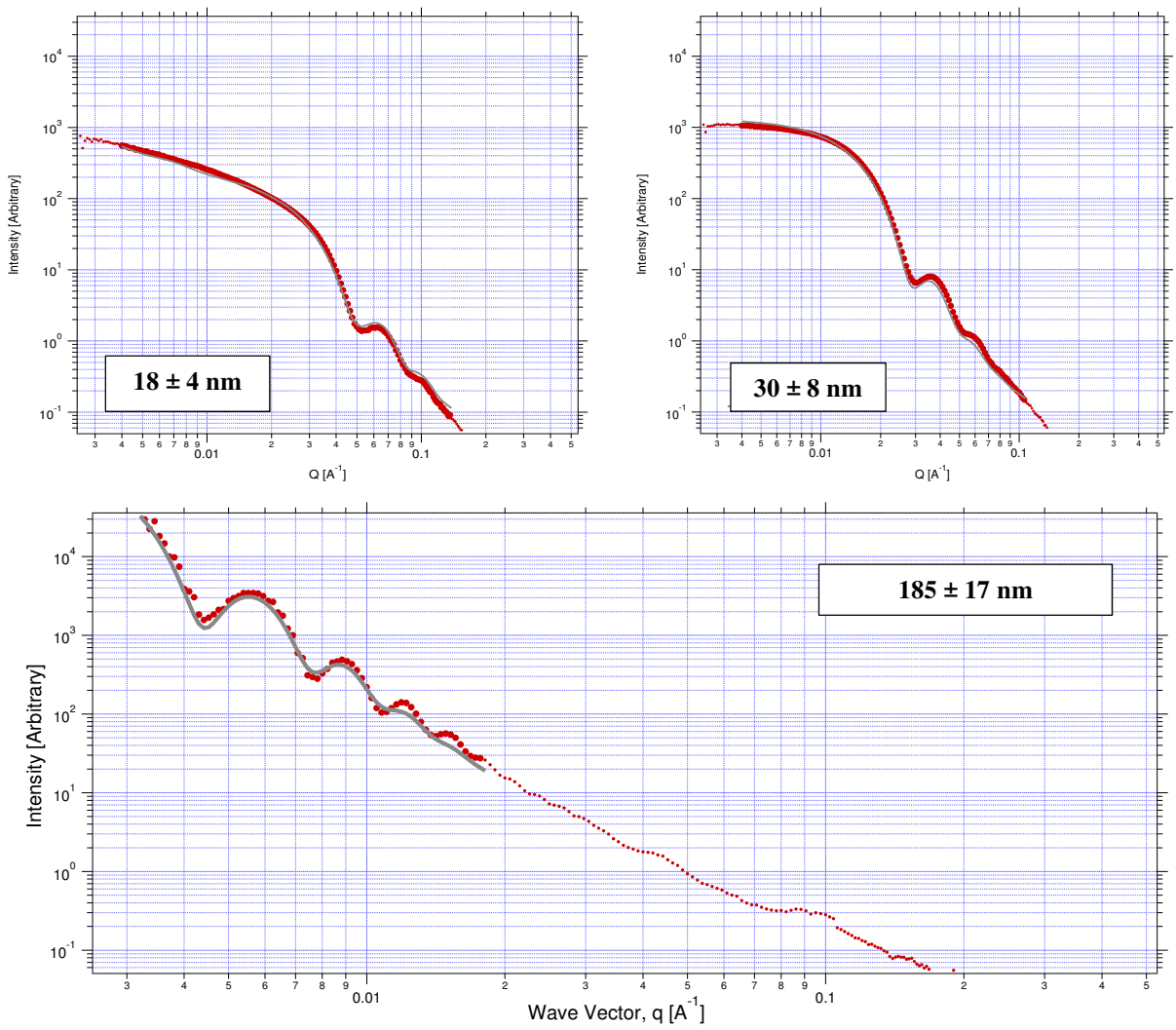

Figure A.1 (Color Online) Intensity vs wave-vector plots for (a) 18 nm, (b) 30 nm and (c) 185 nm particles. Solid red symbol represent fit data points, red dots represent data points excluded from the fit and the grey line represents the hard sphere form factor fit. Plots generated using Igor Pro 7 - USAXS Modeling Toolbox.

APPENDIX B

GEL POINT DETERMINATION

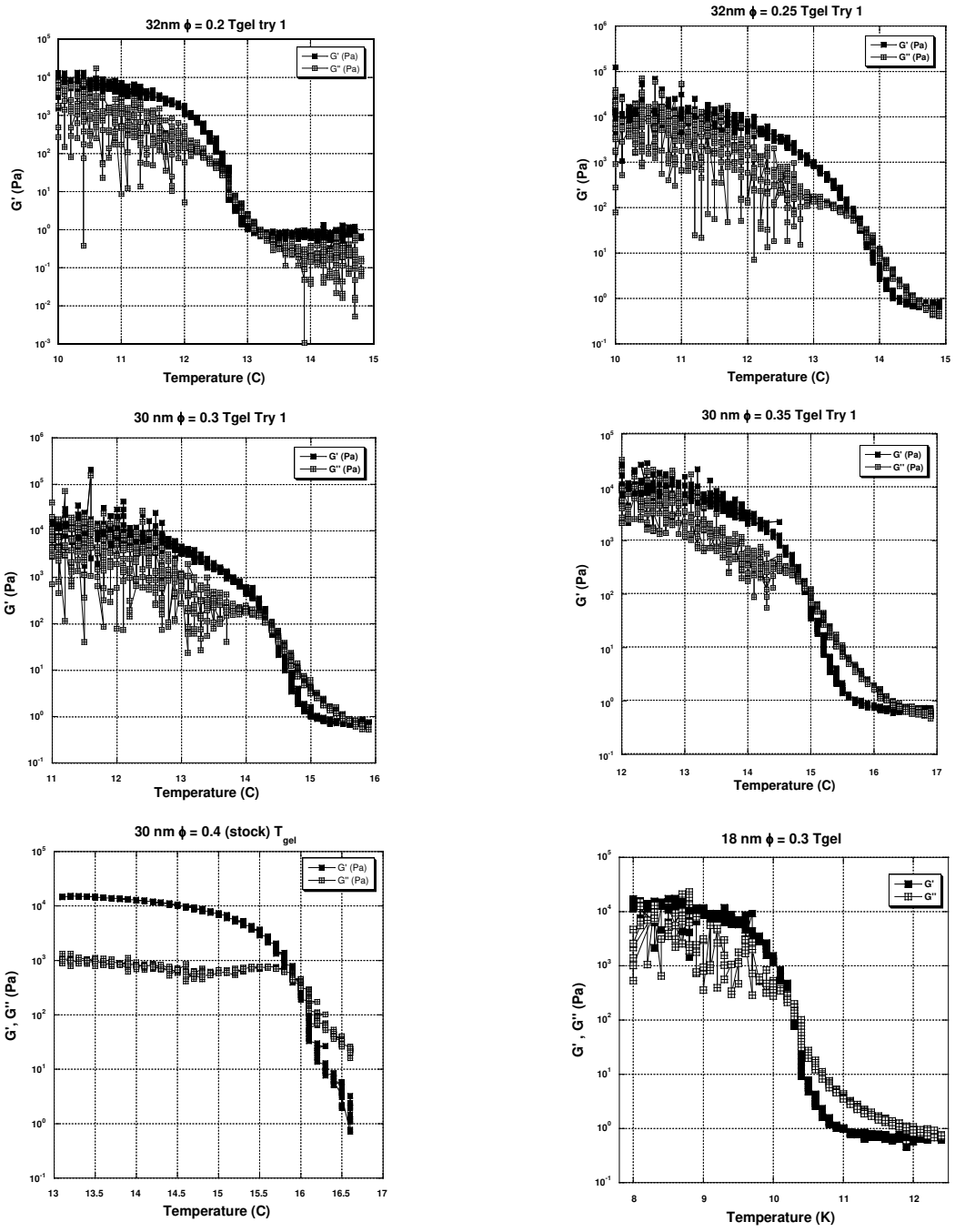

Figure B.1 – Gel Temperature Determination for 30 nm and 18 nm particles at all ϕ

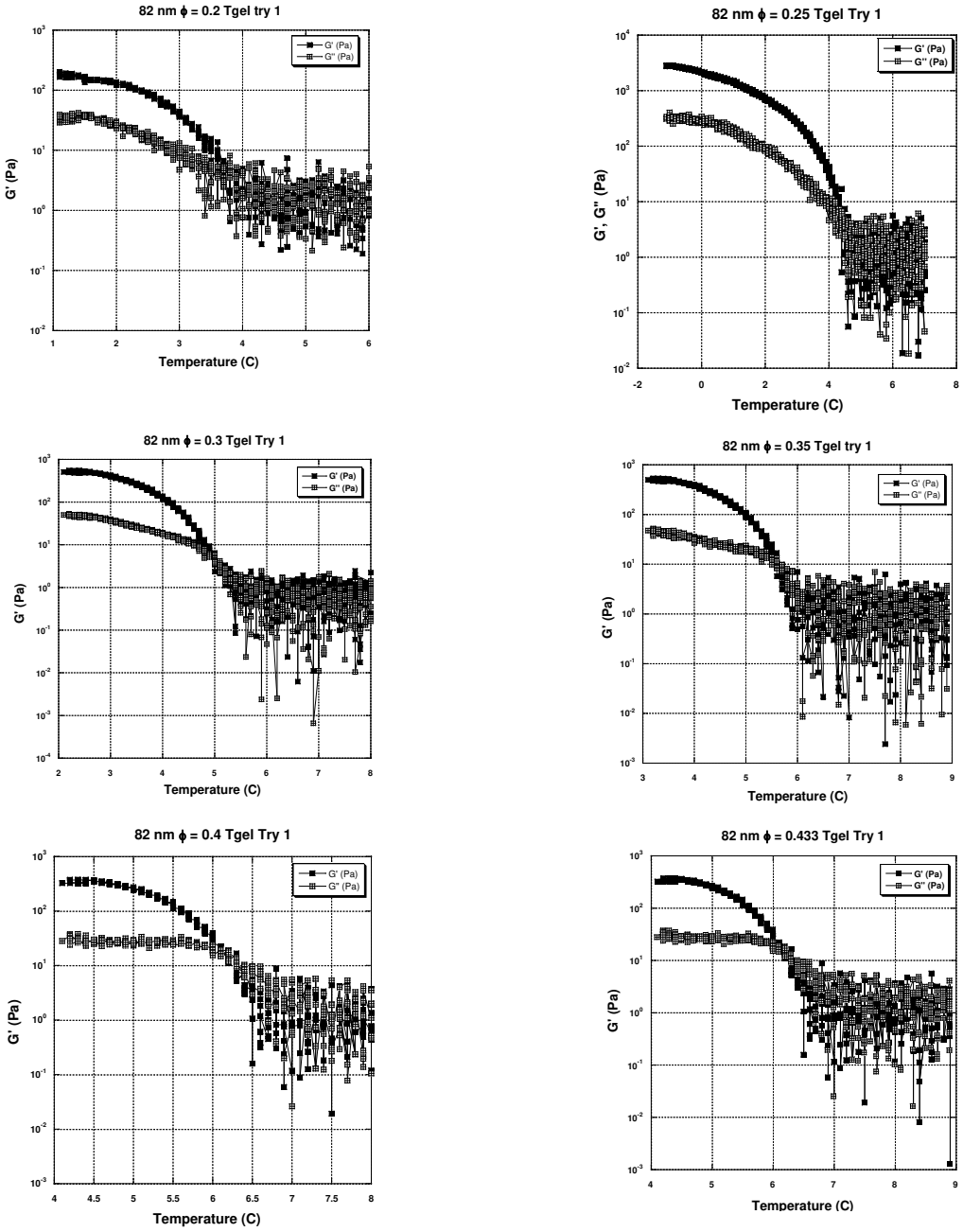

Figure B.2 – Gel Point Determination for 82 nm particles at different ϕ

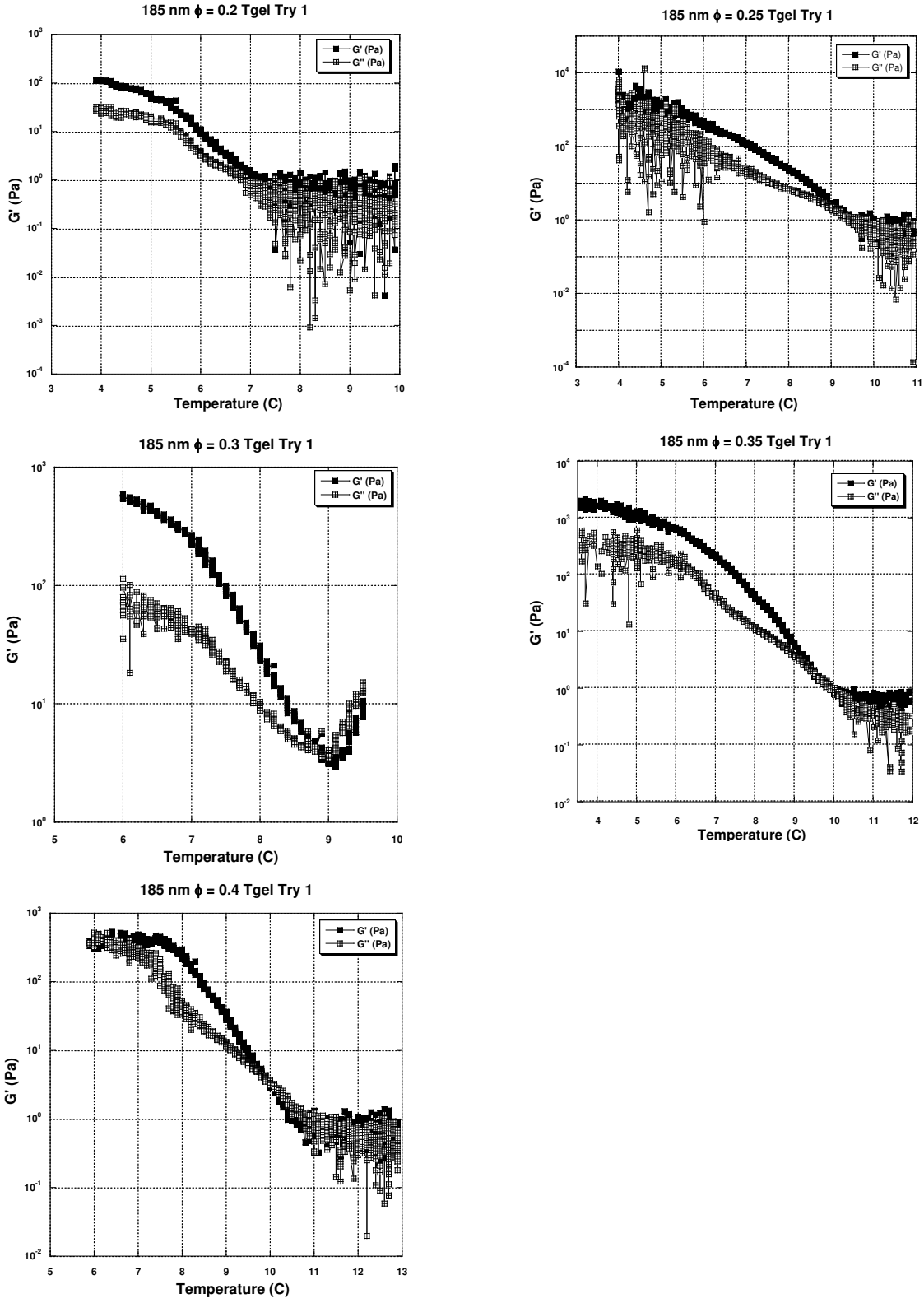

Figure B.3 – Gel Point Determination for 185 nm particles at different ϕ

APPENDIX C

ELASTIC MODULI

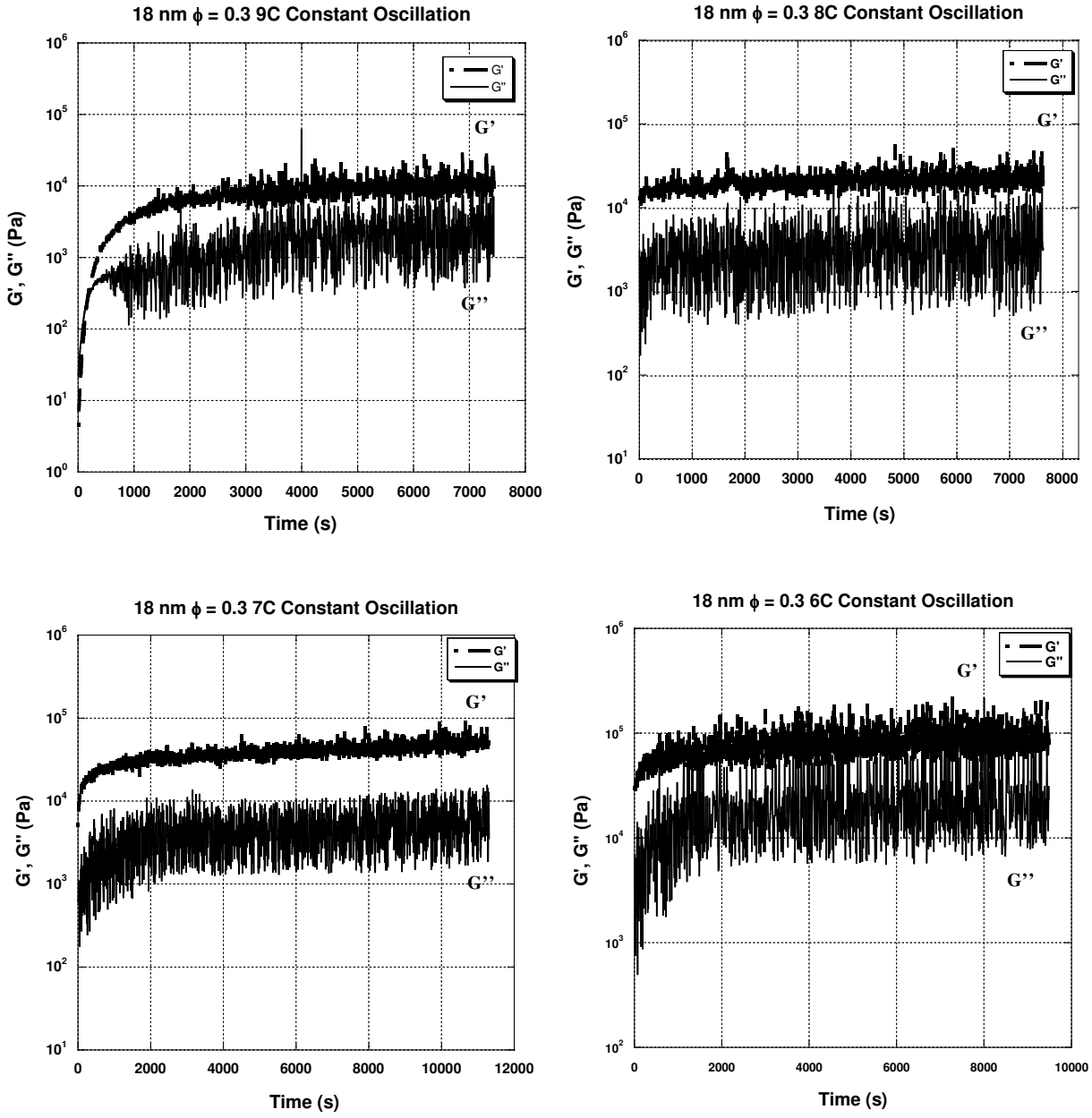

Figure C.1 – Growth of Elastic Modulus in Time for 18 nm particles, ϕ = 0.30

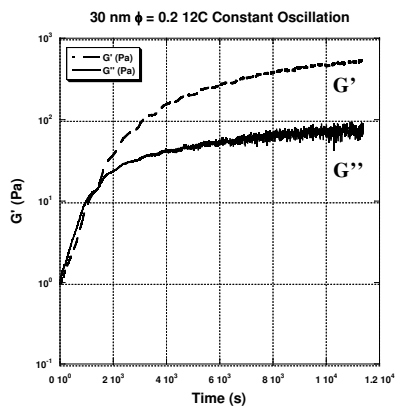

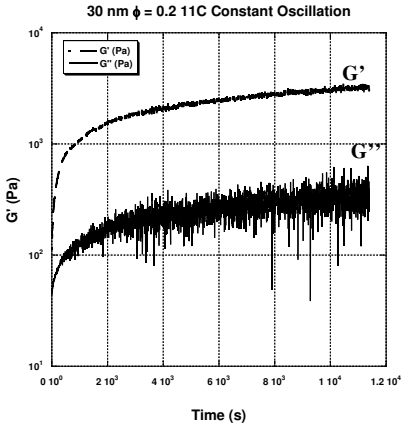

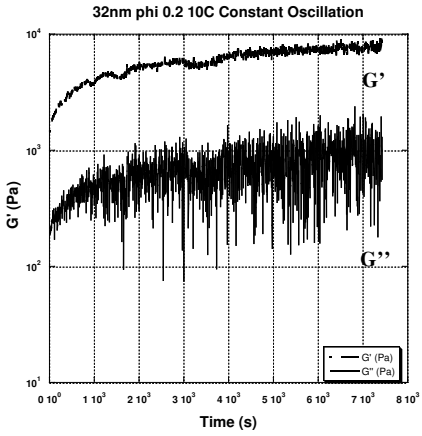

Figure C.2 – Growth of Elastic Modulus in Time for 30 nm particles, ϕ = 0.20

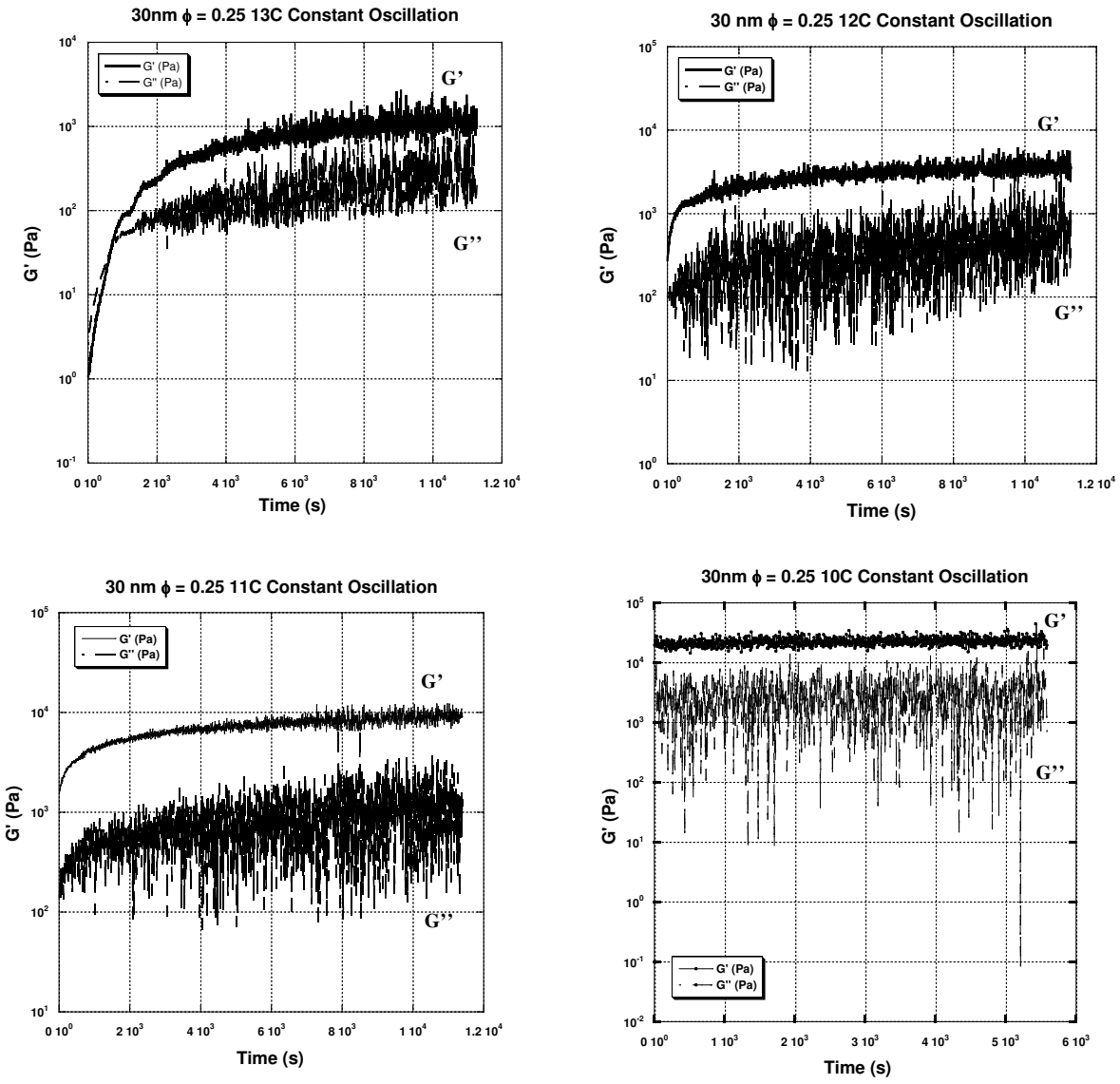

Figure C.3 - Growth of Elastic Modulus in Time for 30 nm particles, ϕ = 0.25

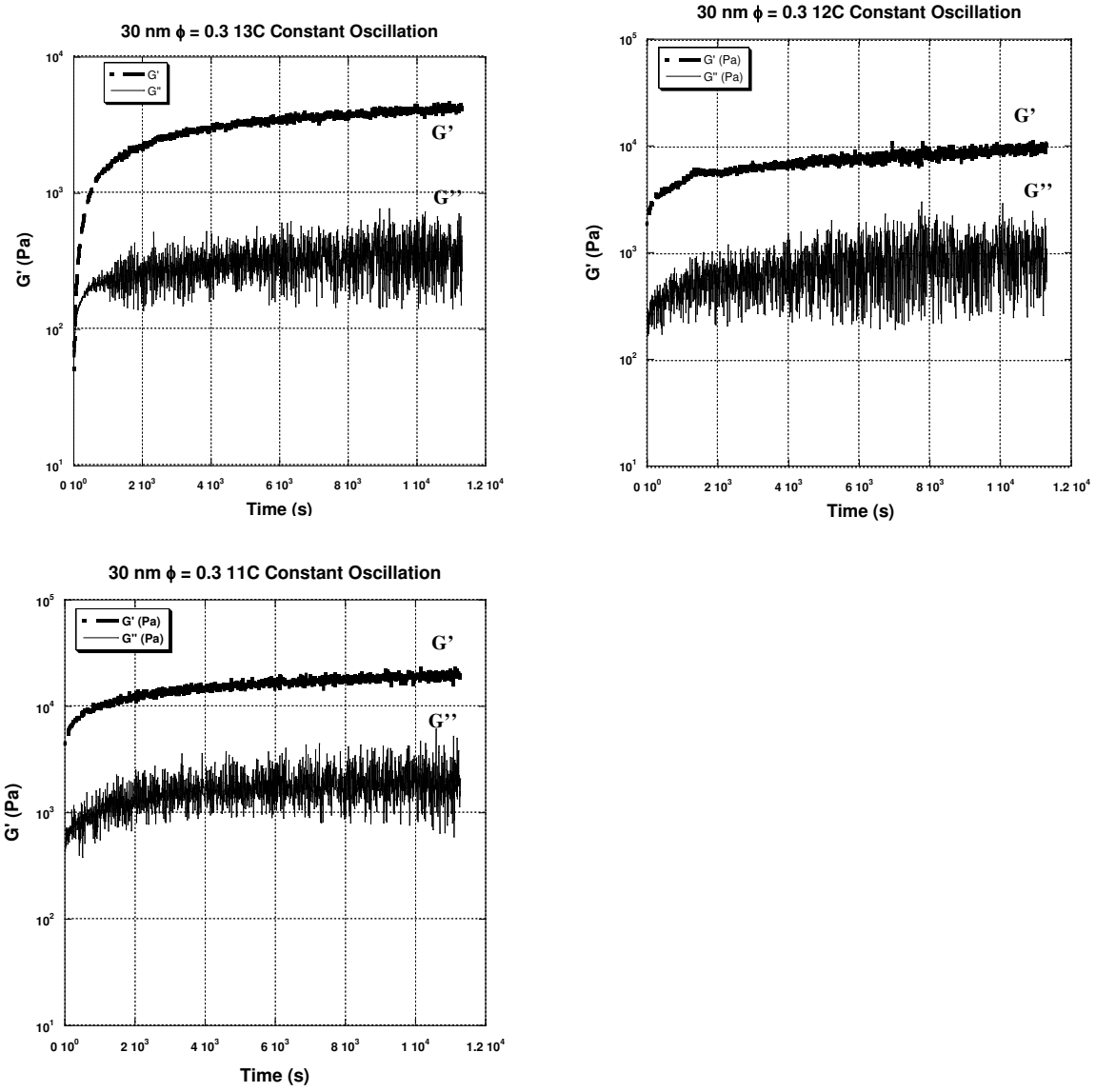

Figure C.4 - Growth of Elastic Modulus in Time for 30 nm particles, ϕ = 0.30

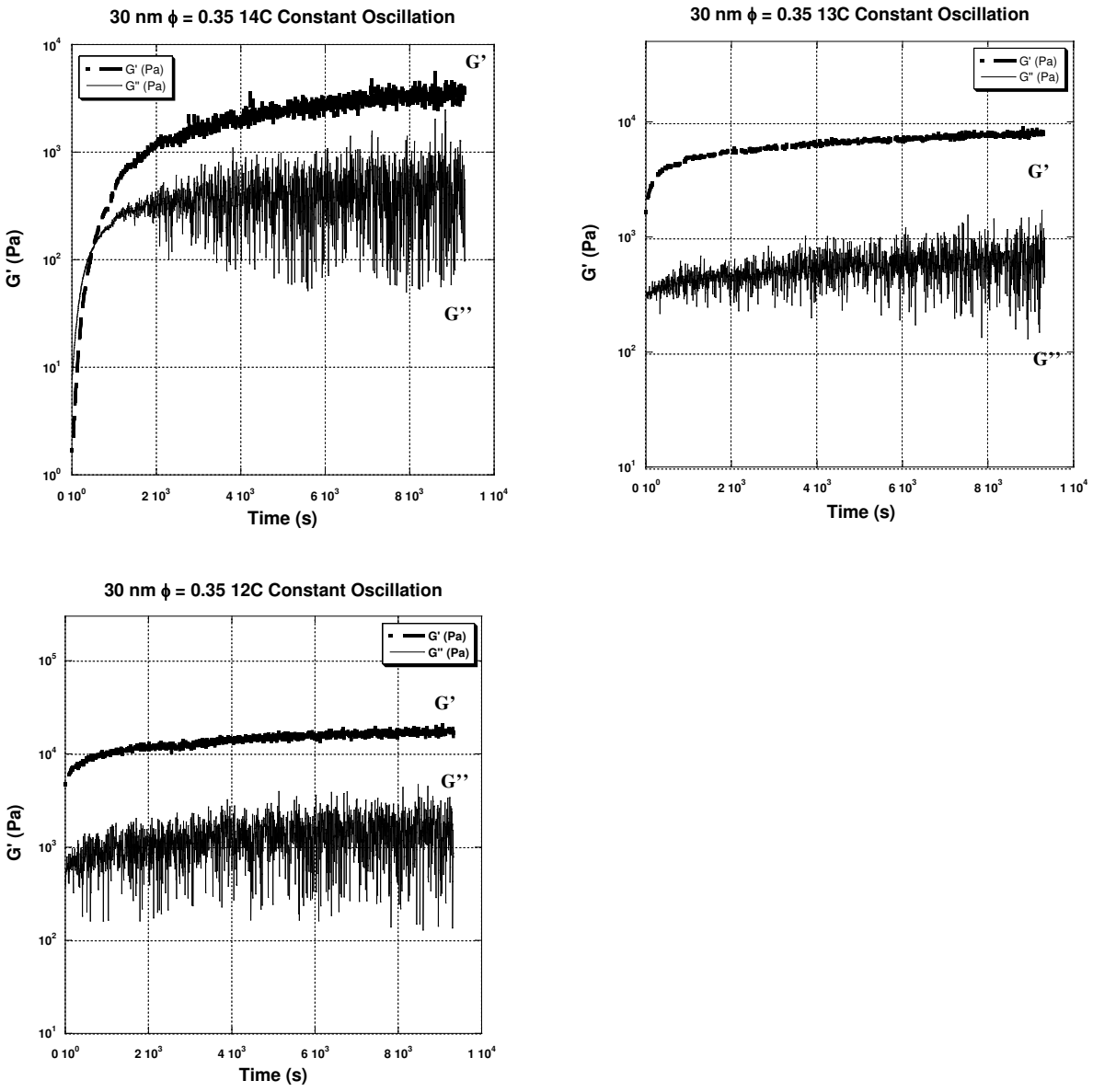

Figure C.5 - Growth of Elastic Modulus in Time for 30 nm particles, ϕ = 0.35

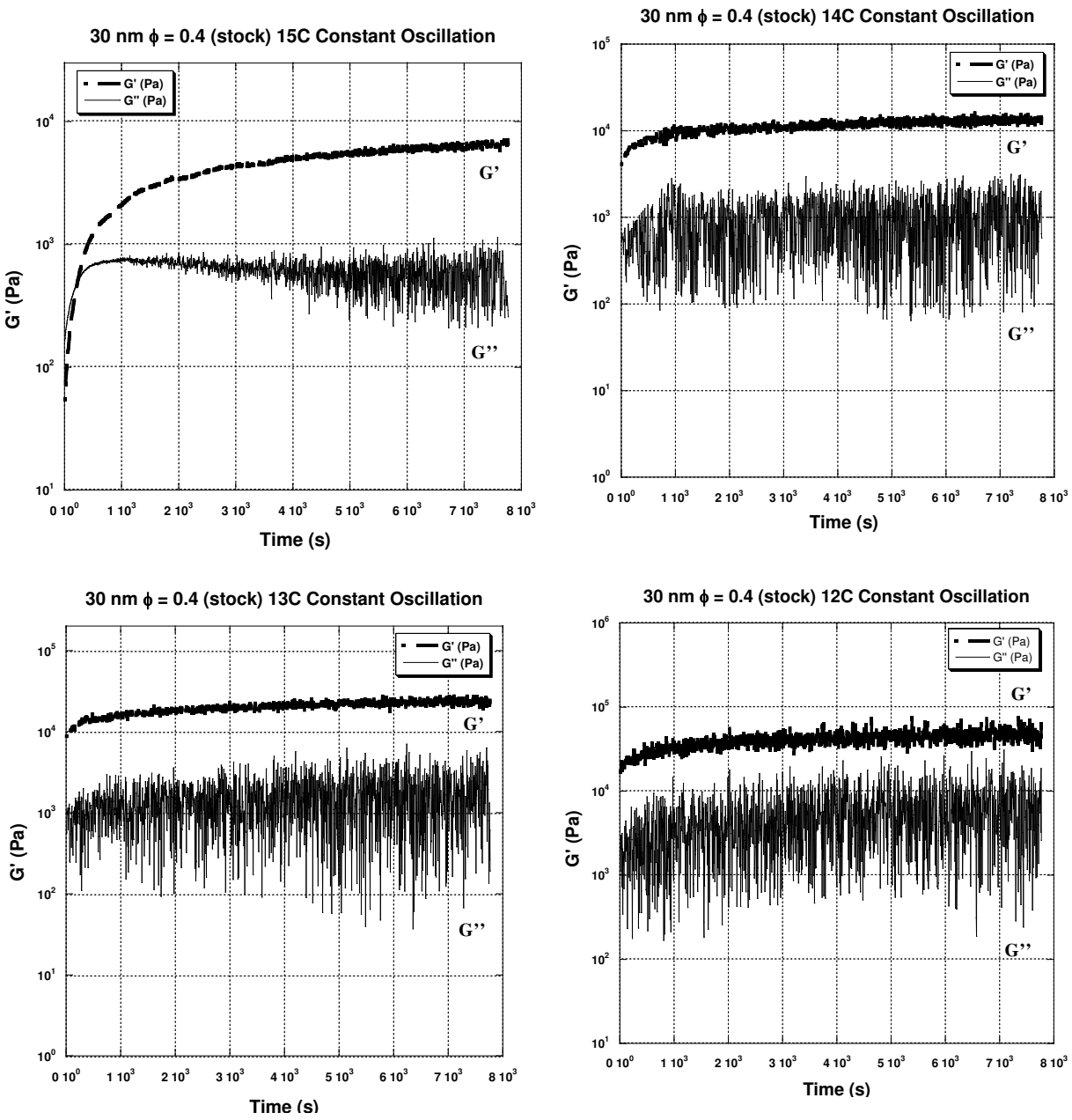

Figure C.6 - Growth of Elastic Modulus in Time for 30 nm particles, ϕ = 0.40

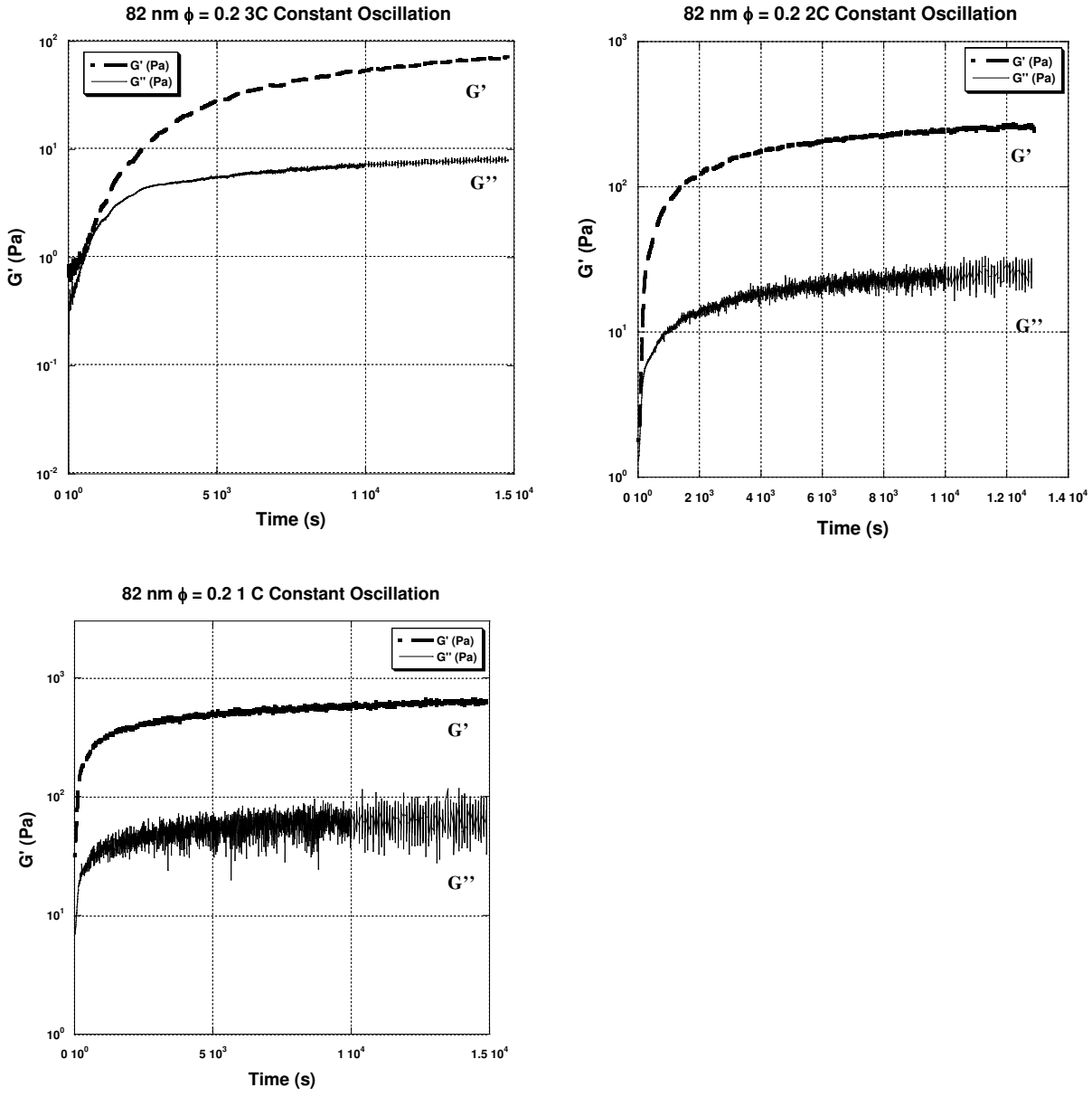

Figure C.7 - Growth of Elastic Modulus in Time for 82 nm particles, ϕ = 0.20

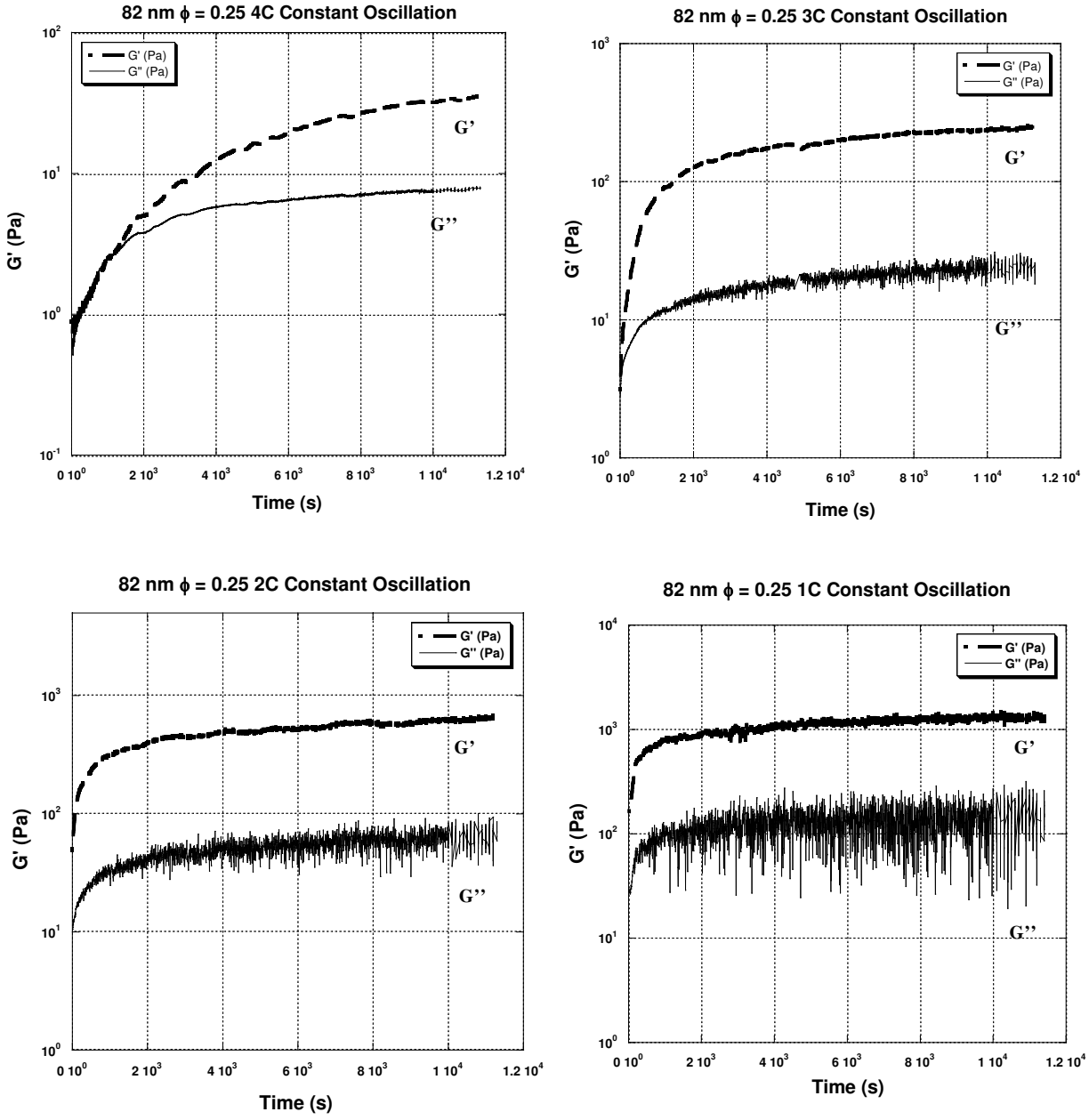

Figure C.8 - Growth of Elastic Modulus in Time for 82 nm particles, ϕ = 0.25

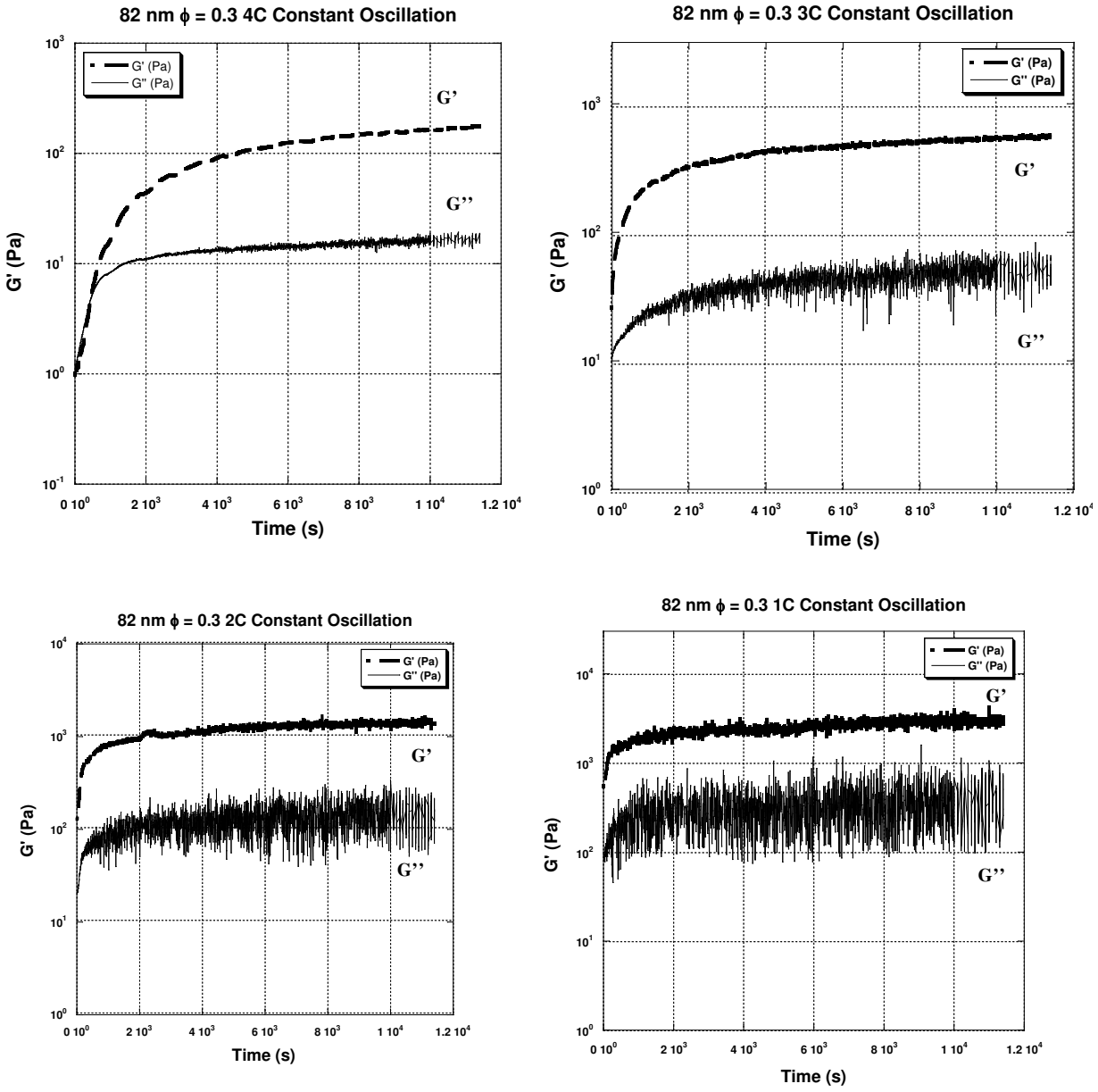

Figure C.9 - Growth of Elastic Modulus in Time for 82 nm particles, ϕ = 0.30

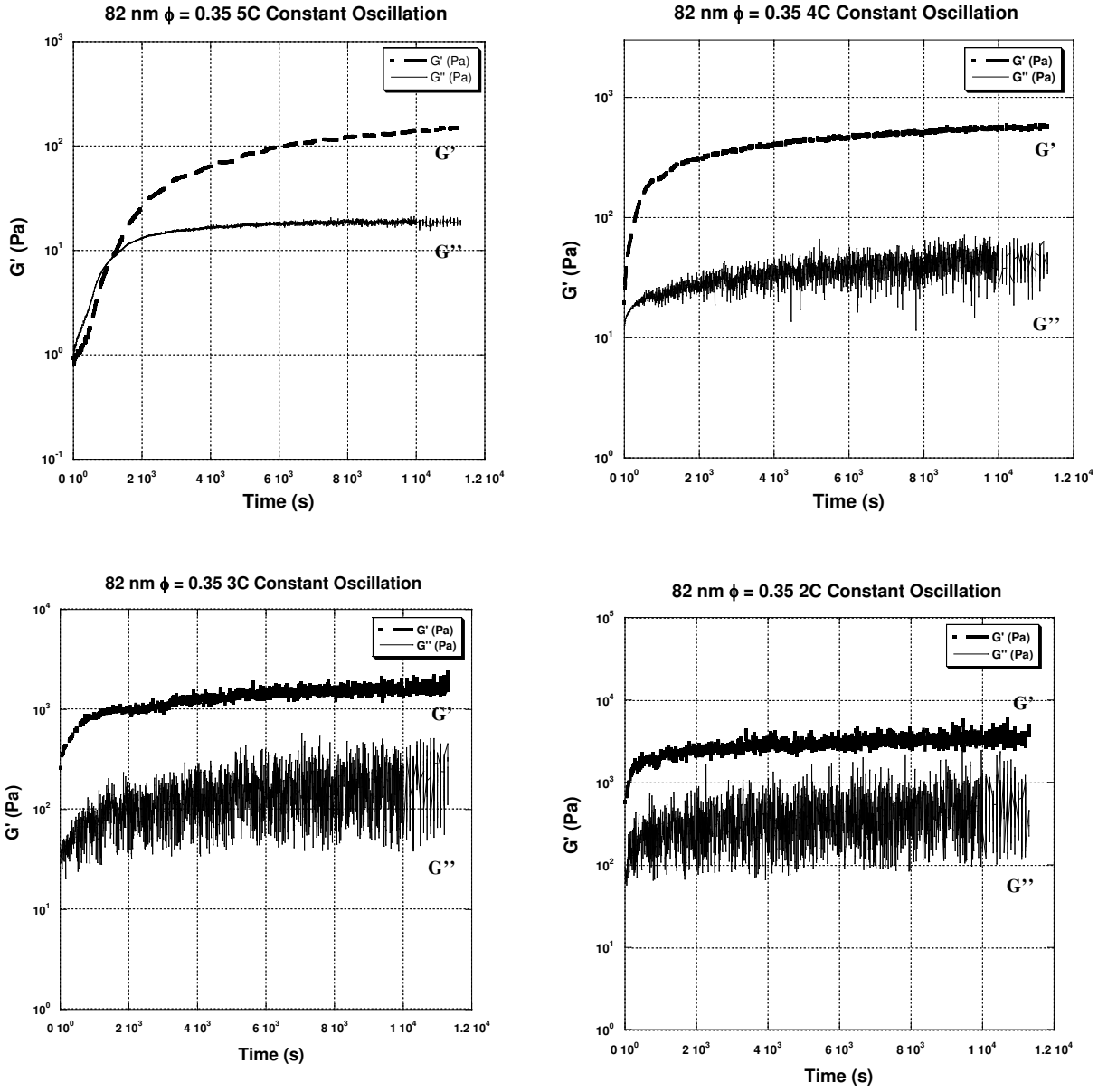

Figure C.10 - Growth of Elastic Modulus in Time for 82 nm particles, ϕ = 0.35

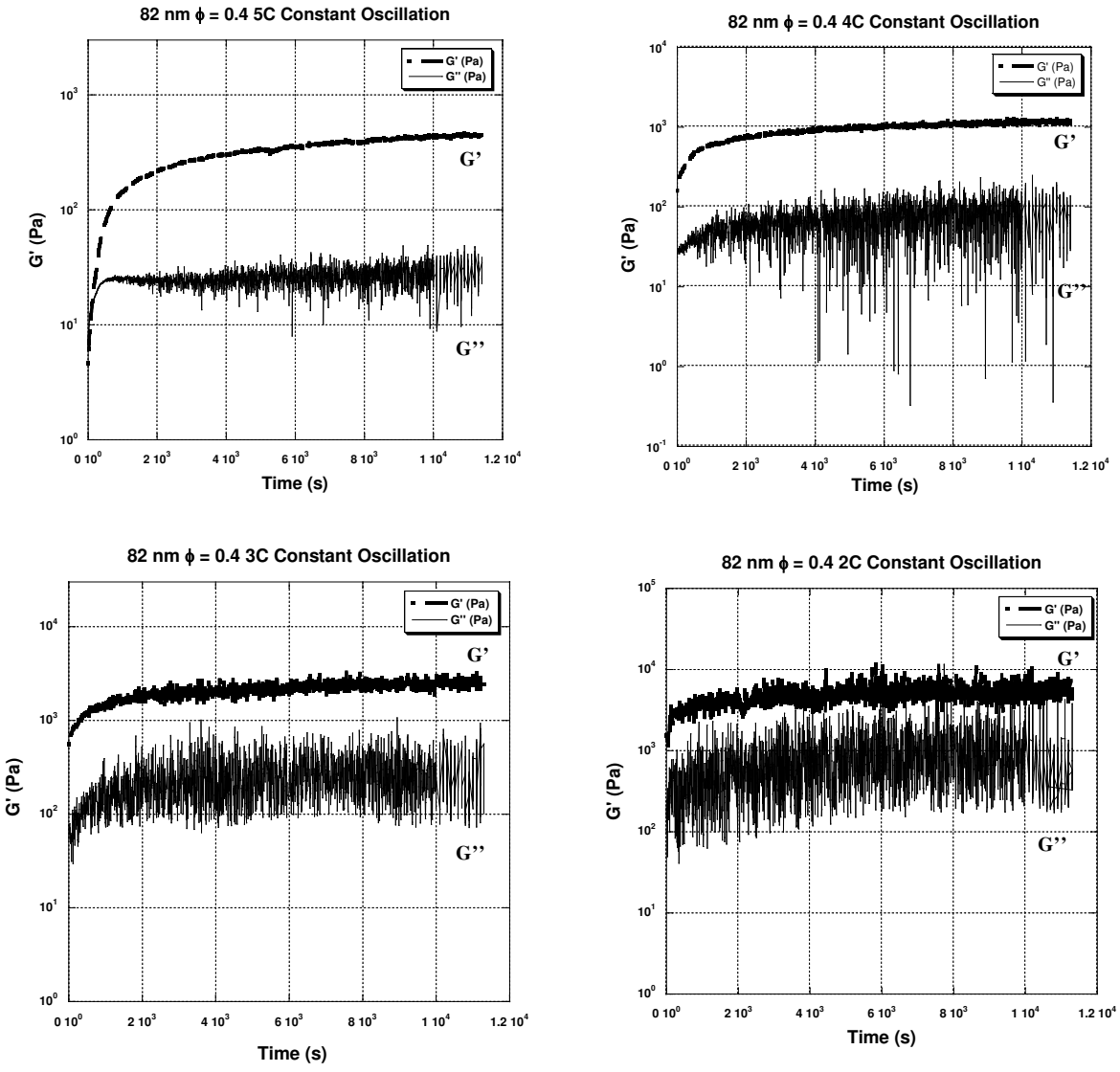

Figure C.11 - Growth of Elastic Modulus in Time for 82 nm particles, ϕ = 0.40

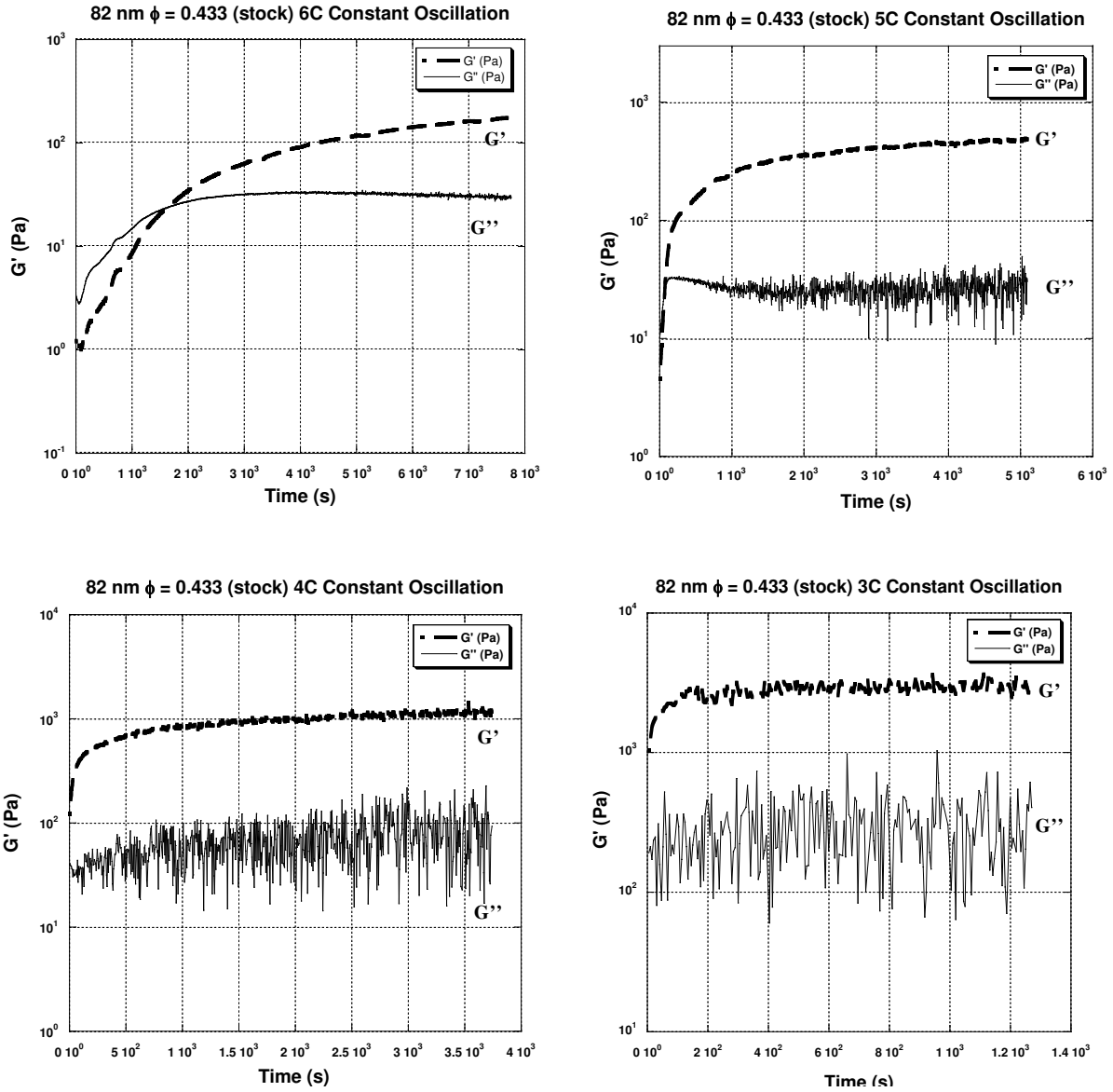

Figure C.12 - Growth of Elastic Modulus in Time for 82 nm particles, ϕ = 0.43

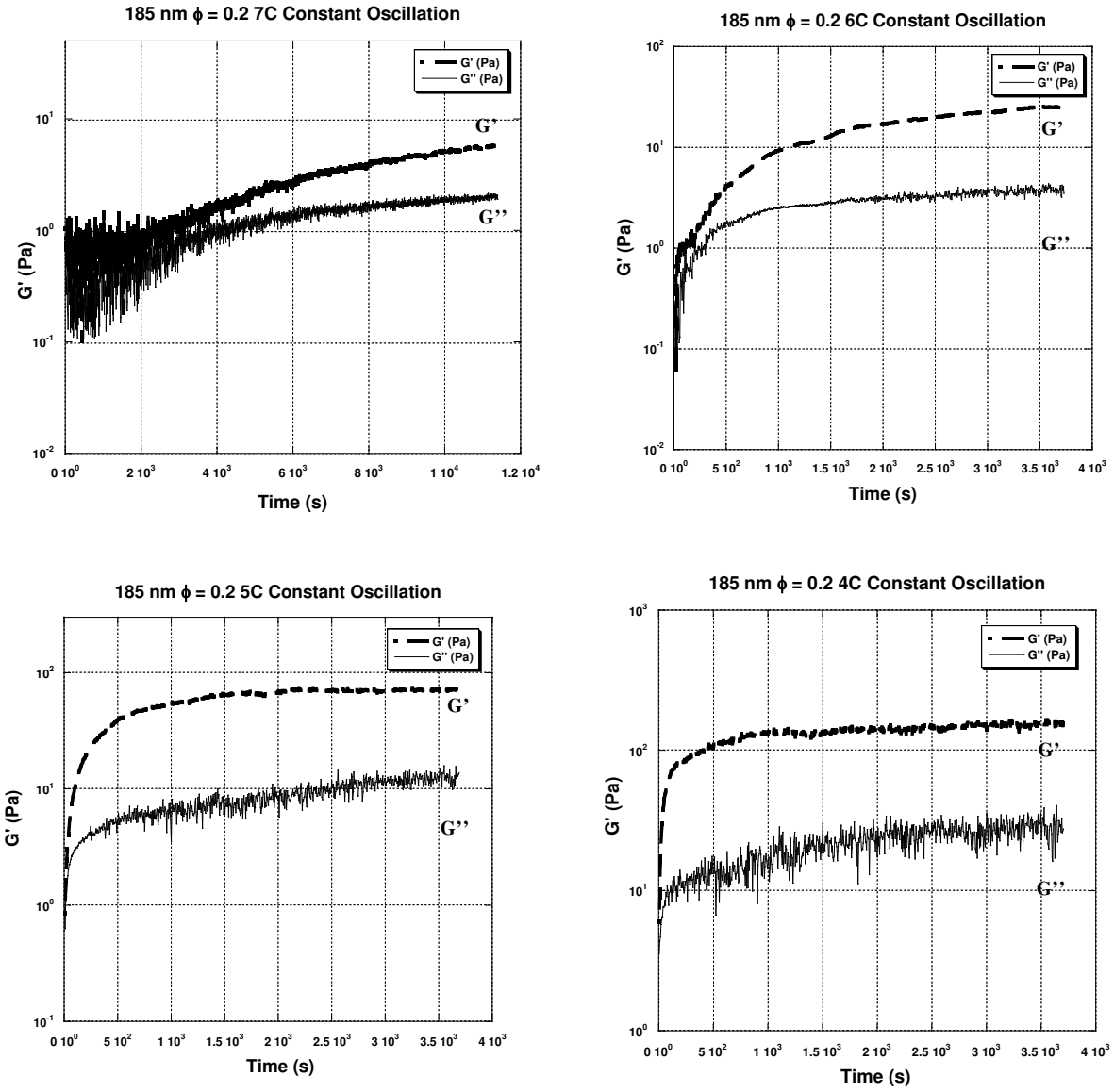

Figure C.13 - Growth of Elastic Modulus in Time for 185 nm particles, ϕ = 0.20

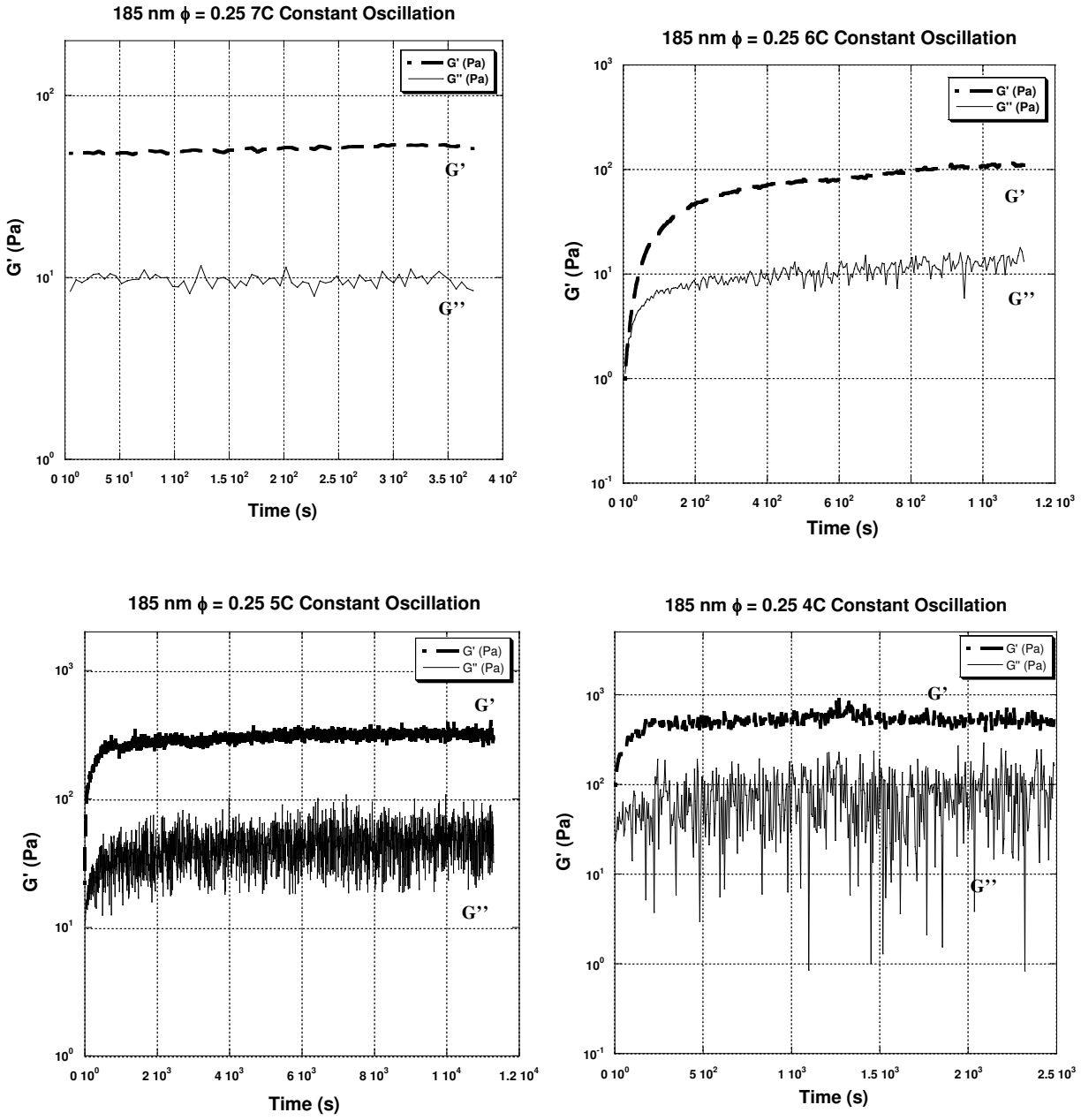

Figure C.14 - Growth of Elastic Modulus in Time for 185 nm particles, ϕ = 0.25

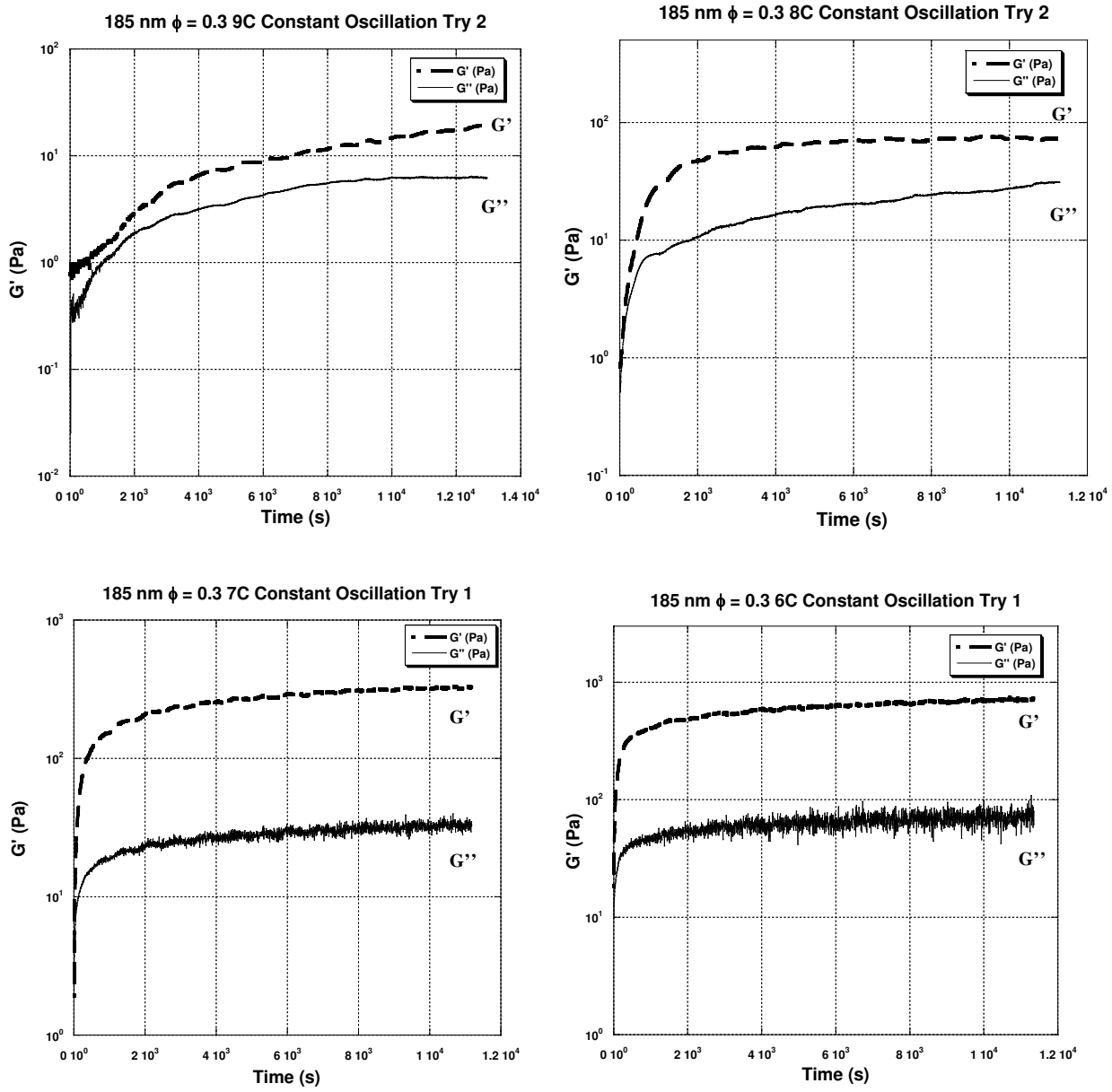

Figure C.15 - Growth of Elastic Modulus in Time for 185 nm particles, ϕ = 0.30

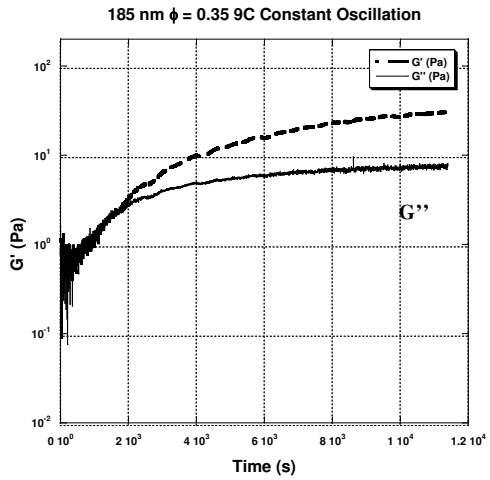

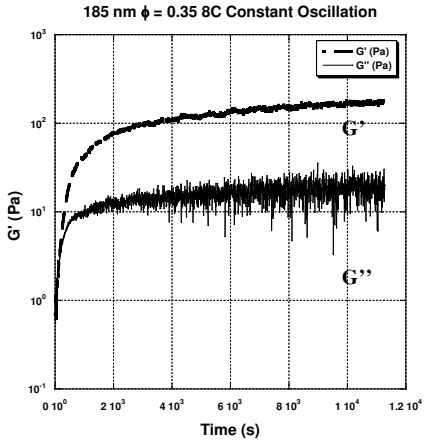

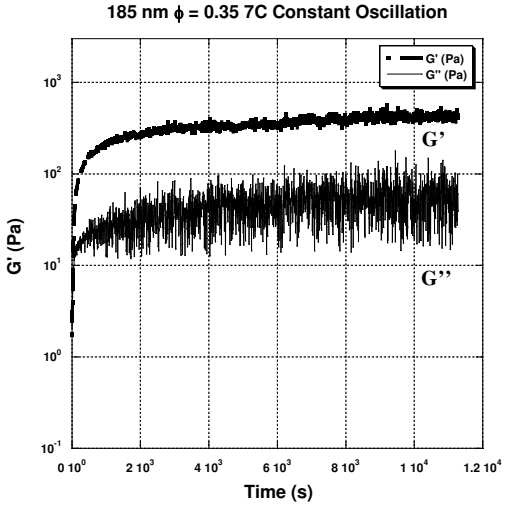

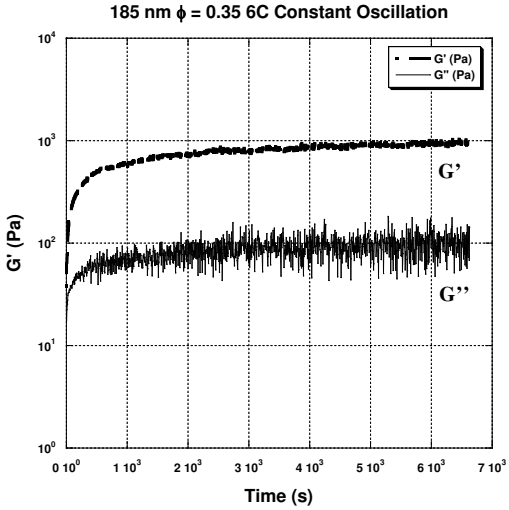

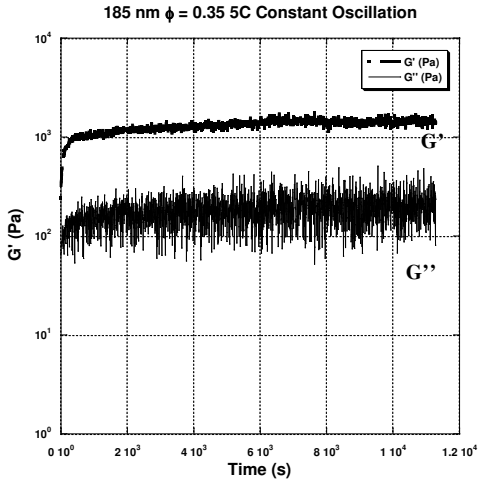

Figure C.16 - Growth of Elastic Modulus in Time for 185 nm particles, ϕ = 0.35

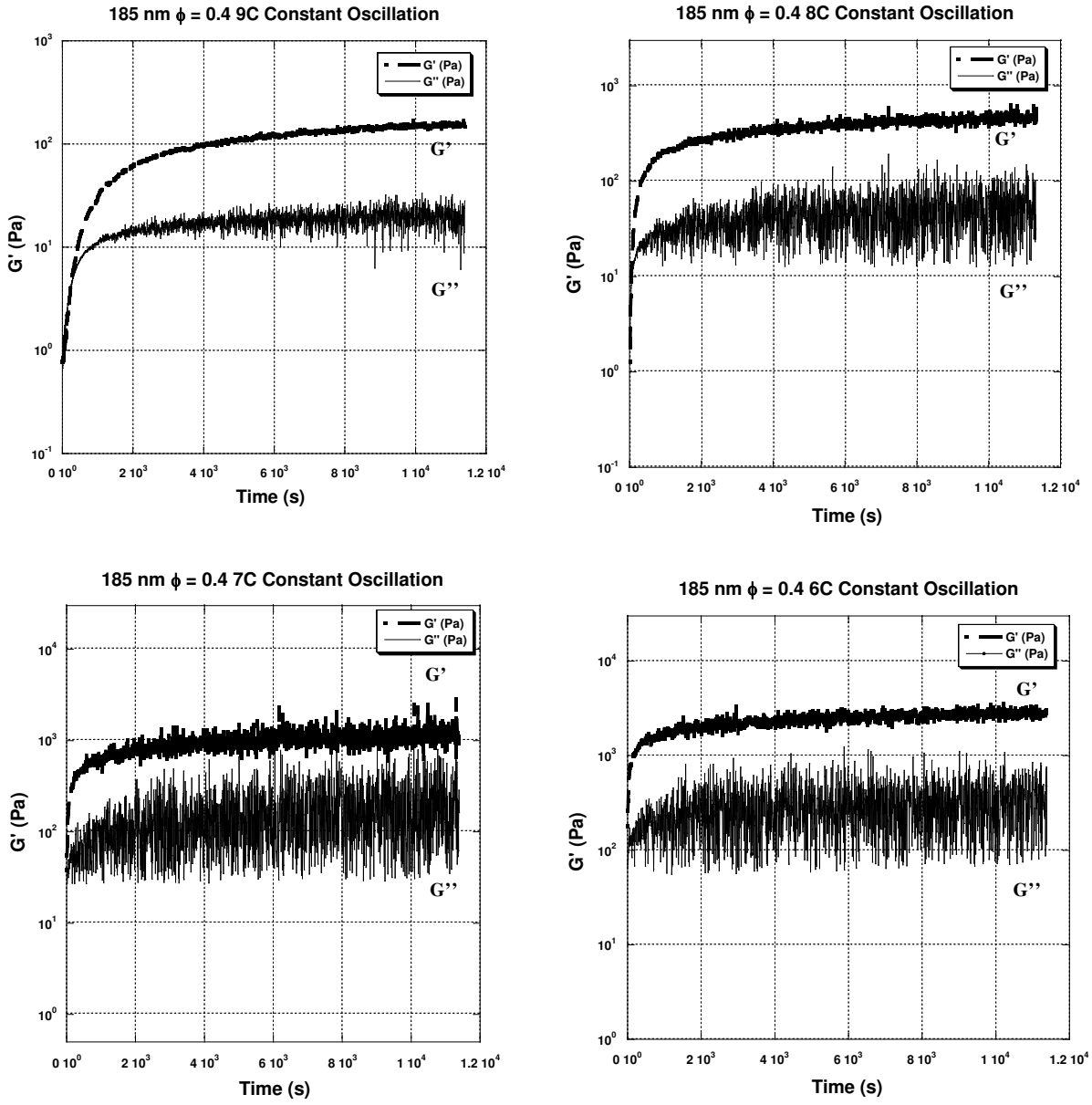

Figure C.17 - Growth of Elastic Modulus in Time for 185 nm particles, ϕ = 0.40

APPENDIX D

FREQUENCY SWEEPS

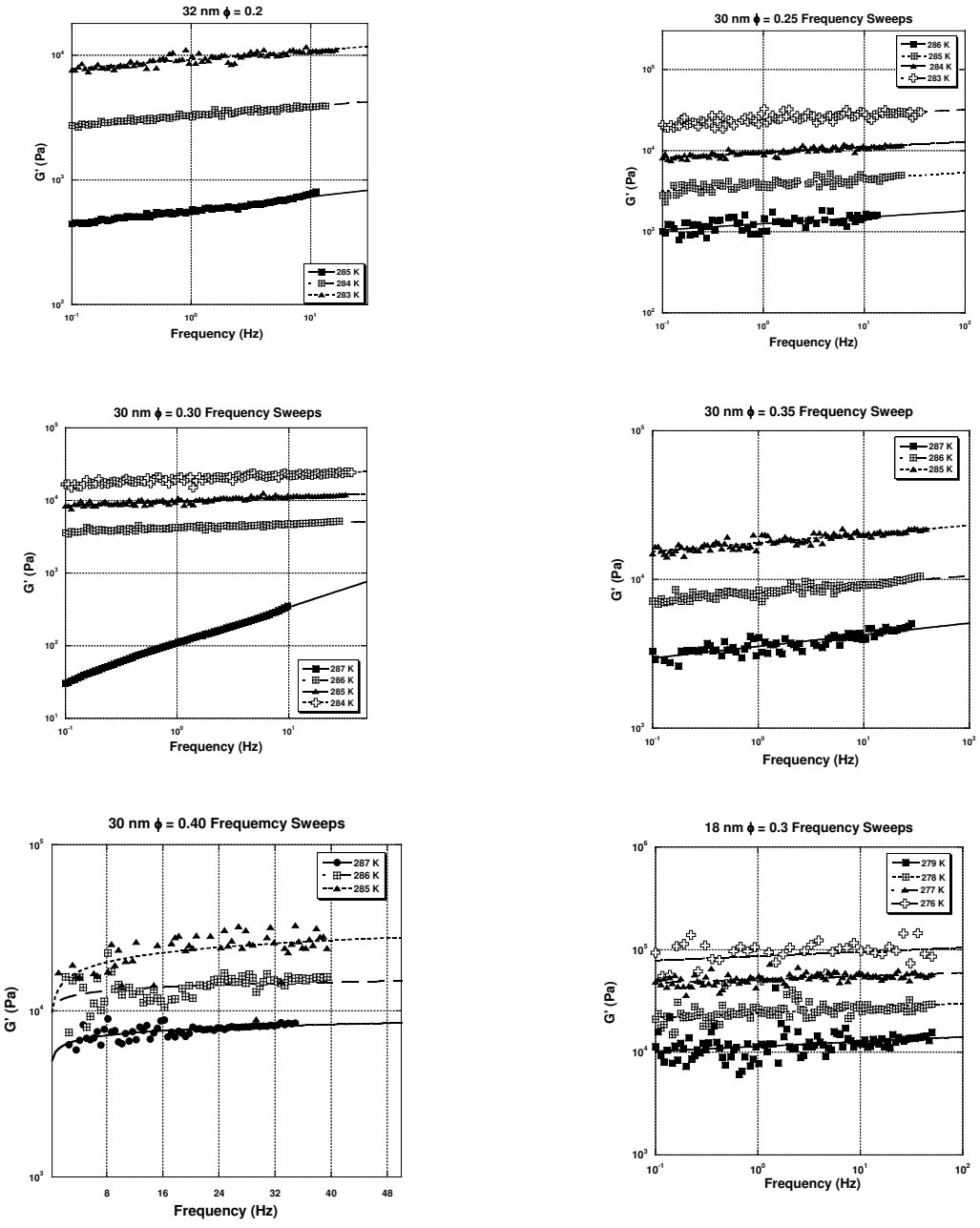

Figure D.1 – Frequency Sweeps for 30 nm and 18 nm particles at different temperatures and volume fractions. Symbols denote data points and the solid and dashed lines represent power law fits to experimental data.

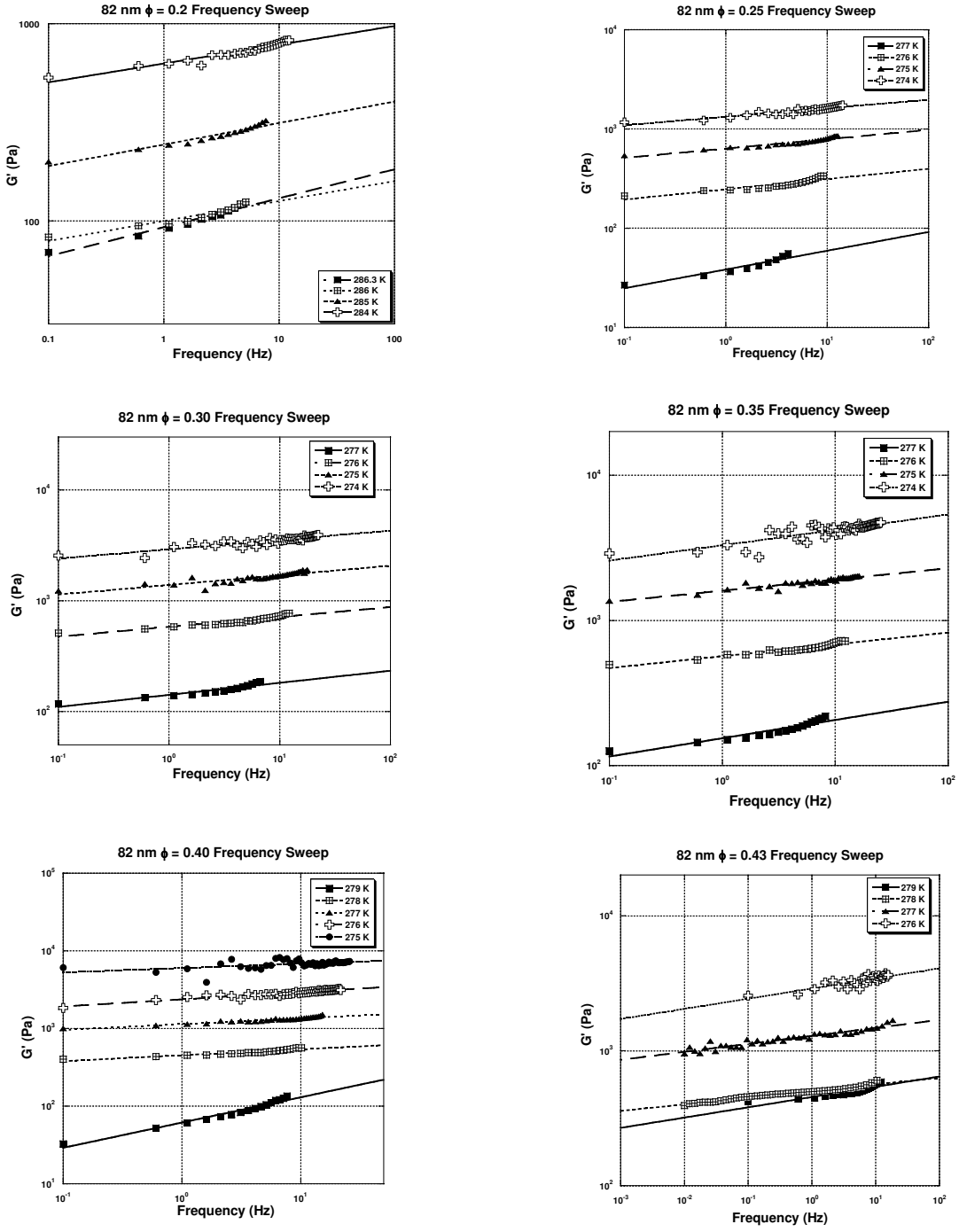

Figure D.2 – Frequency Sweeps for 82 nm particles at different temperatures and volume fractions. Symbols denote data points and the solid and dashed lines represent power law fits to experimental data.

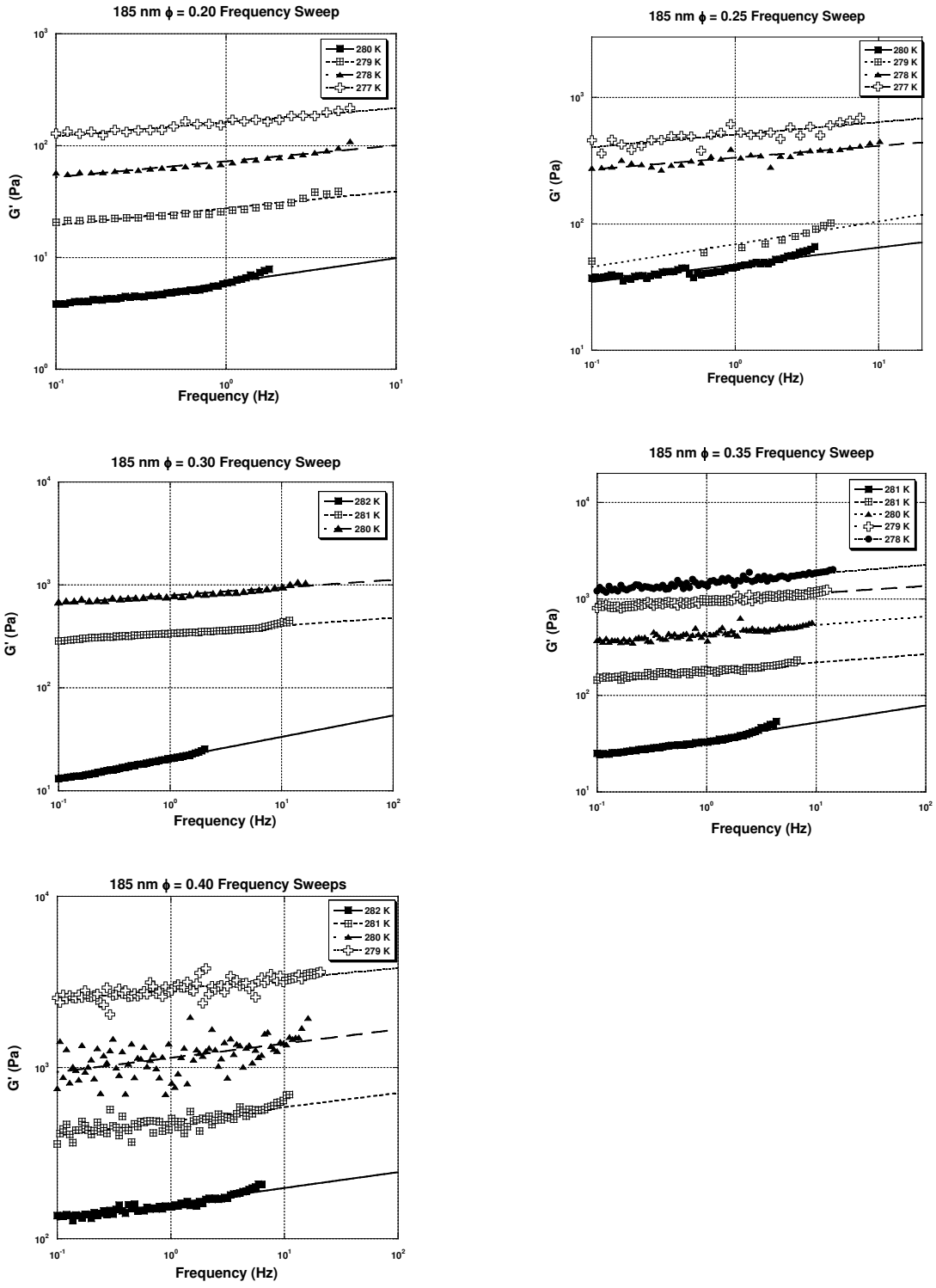

Figure D.3 – Frequency Sweeps for 185 nm particles at different temperatures and volume fractions. Symbols denote data points and the solid and dashed lines represent power law fits to experimental data.

APPENDIX E

YIELD STRESSES

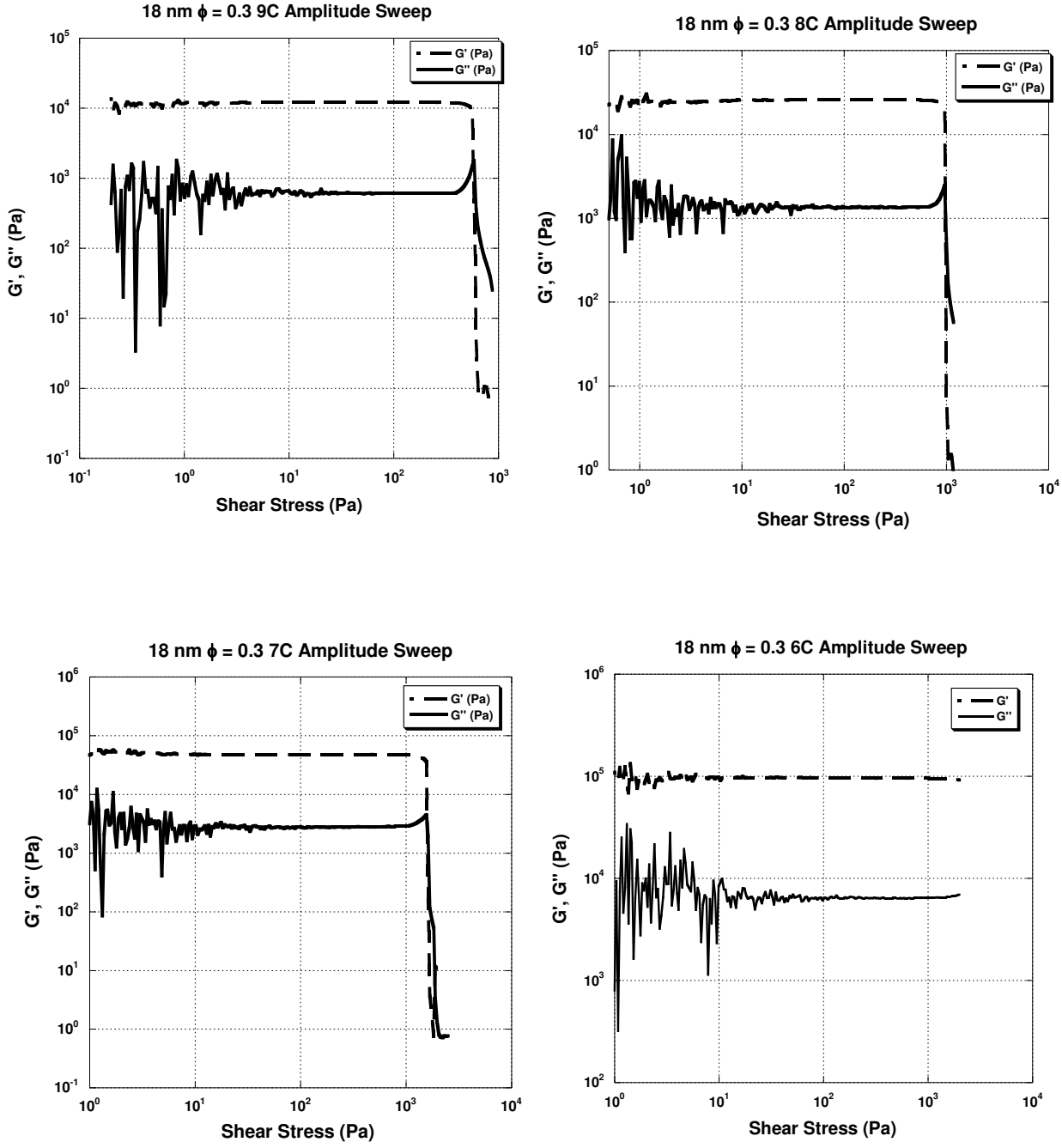

Figure E.1 – Amplitude Sweep plot for 18 nm particles, $\phi = 0.30$

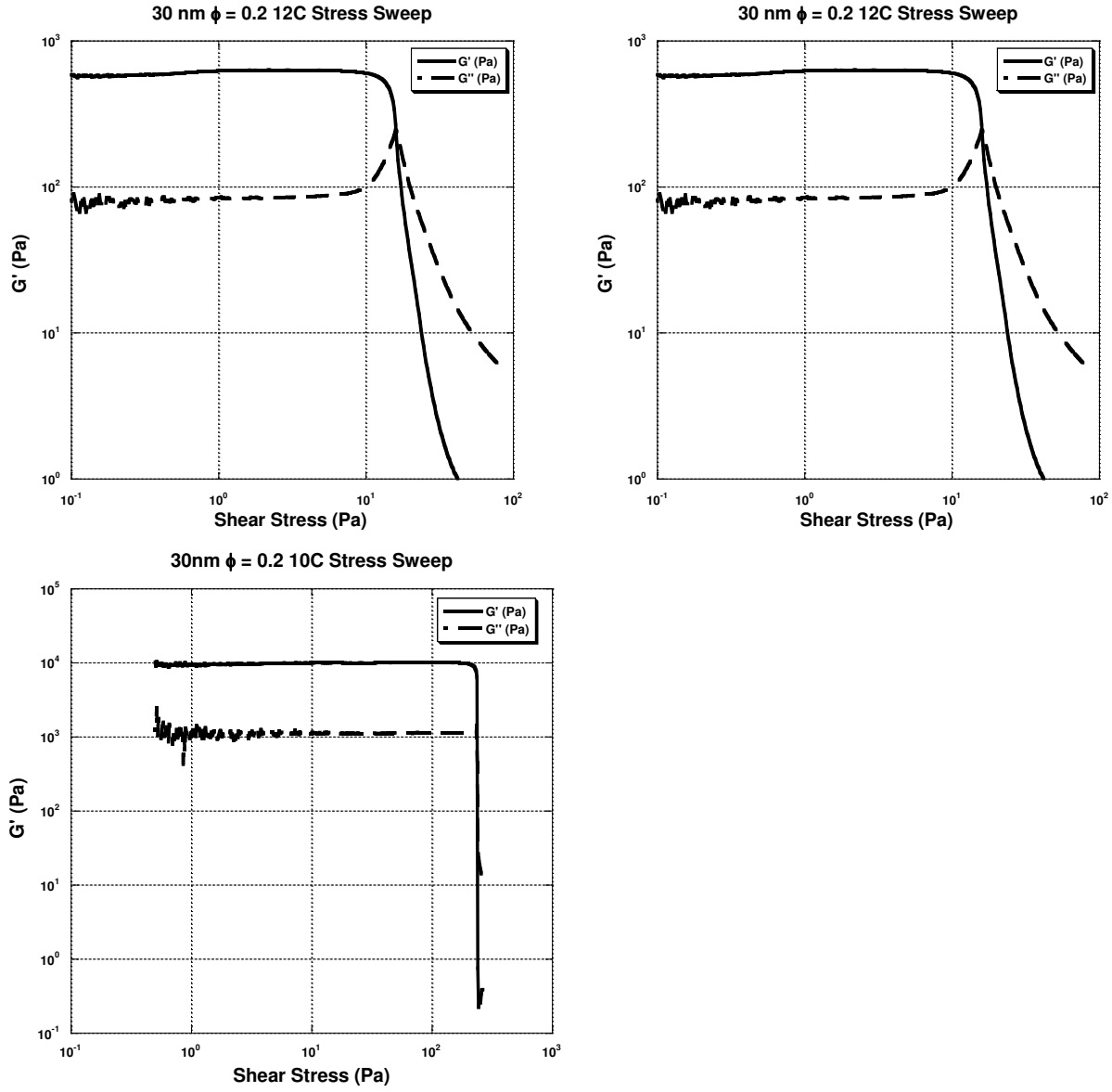

Figure E.2 – Amplitude Sweep plot for 30 nm particles, $\phi = 0.20$

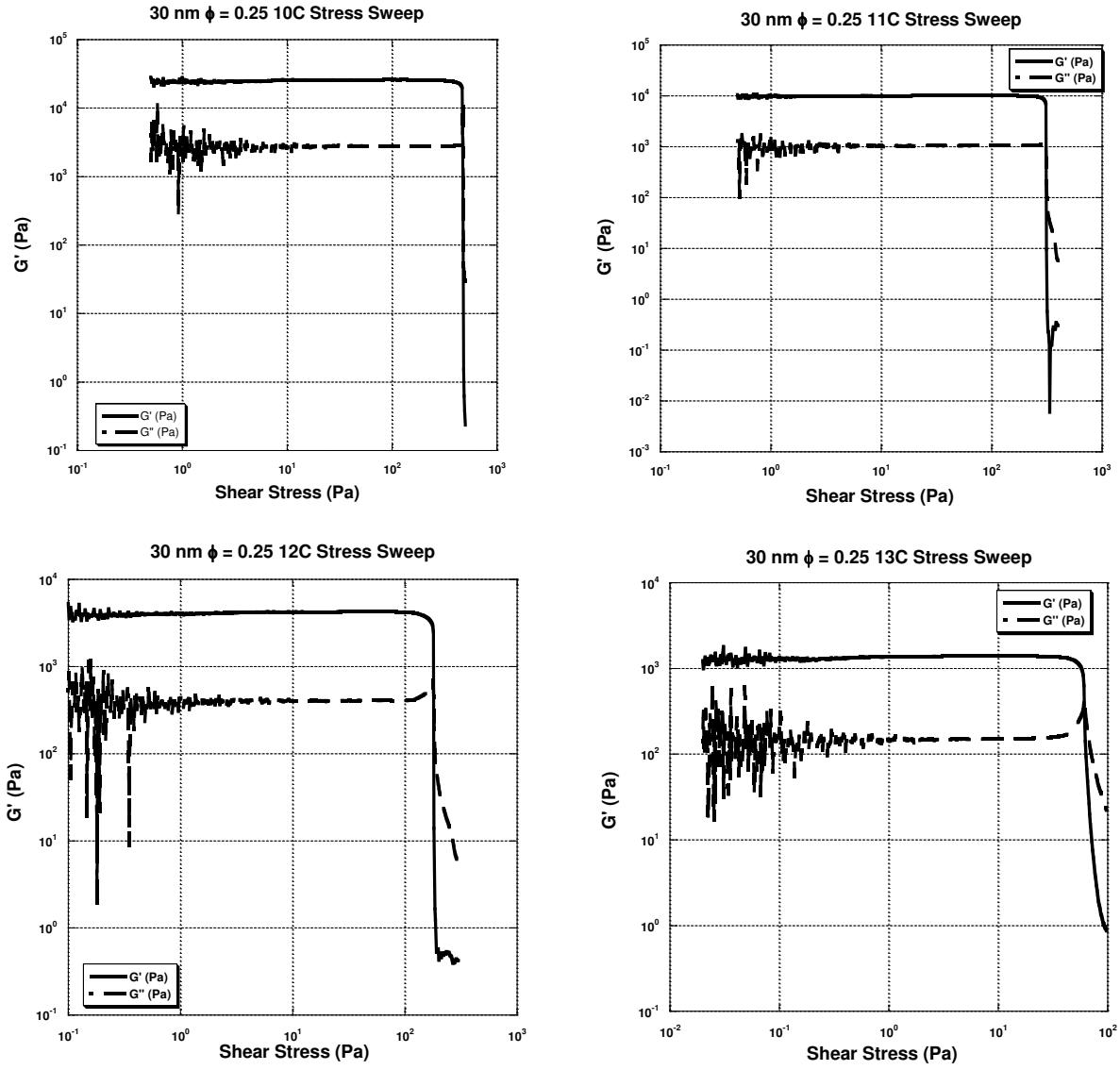

Figure E.3 – Amplitude Sweep plot for 30 nm particles, ϕ = 0.25

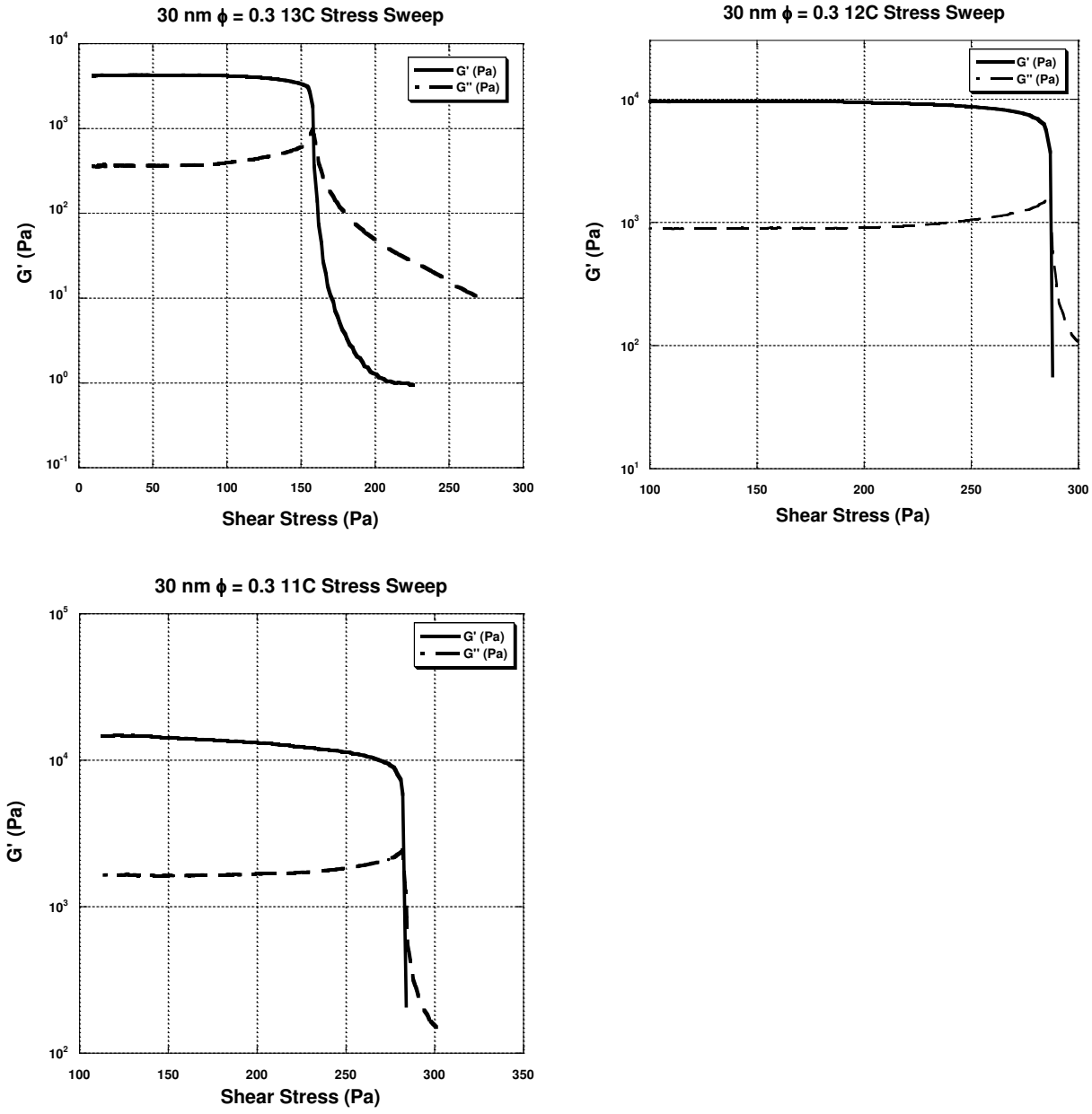

Figure E.4 – Amplitude Sweep plot for 30 nm particles, ϕ = 0.30

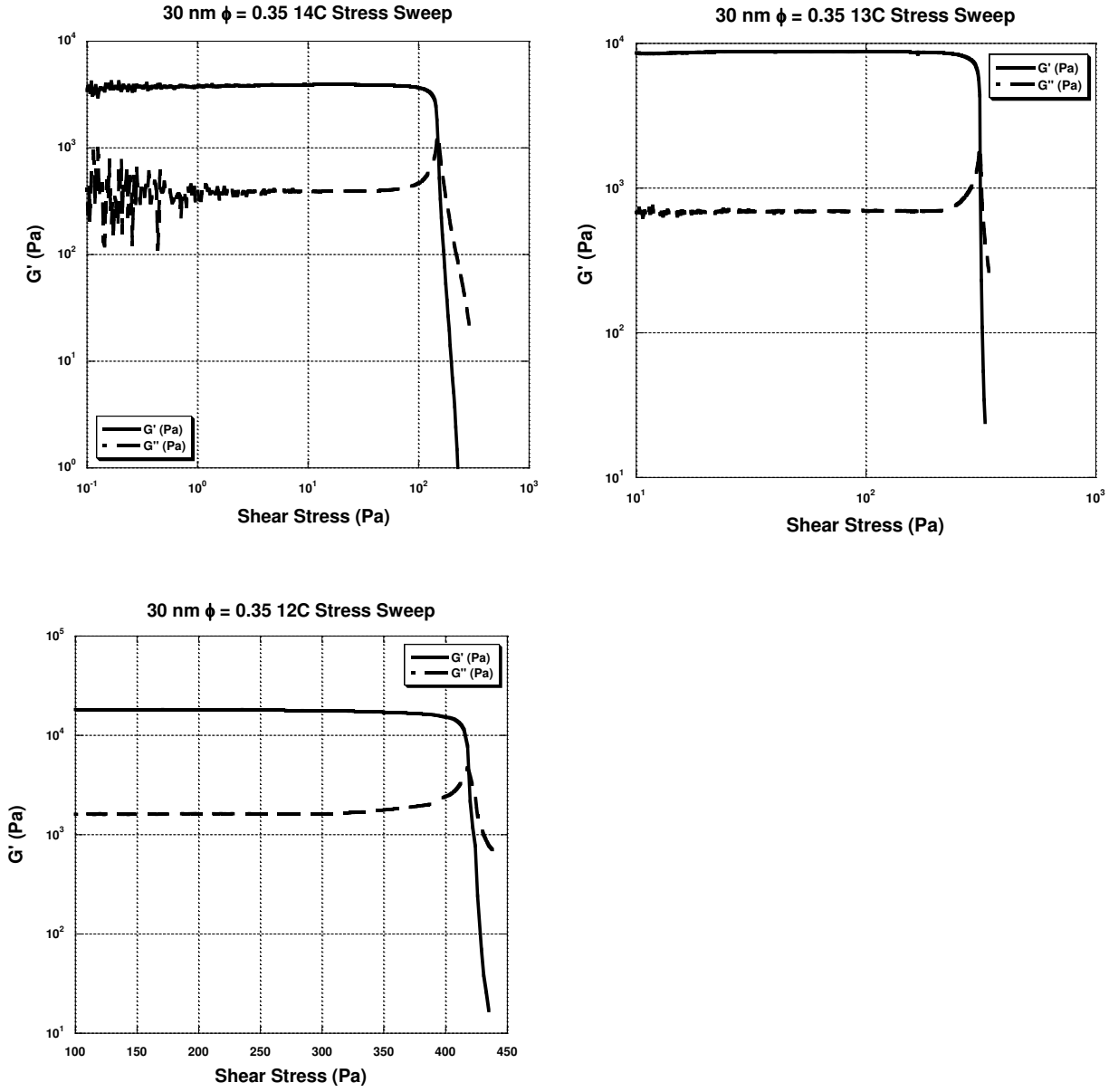

Figure E.5 – Amplitude Sweep plot for 30 nm particles, ϕ = 0.35

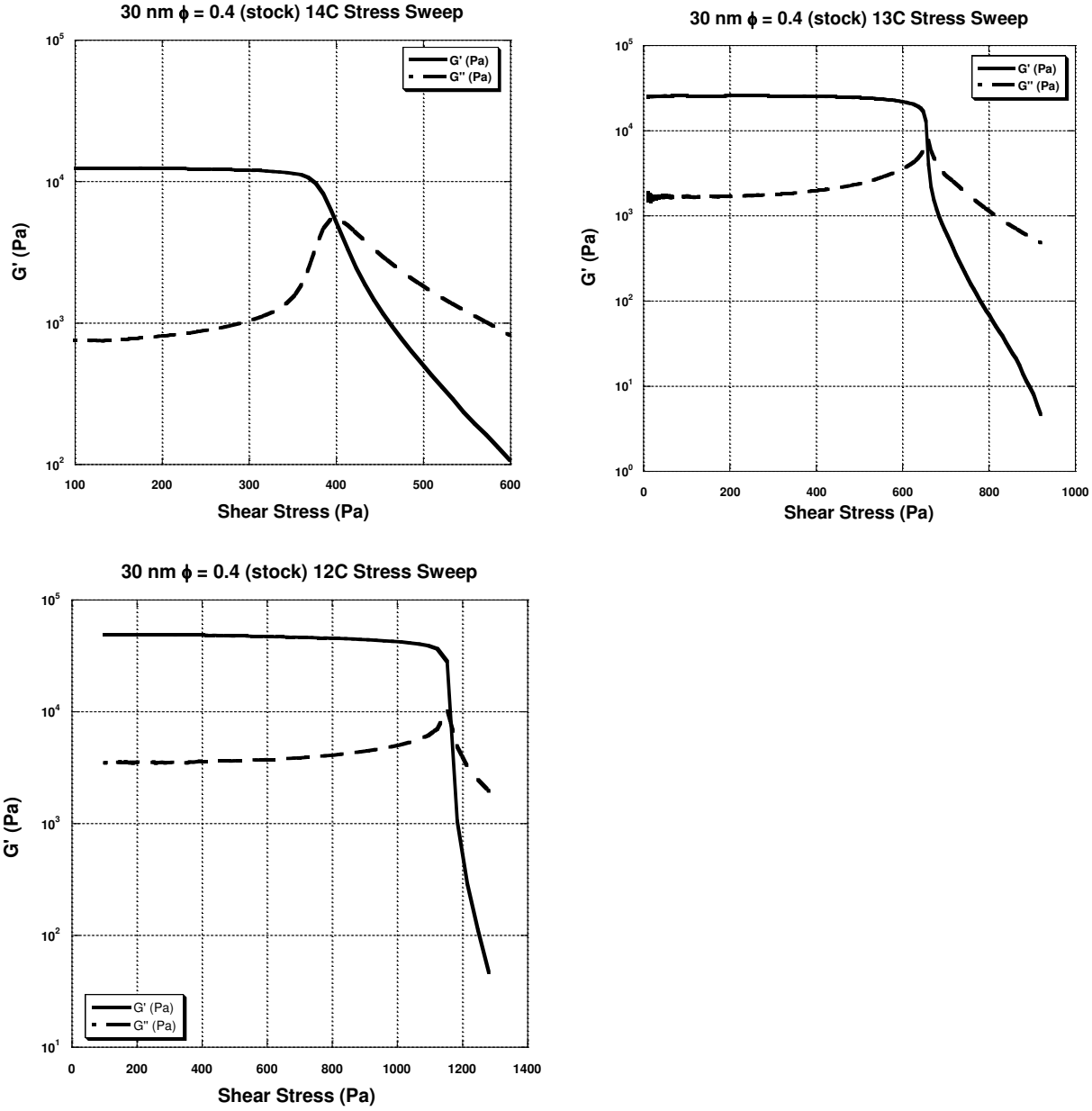

Figure E.6 – Amplitude Sweep plot for 30 nm particles, ϕ = 0.40

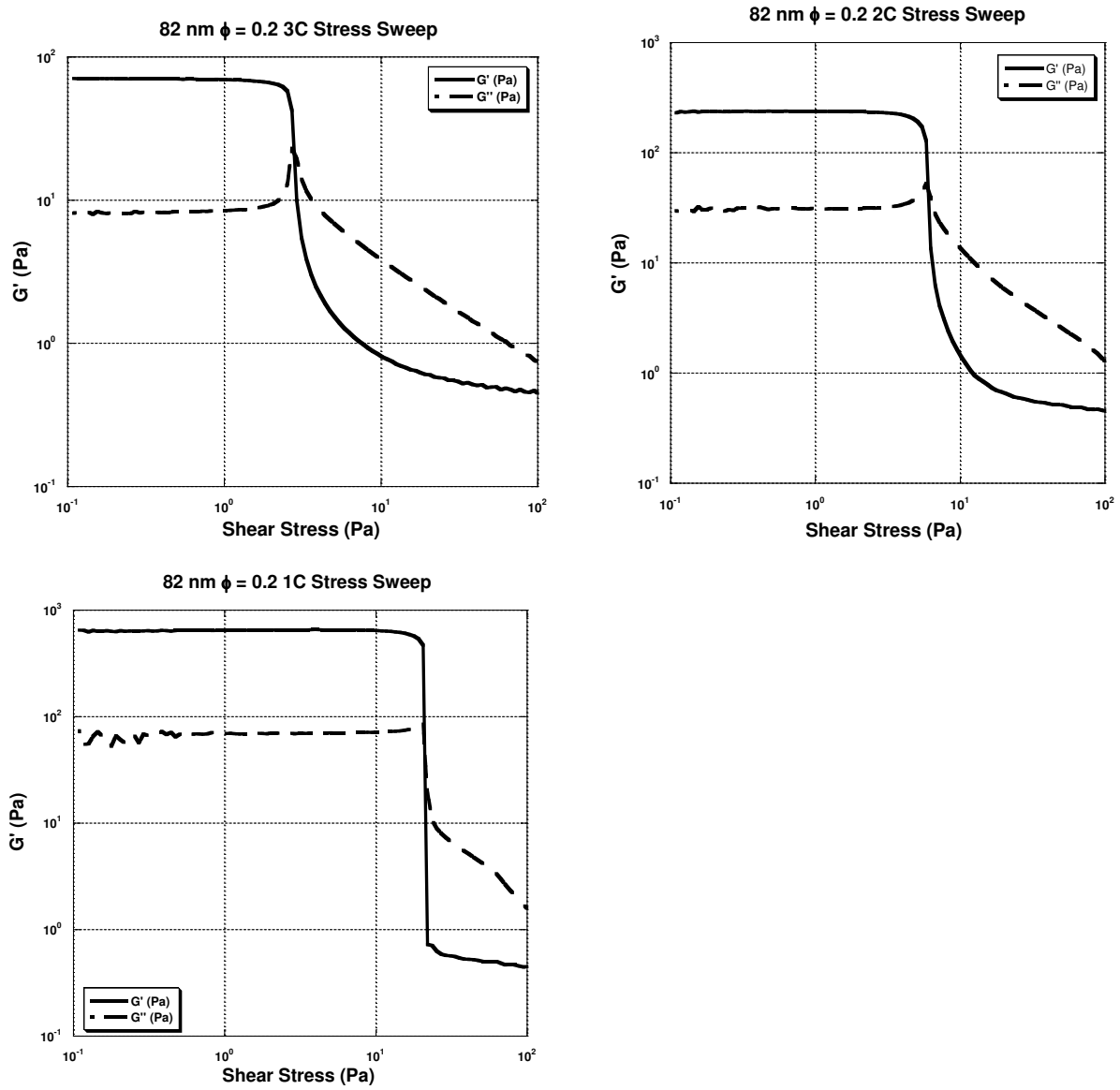

Figure E.7 – Amplitude Sweep plot for 82 nm particles, ϕ = 0.2

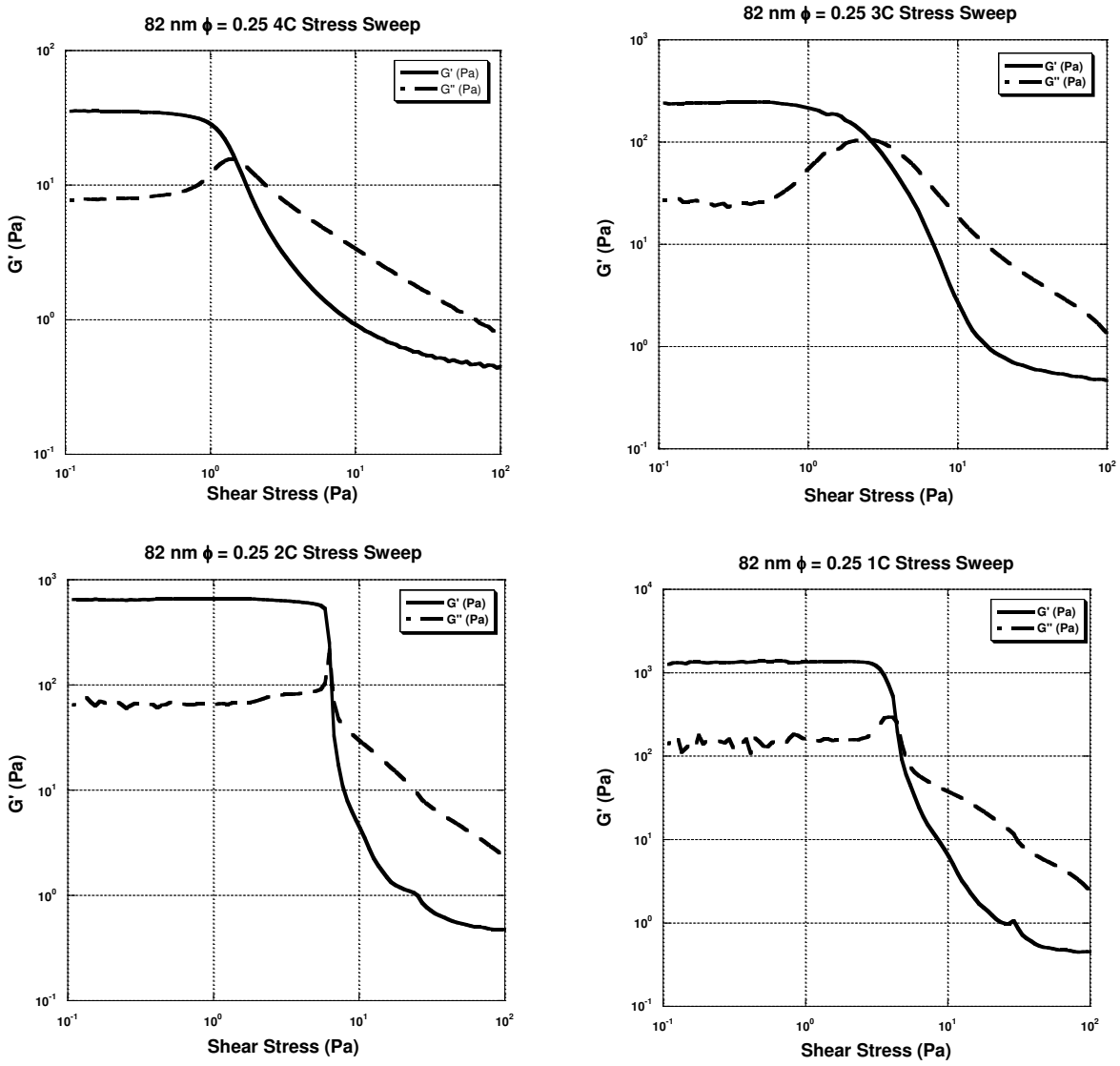

Figure E.8 – Amplitude Sweep plot for 82 nm particles, ϕ = 0.25

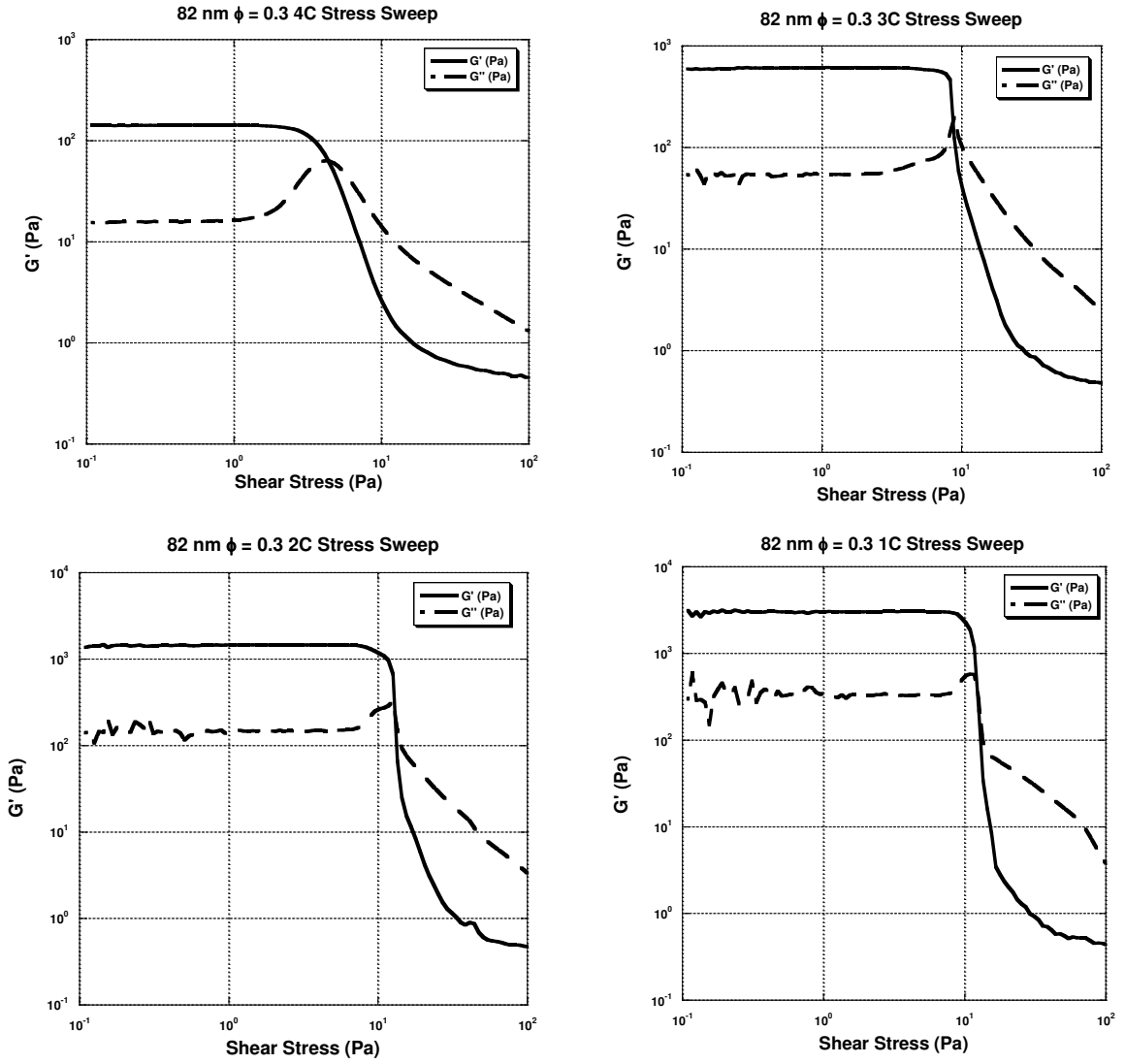

Figure E.9 – Amplitude Sweep plot for 82 nm particles, ϕ = 0.30

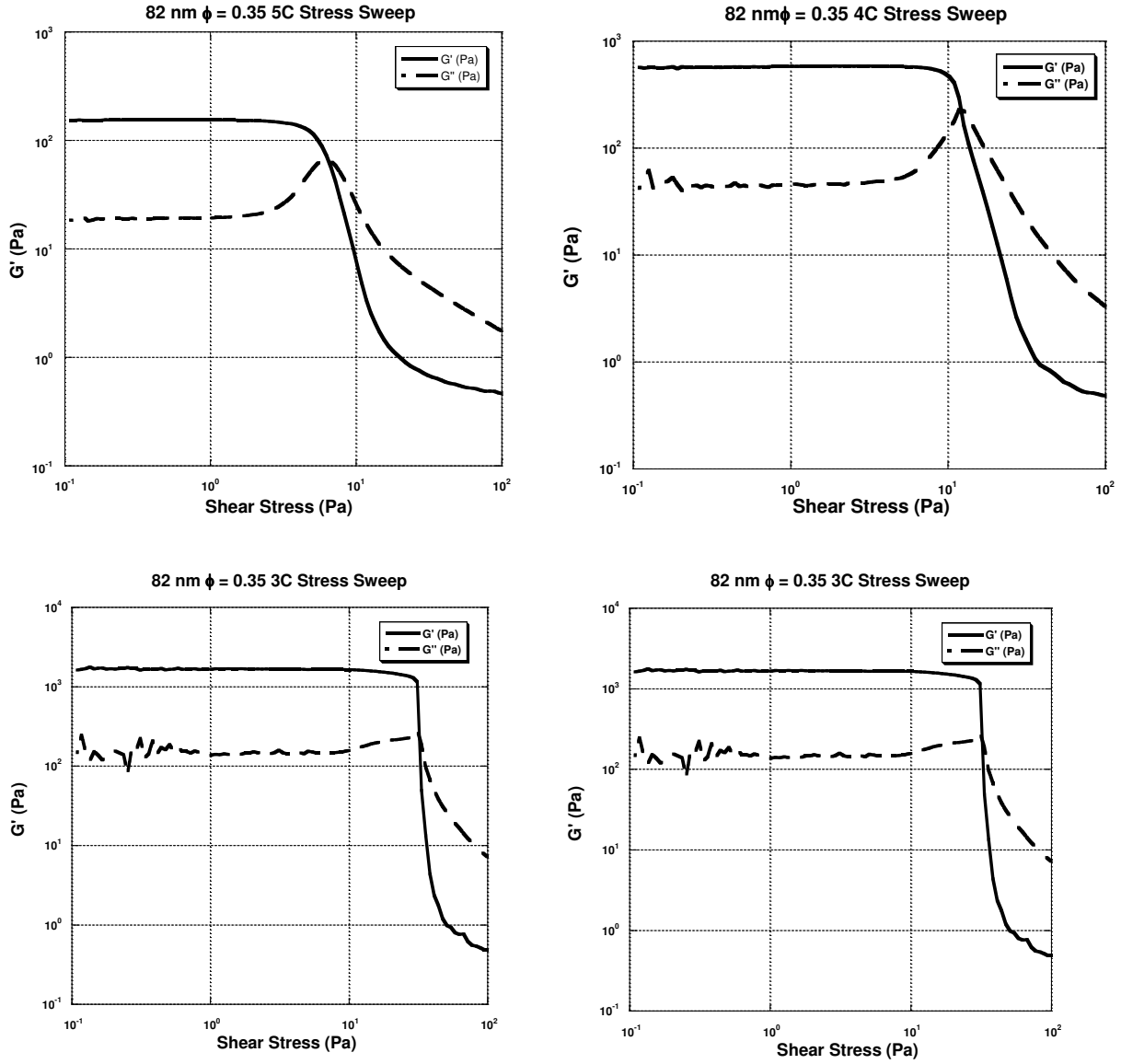

Figure E.10 – Amplitude Sweep plot for 82 nm particles, ϕ = 0.35

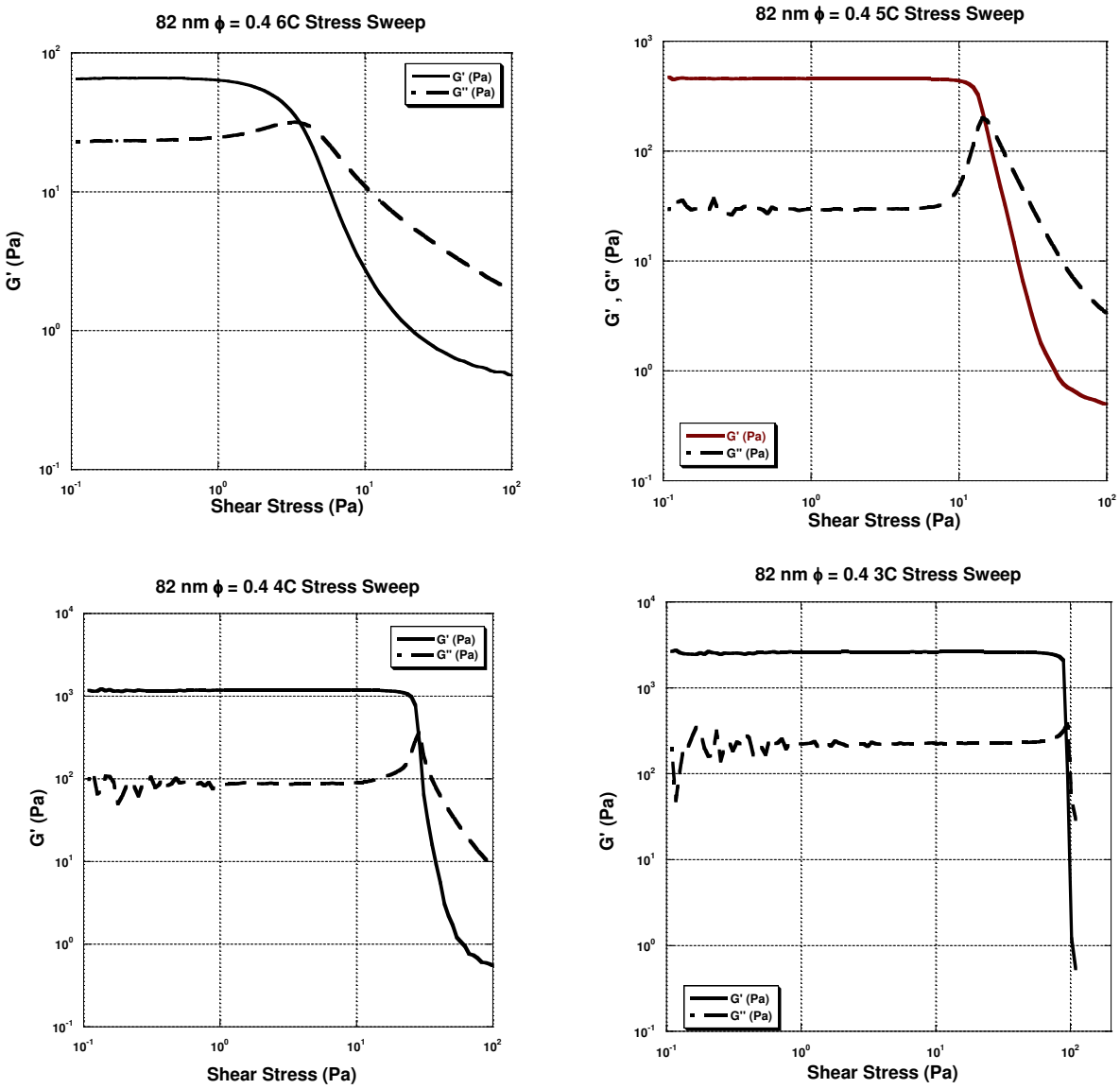

Figure E.11 – Amplitude Sweep plot for 82 nm particles, ϕ = 0.40

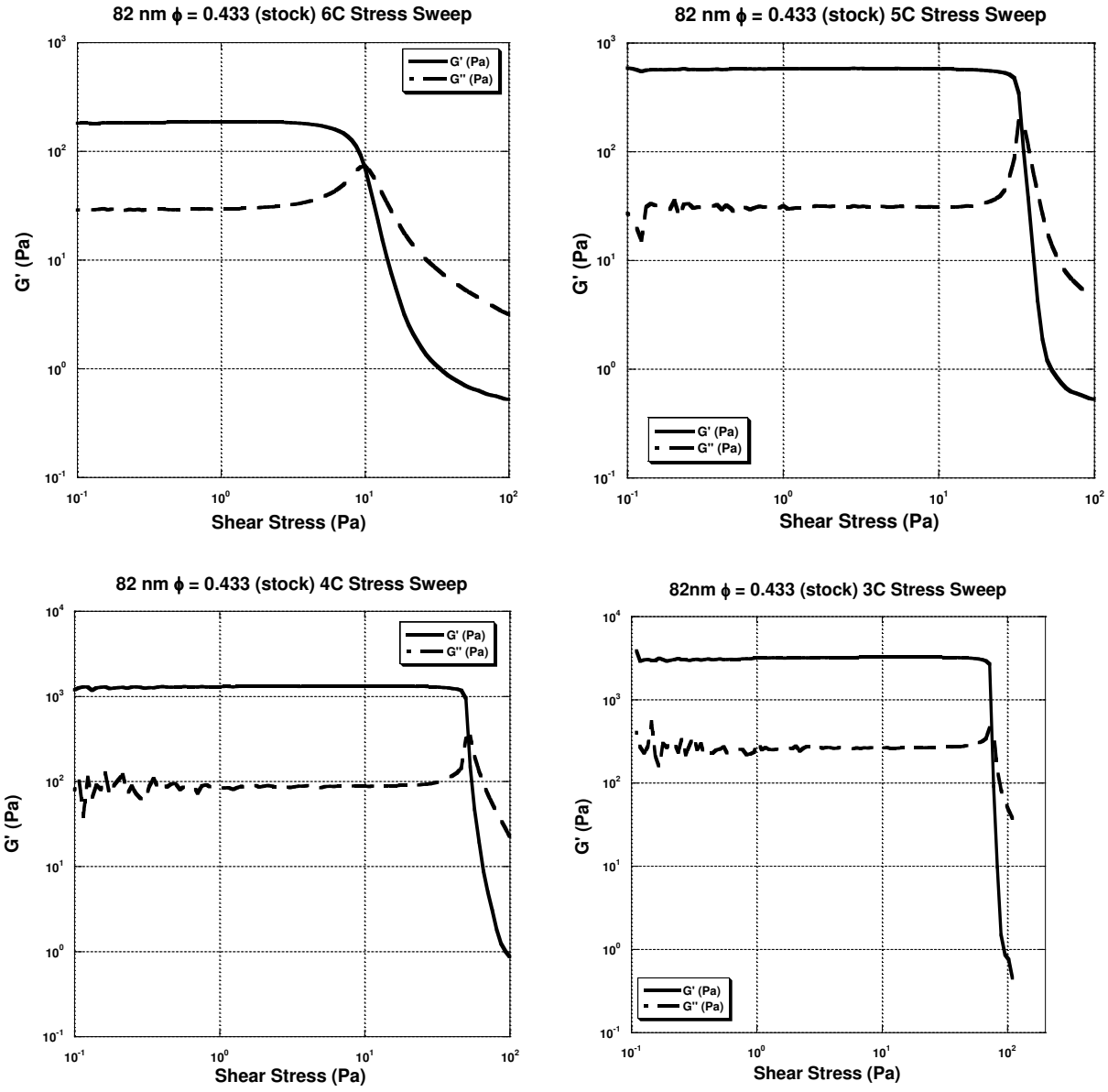

Figure E.12 – Amplitude Sweep plot for 82 nm particles, ϕ = 0.43

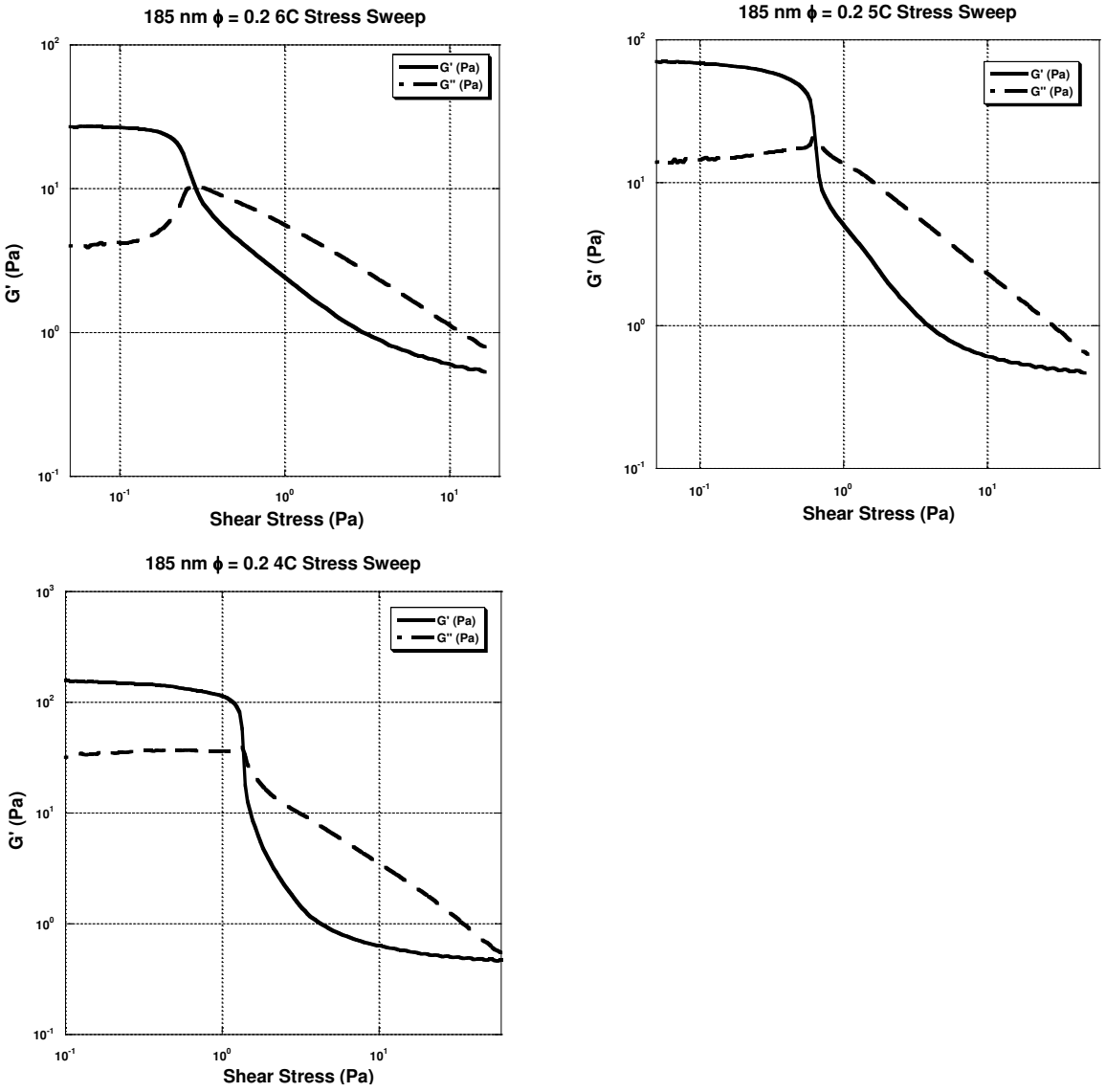

Figure E.13 – Amplitude Sweep plot for 185 nm particles, ϕ = 0.20

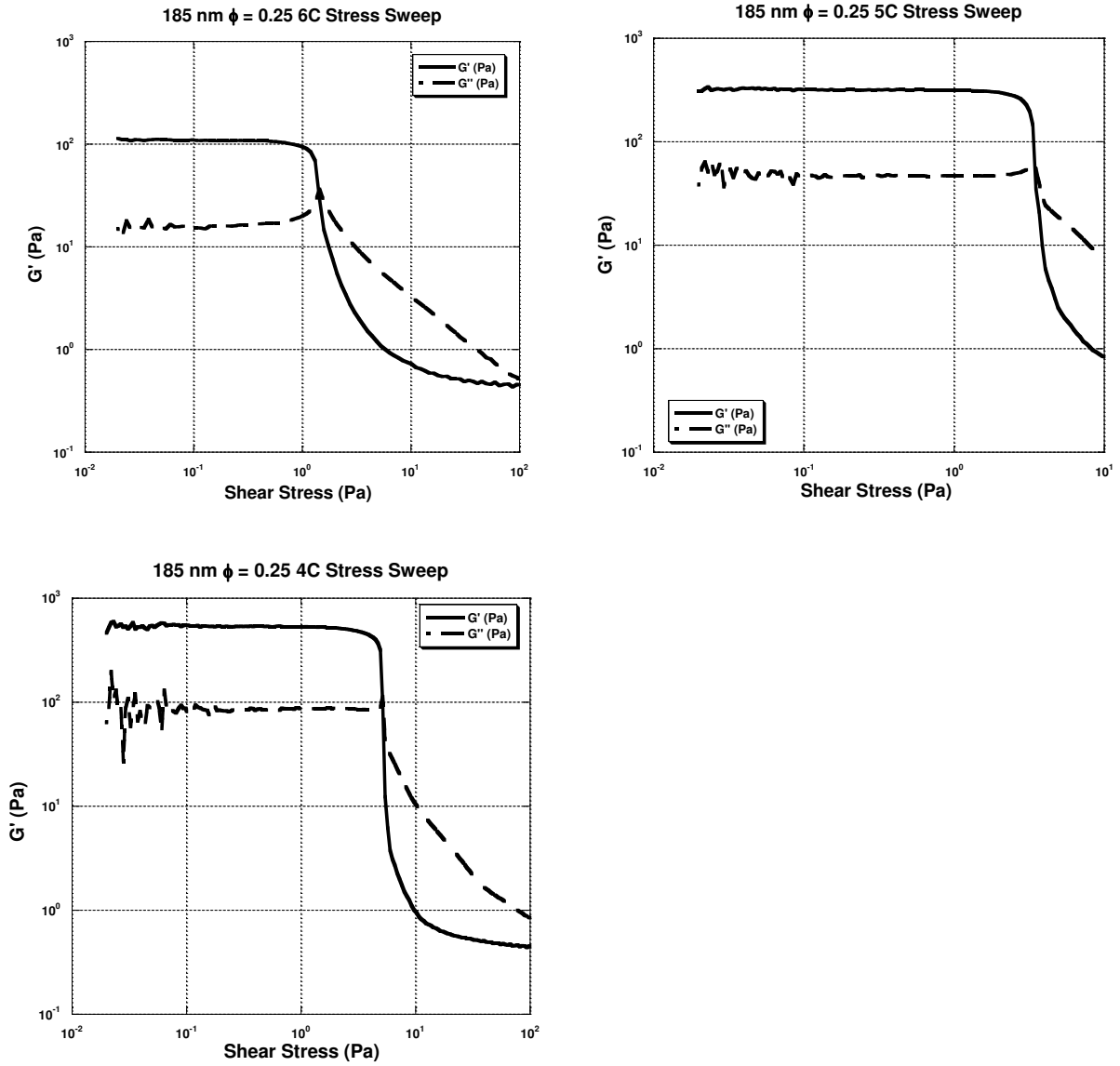

Figure E.14 – Amplitude Sweep plot for 185 nm particles, ϕ = 0.25

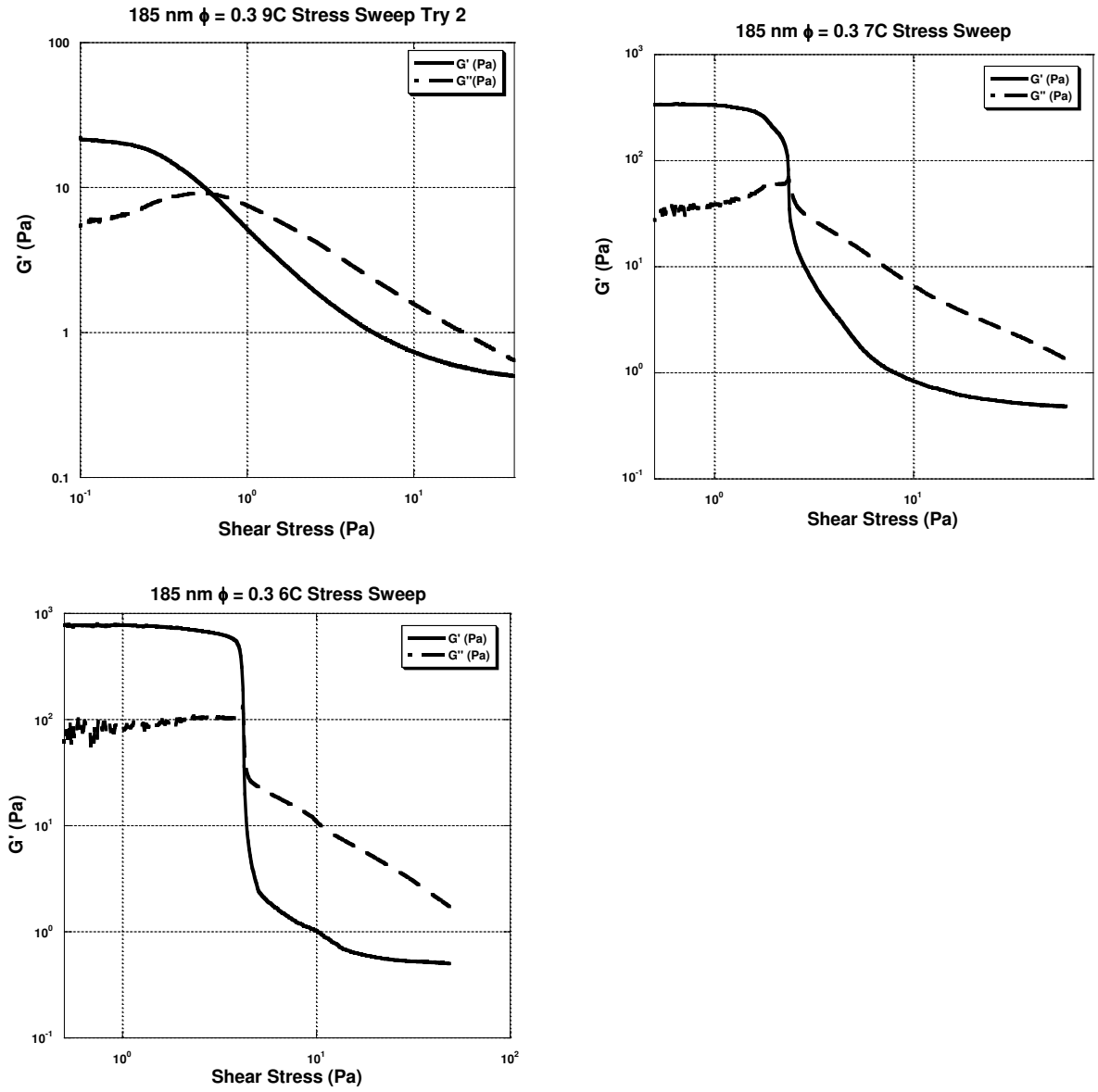

Figure E.15 – Amplitude Sweep plot for 185 nm particles, ϕ = 0.30

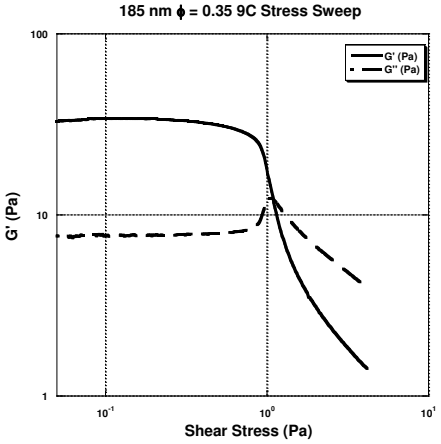

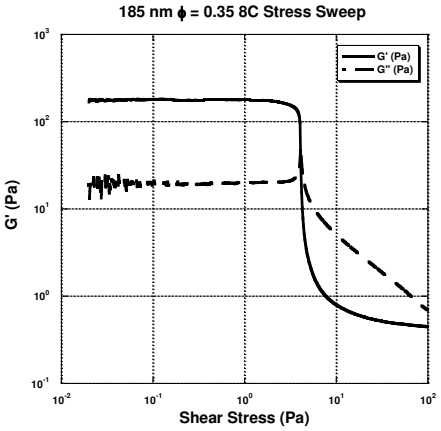

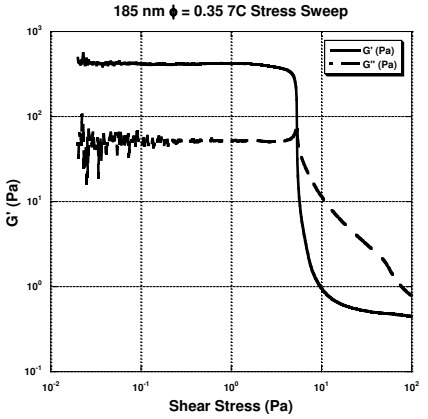

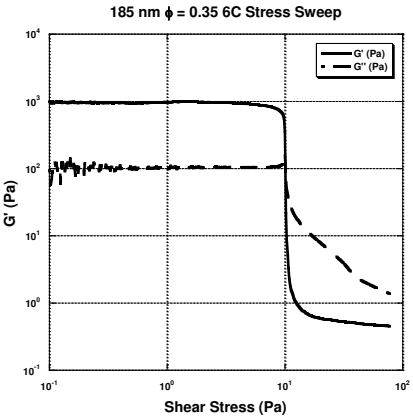

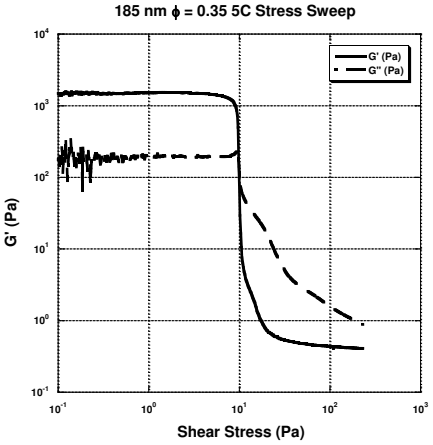

Figure E.16 – Amplitude Sweep plot for 185 nm particles, ϕ = 0.35

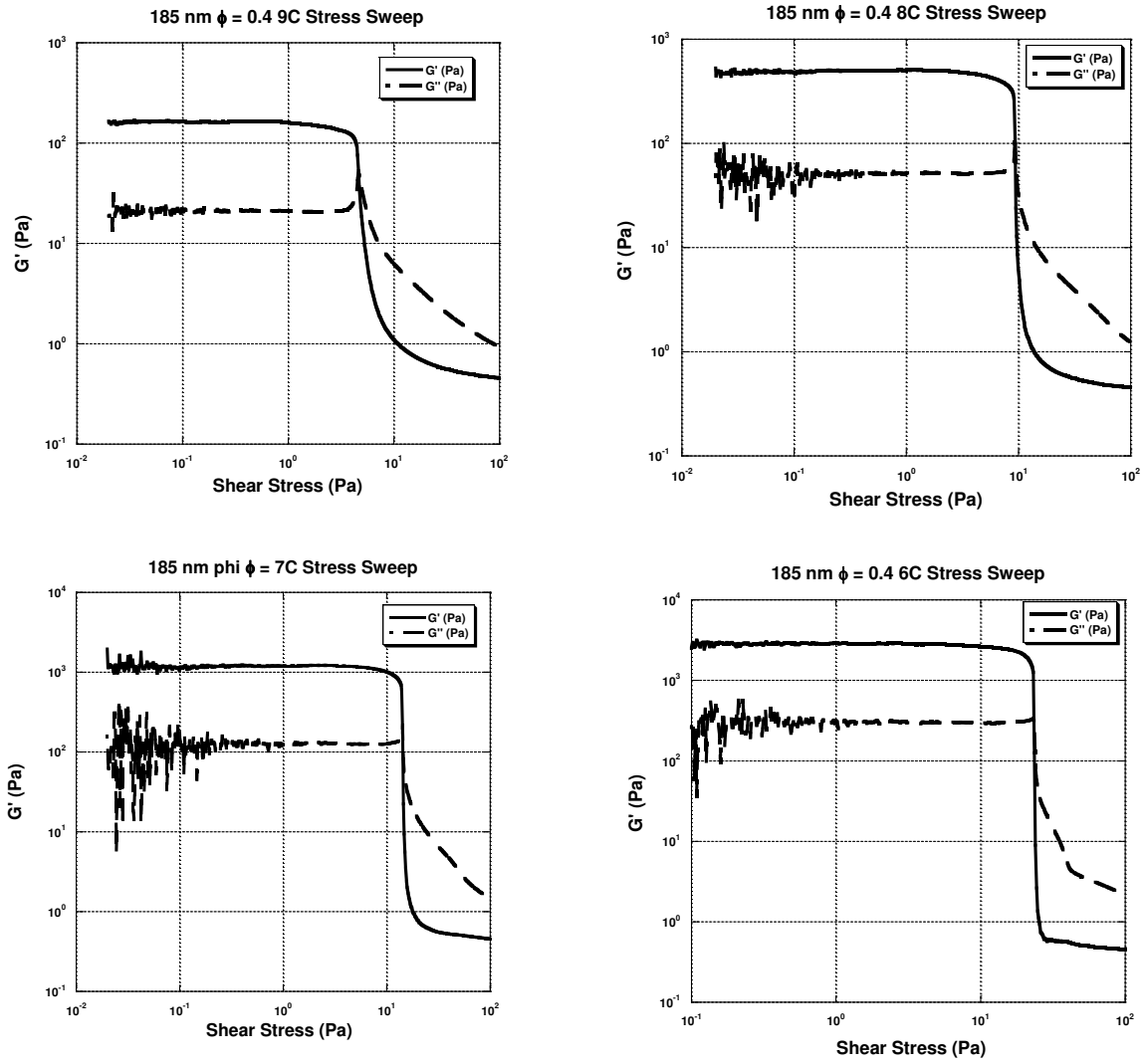

Figure E.17 – Amplitude Sweep plot for 185 nm particles, ϕ = 0.40

APPENDIX F

SCALING DATA FOR DIFFERENT PARTICLE SIZES

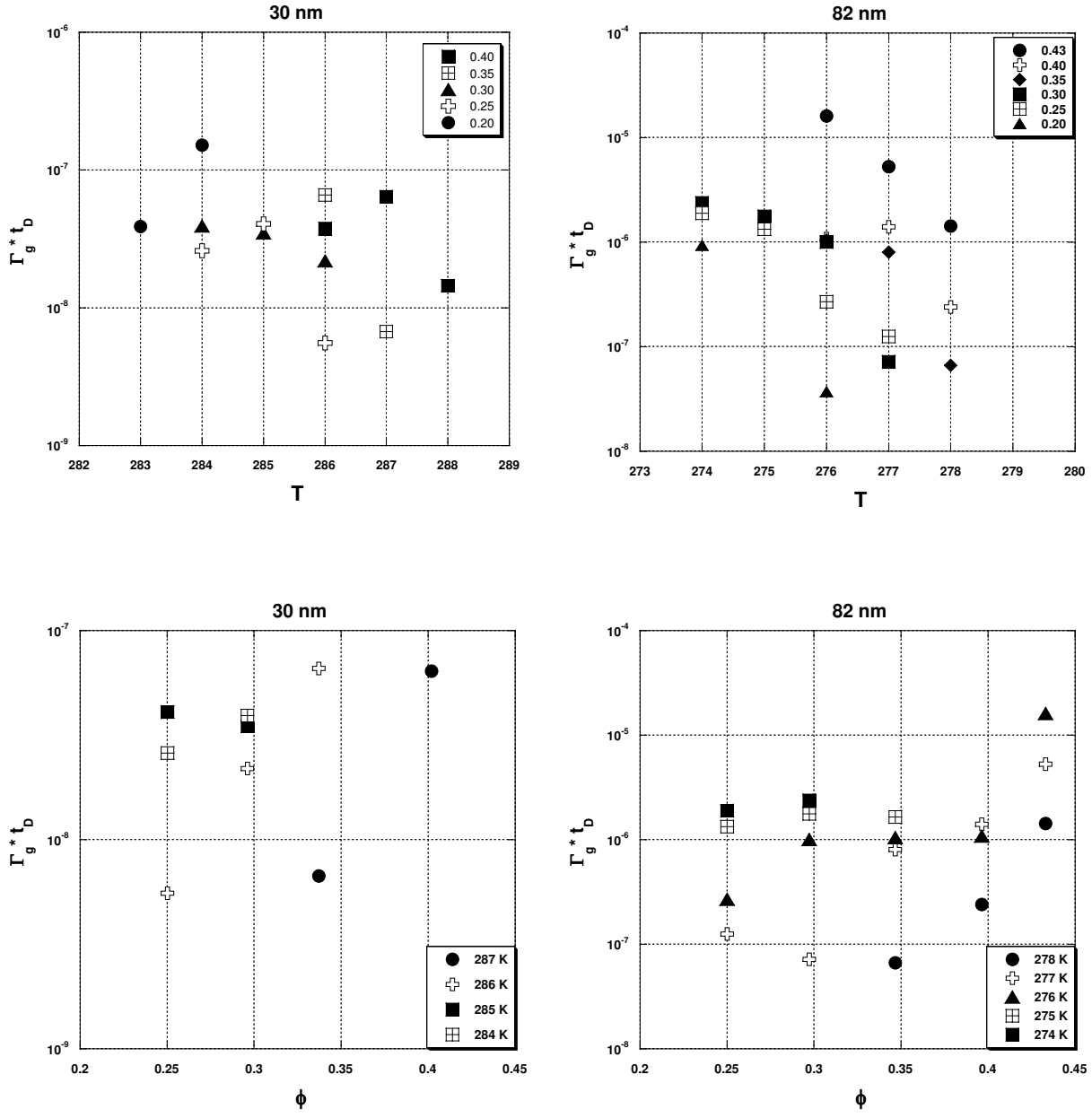

Figure F.1 - $\Gamma_g t_D$ vs Temperature and Volume Fraction for 30 nm and 82 nm particles respectively

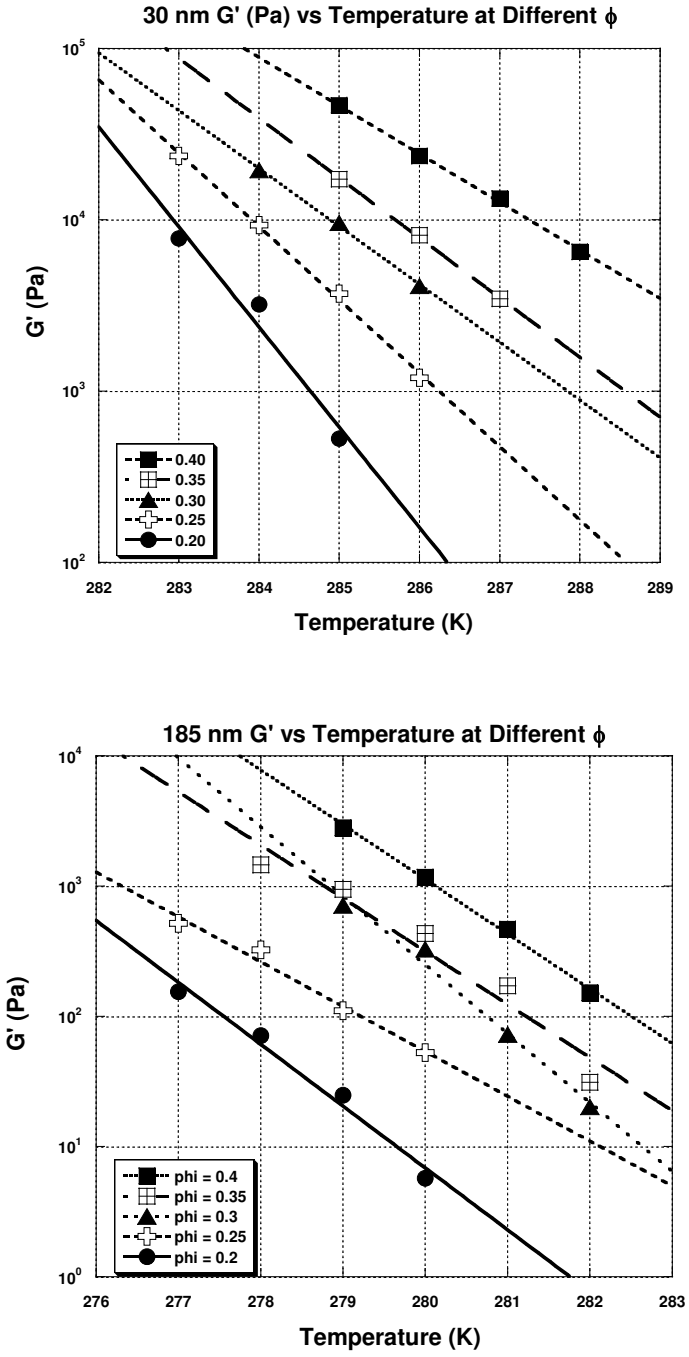

Figure F.2 – G' vs Temperature for 30 nm and 185 nm particles at different volume fractions respectively. Symbols represent experimental data points while the solid and dashed lines represent exponential fits to data.

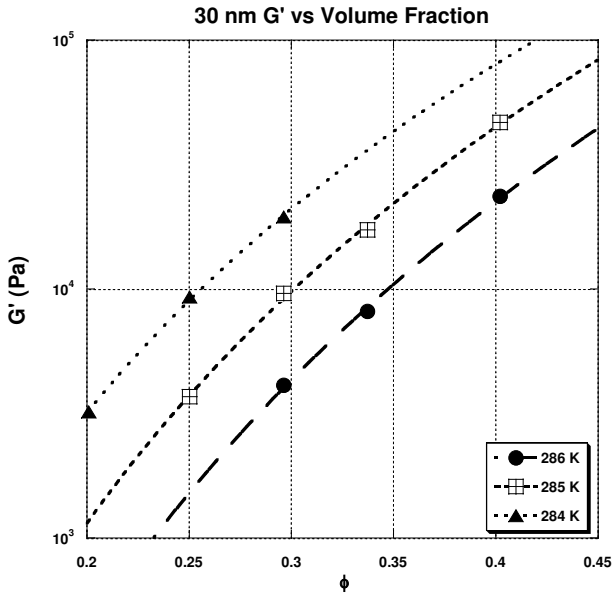

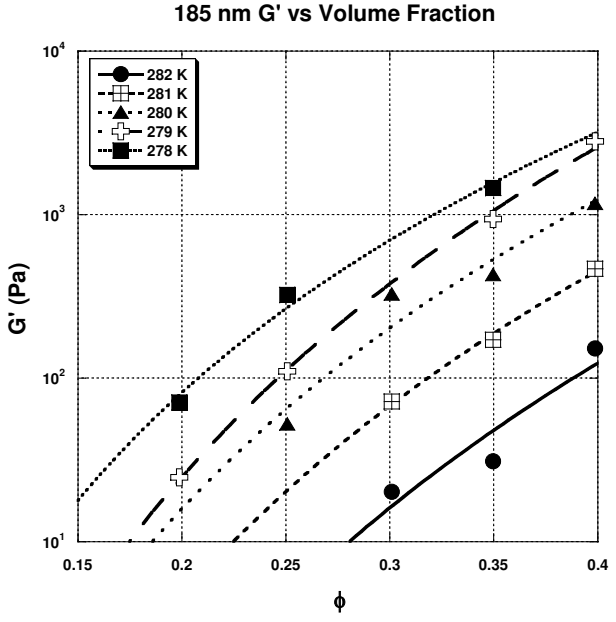

Figure F.3 – G' vs Volume fraction for 30 nm and 185 nm particles at different temperatures respectively. Symbols represent experimental data points while the solid and dashed lines represent power law fits to data.

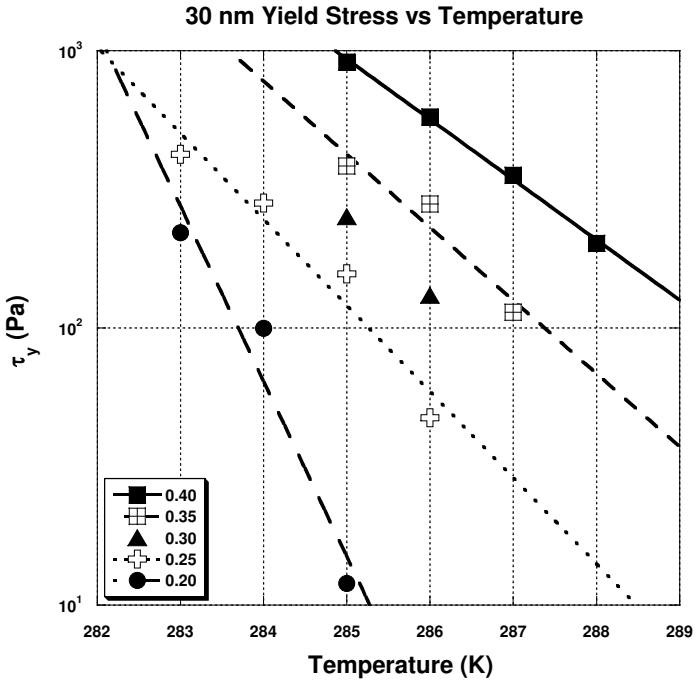

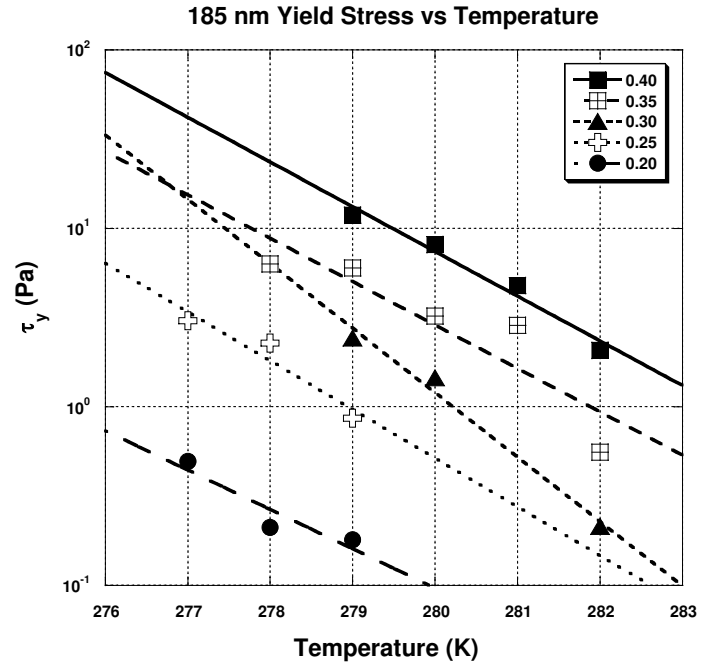

Figure F.4 – Yield Stress vs Temperature for 30 nm and 185 nm particles at different volume fractions respectively. Symbols represent experimental data points while the solid and dashed lines represent exponential fits to data.

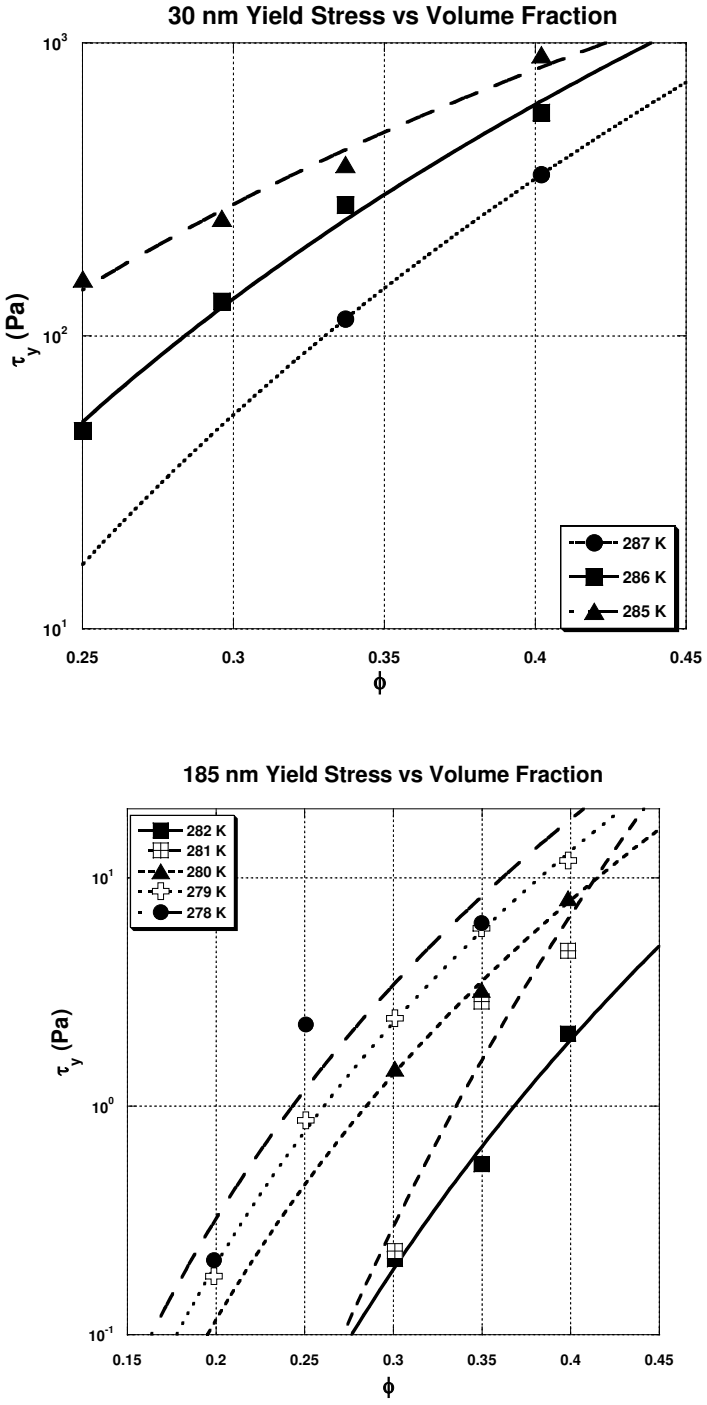

Figure F.5– Yield Stress vs Volume Fraction for 30 nm and 185 nm particles at different temperatures respectively. Symbols represent experimental data points while the solid and dashed lines represent power law fits to data.

REFERENCES

1 Guo, H. Y., Ramakrishnan, S., Harden, J. L. & Leheny, R. L. Connecting Nanoscale Motion And Rheology Of Gel-Forming Colloidal Suspensions. Physical Review E **81**, Doi:10.1103/Physreve.81.050401 (2010).

2 Ramakrishnan, S. & Zukoski, C. F. Microstructure And Rheology Of Thermoreversible Nanoparticle Gels. Langmuir **22**, 7833-7842, Doi:10.1021/La060168j (2006).

3 Gopalakrishnan, V. & Zukoski, C. F. Yielding Behavior Of Thermo-Reversible Colloidal Gels. Langmuir **23**, 8187-8193, Doi:10.1021/1a0620915 (2007).

4 Butterworth, M. D., Illum, L. & Davis, S. S. Preparation Of Ultrafine Silica- And PEG-Coated Magnetite Particles. Colloids And Surfaces A-Physicochemical And Engineering Aspects **179**, 93-102, Doi:10.1016/S0927-7757(00)00633-6 (2001).

5 Liu, J. P. Et Al. Super-Hydrophobic/Icephobic Coatings Based On Silica Nanoparticles Modified By Self-Assembled Monolayers. Nanomaterials **6**, Doi:10.3390/Nano6120232 (2016).

6 Wu, H. X. Et Al. Biocompatibility, MR Imaging And Targeted Drug Delivery Of A Rattle-Type Magnetic Mesoporous Silica Nanosphere System Conjugated With PEG And Cancer-Cell-Specific Ligands. J. Mater. Chem. **21**, 3037-3045, Doi:10.1039/C0jm02863k (2011).

7 Al-Thabaiti, S. A., Al-Nowaiser, F. M., Obaid, A. Y., Al-Youbi, A. O. & Khan, Z. Formation And Characterization Of Surfactant Stabilized Silver Nanoparticles: A Kinetic Study. Colloids And Surfaces B-Biointerfaces **67**, 230-237, Doi:10.1016/J.Colsurfb.2008.08.022 (2008).

8 Farhadi, H., Riahi, S., Ayatollahi, S. & Ahmadi, H. Experimental Study Of Nanoparticle-Surfactant-Stabilized CO2 Foam: Stability And Mobility Control. Chemical Engineering Research & Design **111**, 449-460, Doi:10.1016/J.Cherd.2016.05.024 (2016).

9 Kvitek, L. Et Al. Effect Of Surfactants And Polymers On Stability And Antibacterial Activity Of Silver Nanoparticles (Nps). Journal Of Physical Chemistry C **112**, 5825-5834, Doi:10.1021/Jp711616v (2008).

10 Ramakrishnan, S., Gopalakrishnan, V. & Zukoski, C. F. Clustering And Mechanics In Dense Depletion And Thermal Gels. Langmuir **21**, 9917-9925, Doi:10.1021/La050830w (2005).

11 Ramakrishnan, S., Fuchs, M., Schweizer, K. S. & Zukoski, C. F. Entropy Driven Phase Transitions In Colloid-Polymer Suspensions: Tests Of Depletion Theories. Journal Of Chemical Physics **116**, 2201-2212, Doi:10.1063/1.1426413 (2002).

12 Balazs, A. C., Emrick, T. & Russell, T. P. Nanoparticle Polymer Composites: Where Two Small Worlds Meet. Science **314**, 1107-1110, Doi:10.1126/Science.1130557 (2006).

13 Mohraz, A., Weeks, E. R. & Lewis, J. A. Structure And Dynamics Of Biphasic Colloidal Mixtures. Physical Review E **77**, 4, Doi:10.1103/Physreve.77.060403 (2008).

14 Shevchenko, E. V., Talapin, D. V., Murray, C. B. & O'Brien, S. Structural Characterization Of Self-Assembled Multifunctional Binary Nanoparticle Superlattices. J. Am. Chem. Soc. **128**, 3620-3637, Doi:10.1021/Ja0564261 (2006).

15 Adams, M., Dogic, Z., Keller, S. L. & Fraden, S. Entropically Driven Microphase Transitions In Mixtures Of Colloidal Rods And Spheres. Nature **393**, 349-352 (1998).

16 Adams, M. & Fraden, S. Phase Behavior Of Mixture's Of Rods (Tobacco Mosaic Virus) And Spheres (Polyethylene Oxide, Bovine Serum Albumin). Biophys. J. **74**, 669-677 (1998).

17 Rodriguez-Linan, G. M., Nahmad-Molinari, Y. & Perez-Angel, G. Clustering-Induced Attraction In Granular Mixtures Of Rods And Spheres. Plos One **11**, 11, Doi:10.1371/Journal.Pone.0156153 (2016).

18 Zaccarelli, E. Colloidal Gels: Equilibrium And Non-Equilibrium Routes. Journal Of Physics-Condensed Matter **19**, Doi:10.1088/0953-8984/19/32/323101 (2007).

19 Klinkova, A., Therien-Aubin, H., Choueiri, R. M., Rubinstein, M. & Kumacheva, E. Colloidal Analogs Of Molecular Chain Stoppers. Proceedings Of The National Academy Of Sciences Of The United States Of America **110**, 18775-18779, Doi:10.1073/Pnas.1315381110 (2013).

20 Meng, G. N., Arkus, N., Brenner, M. P. & Manoharan, V. N. The Free-Energy Landscape Of Clusters Of Attractive Hard Spheres. Science **327**, 560-563, Doi:10.1126/Science.1181263 (2010).

21 Manoharan, V. N. Colloidal Matter: Packing, Geometry, And Entropy. Science **349**, Doi:10.1126/Science.1253751 (2015).

22 Mirarefi, A. Y. Et Al. Small-Angle X-Ray Scattering Studies Of The Intact Eye Lens: Effect Of Crystallin Composition And Concentration On Microstructure. Biochim. Biophys. Acta-Gen. Subj. **1800**, 556-564, Doi:10.1016/J.Bbagen.2010.02.004 (2010).

23 Belyi, V. A. & Muthukumar, M. Electrostatic Origin Of The Genome Packing In Viruses. Proceedings Of The National Academy Of Sciences Of The United States Of America **103**, 17174-17178, Doi:10.1073/Pnas.0608311103 (2006).

24 Starruss, J., Peruani, F., Bar, M. & Deutsch, A. Bacterial Swarming Driven By Rod Shape. (2007).

25 Yethiraj, A. & Van Blaaderen, A. A Colloidal Model System With An Interaction Tunable From Hard Sphere To Soft And Dipolar. Nature **421**, 513-517, Doi:10.1038/Nature01328 (2003).

26 Eberle, A. P. R., Wagner, N. J. & Castaneda-Priego, R. Dynamical Arrest Transition In Nanoparticle Dispersions With Short-Range Interactions. Physical Review Letters **106**, Doi:10.1103/Physrevlett.106.105704 (2011).

27 Jansen, J. W., Dekruif, C. G. & Vrij, A. Attractions In Sterically Stabilized Silica Dispersions .1. Theory Of Phase-Separation. Journal Of Colloid And Interface Science **114**, 471-480, Doi:10.1016/0021-9797(86)90432-7 (1986).

28 Roth, R., Evans, R. & Dietrich, S. Depletion Potential In Hard-Sphere Mixtures: Theory And Applications. Physical Review E **62**, 5360-5377, Doi:10.1103/Physreve.62.5360 (2000).

29 Dijkstra, M., Brader, J. M. & Evans, R. Phase Behaviour And Structure Of Model Colloid-Polymer Mixtures. Journal Of Physics-Condensed Matter **11**, 10079-10106, Doi:10.1088/0953-8984/11/50/304 (1999).

30 Sciortino, F. Disordered Materials - One Liquid, Two Glasses. Nat. Mater. **1**, 145-146, Doi:10.1038/Nmat752 (2002).

31 Eckert, T. & Bartsch, E. Re-Entrant Glass Transition In A Colloid-Polymer Mixture With Depletion Attractions. Physical Review Letters **89**, 4, Doi:10.1103/Physrevlett.89.125701 (2002).

32 Pham, K. N. Et Al. Multiple Glassy States In A Simple Model System. Science **296**, 104-106, Doi:10.1126/Science.1068238 (2002).

33 Jan Mewis, N. J. W. Colloidal Suspension Rheology. (Cambridge University Press, 2012).

34 Shih, W. H., Shih, W. Y., Kim, S. I., Liu, J. & Aksay, I. A. Scaling Behavior Of The Elastic Properties Of Colloidal Gels. Physical Review A **42**, 4772-4779, Doi:10.1103/Physreva.42.4772 (1990).

35 Derooij, R., Potanin, A. A., Vandenende, D. & Mellema, J. Steady Shear Viscosity Of Weakly Aggregating Polystyrene Latex Dispersions. Journal Of Chemical Physics **99**, 9213-9223, Doi:10.1063/1.465537 (1993).

36 Stauffer, D., Coniglio, A. & Adam, M. Gelation And Critical Phenomena. Advances In Polymer Science **44**, 103-158 (1982).

37 Grant, M. C. & Russel, W. B. Volume-Fraction Dependence Of Elastic-Moduli And Transition-Temperatures For Colloidal Silica-Gels. Physical Review E **47**, 2606-2614, Doi:10.1103/Physreve.47.2606 (1993).

38 Schweizer, K. S. & Yatsenko, G. Collisions, Caging, Thermodynamics, And Jamming In The Barrier Hopping Theory Of Glassy Hard Sphere Fluids. Journal Of Chemical Physics **127**, Doi:10.1063/1.2780861 (2007).

39 Lin, M. Y. Et Al. Universality Of Fractal Aggregates As Probed By Light-Scattering. Proc. R. Soc. London Ser. A-Math. Phys. Eng. Sci. **423**, 71-87, Doi:10.1098/Rspa.1989.0042 (1989).

40 Ramakrishnan, S., Chen, Y. L., Schweizer, K. S. & Zukoski, C. F. Elasticity And Clustering In Concentrated Depletion Gels. Physical Review E **70**, Doi:10.1103/Physreve.70.040401 (2004).

41 Rueb, C. J. & Zukoski, C. F. Viscoelastic Properties Of Colloidal Gels. Journal Of Rheology **41**, 197-218, Doi:10.1122/1.550812 (1997).

42 Eberle, A. P. R., Castaneda-Priego, R., Kim, J. M. & Wagner, N. J. Dynamical Arrest, Percolation, Gelation, And Glass Formation In Model Nanoparticle Dispersions With Thermoreversible Adhesive Interactions. Langmuir **28**, 1866-1878, Doi:10.1021/La2035054 (2012).

43 Gordon, M. B., Kloxin, C. J. & Wagner, N. J. The Rheology And Microstructure Of An Aging Thermoreversible Colloidal Gel. Journal Of Rheology **61**, 23-34, Doi:10.1122/1.4966039 (2017).

44 Sonntag, R. C. & Russel, W. B. Structure And Breakup Of Flocs Subjected To Fluid Stresses .1. Shear Experiments. Journal Of Colloid And Interface Science **113**, 399-413, Doi:10.1016/0021-9797(86)90175-X (1986).

45 Buscall, R., Mills, P. D. A. & Yates, G. E. Viscoelastic Properties Of Strongly Flocculated Polystyrene Latex Dispersions. Colloids And Surfaces **18**, 341-358, Doi:10.1016/0166-6622(86)80322-5 (1986).

46 Buscall, R., Mills, P. D. A., Goodwin, J. W. & Lawson, D. W. Scaling Behavior Of The Rheology Of Aggregate Networks Formed From Colloidal Particles. Journal Of The Chemical Society-Faraday Transactions I **84**, 4249-4260, Doi:10.1039/F19888404249 (1988).

47 Buscall, R., Mcgowan, I. J. & Mummeyoung, C. A. Rheology Of Weakly Interacting Colloidal Particles At High-Concentration. Faraday Discussions **90**, 115-127, Doi:10.1039/Dc9909000115 (1990).

48 Derooij, R., Vandenende, D., Duits, M. H. G. & Mellema, J. Elasticity Of Weakly Aggregating Polystyrene Latex Dispersions. Physical Review E **49**, 3038-3049, Doi:10.1103/Physreve.49.3038 (1994).

49 Potanin, A. A., Derooij, R., Vandenende, D. & Mellema, J. Microrheological Modeling Of Weakly Aggregated Dispersions. Journal Of Chemical Physics **102**, 5845-5853, Doi:10.1063/1.469317 (1995).

50 Potanin, A. A. & Russel, W. B. Fractal Model Of Consolidation Of Weakly Aggregated Colloidal Dispersions. Physical Review E **53**, 3702-3709, Doi:10.1103/Physreve.53.3702 (1996).

51 Schweizer, K. S. & Saltzman, E. J. Entropic Barriers, Activated Hopping, And The Glass Transition In Colloidal Suspensions. Journal Of Chemical Physics **119**, 1181-1196, Doi:10.1063/1.1578632 (2003).

52 Kobelev, V. & Schweizer, K. S. Yielding, Strain Softening And Shear Thinning In Glassy Colloidal Suspensions. Abstr. Pap. Am. Chem. Soc. **229**, U652-U652 (2005).

53 Yatsenko, G. & Schweizer, K. S. Glassy Dynamics And Kinetic Vitrification Of Isotropic Suspensions Of Hard Rods. Langmuir **24**, 7474-7484, Doi:10.1021/La8002492 (2008).

54 Guo, H. Y., Ramakrishnan, S., Harden, J. L. & Leheny, R. L. Gel Formation And Aging In Weakly Attractive Nanocolloid Suspensions At Intermediate Concentrations. Journal Of Chemical Physics **135**, Doi:10.1063/1.3653380 (2011).

55 Jansen, J. W., Dekruif, C. G. & Vrij, A. Attractions In Sterically Stabilized Silica Dispersions .4. Sedimentation. Journal Of Colloid And Interface Science **114**, 501-504, Doi:10.1016/0021-9797(86)90435-2 (1986).

56 Dekruif, C. G. Et Al. Adhesive Hard-Sphere Colloidal Dispersions - A Small-Angle Neutron-Scattering Study Of Stickiness And The Structure Factor. Langmuir **5**, 422-428, Doi:10.1021/La00086a023 (1989).

57 Bogush, G. H., Tracy, M. A. & Zukoski, C. F. Preparation Of Monodisperse Silica Particles - Control Of Size And Mass Fraction. Journal Of Non-Crystalline Solids **104**, 95-106, Doi:10.1016/0022-3093(88)90187-1 (1988).

58 Vanhelden, A. K., Jansen, J. W. & Vrij, A. Preparation And Characterization Of Spherical Monodisperse Silica Dispersions In Non-Aqueous Solvents. Journal Of Colloid And Interface Science **81**, 354-368, Doi:10.1016/0021-9797(81)90417-3 (1981).

59 Stober, W., Fink, A. & Bohn, E. Controlled Growth Of Monodisperse Silica Spheres In Micron Size Range. Journal Of Colloid And Interface Science **26**, 62-&, Doi:10.1016/0021-9797(68)90272-5 (1968).

60 Guo, H., Ramakrishnan, S., Harden, J. L. & Leheny, R. L. Gel Formation And Aging In Weakly Attractive Nanocolloid Suspensions At Intermediate Concentrations. Journal Of Chemical Physics **135**, Doi:10.1063/1.3653380 (2011).

61 Chambon, F. & Winter, H. H. Stopping Of Crosslinking Reaction In A Pdms Polymer At The Gel Point. Polym. Bull. **13**, 499-503 (1985).

62 Breuer, K. Rheology Of Colloidal Gels Undergraduate Thesis, Florida State University, (2008).

63 Melrose, J. R. & Heyes, D. M. Rheology Of Weakly Flocculated Suspensions - Simulation Of Agglomerates Under Shear. Journal Of Colloid And Interface Science **157**, 227-234, Doi:10.1006/Jcis.1993.1180 (1993).

64 Chen, D. H. & Doi, M. Microstructure And Viscosity Of Aggregating Colloids Under Strong Shearing Force. Journal Of Colloid And Interface Science **212**, 286-292, Doi:10.1006/Jcis.1998.6011 (1999).

65 Lin, M. Y. Et al. The Structure Of Fractal Colloidal Aggregates Of Finite Extent. Journal Of Colloid And Interface Science **137**, 263-280, Doi:10.1016/0021-9797(90)90061-R (1990).

66 Muzny, C. D., Hansen, D., Straty, G. C., Evans, D. J. & Hanley, H. J. M. Simulation And Sans Studies Of Gelation Under Shear. International Journal Of Thermophysics **16**, 337-346, Doi:10.1007/Bf01441899 (1995).

67 Chen, M. & Russel, W. B. Characteristics Of Flocculated Silica Dispersions. Journal Of Colloid And Interface Science **141**, 564-577, Doi:10.1016/0021-9797(91)90353-A (1991).

68 Jiang, T. Y. & Zukoski, C. F. Dynamic Localization And Shear-Induced Hopping Of Particles: A Way To Understand The Rheology Of Dense Colloidal Dispersions. Journal Of Rheology **58**, 1277-1299, Doi:10.1122/1.4866038 (2014).

BIOGRAPHICAL SKETCH

Divya Bahadur was born on December 07, 1991 in New Delhi, India. She received her high school diploma from The Mother's International School, New Delhi in 2010. Ms Bahadur was an undergraduate student at the Vellore Institute of Technology in Tamil Nadu, India where she was exposed to a variety of research and she pursued projects in fluid dynamics, chemical waste recycling, reactor and plant design, wind resource assessment and environmental impact studies. During her undergraduate studies, she worked as a summer intern at the Materials Development Division at Moser Baer Solar Pvt. Ltd. in New Delhi. Her senior year thesis, under the supervision of Dr David K Daniel, involved exploring a cost effective way to synthesize and rheologically characterize ferrofluids. Her fascination with these materials led her to design interactive art displays using the same. She served as the President of the Indian Institute of Chemical Engineers – VIT Student Chapter for the year 2013 – 2014 and was awarded the Special Achievers' Award for the outgoing batch of 2013 – 14. At FSU, she is pursuing a Master's Degree in Chemical Engineering with a focus on Materials Science and is advised by Dr Subramanian Ramakrishnan. Her research focusses on understanding the structure and dynamics of nano-colloidal gels by probing the gelation transition using rheological and x-ray photon correlation spectroscopy techniques. She has also served as a Teaching Assistant for two courses and a lab at FSU. She was awarded the Dean Scholarship for Academic Excellence in December 2014 and May 2015 at FSU. In 2016, as a visiting student at Dr David Weitz's lab at Harvard, she worked on developing a technique to study interaction pathways between different cell types by co-culturing them in hydrogel capsules using droplet microfluidics.